LUND UNIVERSITY

fMRI for mapping the plastic somatotopy of primary somatosensory cortex - Development and clinical applications

Weibull, Andreas

2009

Link to publication

Citation for published version (APA):
Weibull, A. (2009). *fMRI for mapping the plastic somatotopy of primary somatosensory cortex - Development and clinical applications*. [Doctoral Thesis (compilation), Medical Radiation Physics, Malmö]. Medical Radiation Physics, Lund University.

Total number of authors:
1

General rights
Unless other specific re-use rights are stated the following general rights apply:
Copyright and moral rights for the publications made accessible in the public portal are retained by the authors and/or other copyright owners and it is a condition of accessing publications that users recognise and abide by the legal requirements associated with these rights.
• Users may download and print one copy of any publication from the public portal for the purpose of private study or research.
• You may not further distribute the material or use it for any profit-making activity or commercial gain
• You may freely distribute the URL identifying the publication in the public portal

Read more about Creative commons licenses: https://creativecommons.org/licenses/

Take down policy
If you believe that this document breaches copyright please contact us providing details, and we will remove access to the work immediately and investigate your claim.

LUND UNIVERSITY

PO Box 117
221 00 Lund
+46 46-222 00 00

fMRI for mapping the plastic somatotopy of primary somatosensory cortex

Development and clinical applications

Andreas Weibull

Medical Radiation Physics
Department of Clinical Sciences, Malmö
Faculty of Medicine, Lund University
Malmö University Hospital
2009

LUND
UNIVERSITY

Thesis for the Degree of Doctor of Medicine
Lund University
Faculty of Medicine Doctoral Dissertation Series 2009:119
Medical Radiation Physics and Hand Surgery
Department of Clinical Sciences, Malmö
Malmö University Hospital
SE-205 02 Malmö, Sweden

Copyright © 2009 Andreas Weibull (pp 1-71)
ISBN 978-91-86443-08-5
Printed in Sweden by Media-tryck, Lund, 2009

Till min familj

Abstract

Functional magnetic resonance imaging (fMRI) is a widely used tool for studying brain function *in vivo*. The technique is based on acquiring brain images sensitive to the physiological response following neural activation, and hence, allows brain activity to be examined and documented.

In this thesis, methods for fMRI mapping of the primary somatosensory cortex (S1) are optimised and subsequently applied in studies where a plastic reorganisation of S1 is hypothesised.

Initially, the impact of spatial resolution and smoothing on fMRI data of detailed S1 activation was investigated using a theoretical model of fMRI performance. The impact of these parameters was also examined in healthy volunteers where different fingers were mapped in S1. This was accomplished using computer controlled and reproducible tactile stimulation. It was found that both the optimal spatial resolution and preferred level of smoothing were intimately coupled to the experiment's contrast-to-noise.

These results were utilised for monitoring sensory activation of S1 in three cohorts where cortical reorganisation was anticipated: (i) In healthy volunteers where the volar part of the forearm was anaesthetised, (ii) in hand amputees and (iii) in subjects suffering from long-term exposure to vibrating tools. In all these groups, evidence of plastic changes in the sensorimotor system were found. This suggests that plastic processes could be an underlying mechanism for the symptoms experienced in patients following nerve injury and neuropathy.

Finally, alternative methods for mapping functional networks of the sensorimotor cortex during rest were explored. We found that the resulting networks were comparable to activation maps during a finger-tapping task, although only partly overlapping. Such network maps could potentially add to our understanding of brain plasticity in this region of the brain.

In conclusion, this work has improved the feasibility of monitoring plastic reorganisation in S1. This may contribute to the process of rehabilitation in patients suffering from sensory disorders following nerve injury and neuropathy.

Summary in Swedish

Vår hjärna får information från omvärlden via våra sinnen. Olika delar av hjärnan behandlar information från vår syn, hörsel, känsel etc. Inom varje sådant område finns även en funktionell uppdelning. I somatosensoriska kortex (S1) till exempel, där sensorisk information bearbetas, finns en hel kroppskarta där varje liten region svarar mot beröring av en viss kroppsdel. Dessa funktionella kartor är inte permanenta utan förändras kontinuerligt på grund av hjärnans förmåga att anpassa sig till omvärlden - även kallat hjärnans plasticitet. Efter nervskada eller nervsjukdom kan en plastisk reorganisation av handens område i S1 orsaka känselbortfall, försämrad finmotorik eller smärta. Att identifiera sådana förändringar är relevant för att förstå symptom och förbättra rehabilitering av dessa patienter.

Att ta bilder av kroppens insida med hjälp av en magnetkamera (MRI) är ett viktigt diagnostiskt verktyg i sjukvården. Med funktionell MRI (fMRI) är det idag även möjligt att avbilda hjärnans arbete. Med denna teknik kan man se skillnad på syrerikt och syrefattigt blod, vilket ger information om hjärnans aktivitet lokalt. Med fMRI är det även möjligt att studera förändringar till följd av plastisk reorganisation. Handens område i hjärnan är dock litet och väldigt detaljerat vilket kan leda till att aktivering missas med fMRI. Därför är det viktigt att optimera metoden för mätningar i S1. Med fMRI kan man inte bara få information om hur hjärnan arbetar vid ett visst tillfälle utan även hur utbredningen av ett nätverk inom en viss funktion ser ut. Detta kan potentiellt ge ytterligare information om de symptom som är typiska för patienter med nervskada eller nervsjukdom.

I detta arbete har jag, i modeller samt i en grupp av friska frivilliga, studerat hur valet av upplösning i de insamlade bilderna påverkar fMRI-studier av den detaljerade aktiveringen i S1. En apparat för sensorisk stimulering av hudytan har utvecklats som tillsammans med den optimerade upplösningen har förbättrat möjligheten att studera det sensoriska området i hjärnan. Plastiska förändringar i S1 har sedan påvisats i grupper där en reorganisation har varit förväntad: (i) Efter lokal bedövning av huden, (ii) hos handamputerade samt (iii) hos personer som arbetat med vibrerande verktyg under lång tid. Slutligen har sensorisk handaktivering jämförts med de funktionella nätverk som utgör den sensoriska utbredningen i hjärnan.

Den forskning som presenteras här har förbättrat möjligheterna att studera plastisk reorganisation i handens sensoriska område i hjärnan. Detta ökar utsikterna för rehabilitering av individer som lider av sensoriska besvär till följd av nervskador och nervsjukdomar.

Original papers and preliminary reports

This thesis is based on the following papers, which will be referred to in the text by their Roman numerals.

I. *Investigation of spatial resolution, partial volume effects and smoothing in functional MRI using artificial 3D time series*
Weibull A, Gustavsson H, Mattsson S, Svensson J.
Neuroimage 2008; 41(2):346-53

II. *Optimizing the mapping of finger areas in primary somatosensory cortex using functional MRI*
Weibull A, Björkman A, Hall H, Rosén B, Lundborg G, Svensson J.
Magn Reson Imaging 2008; 26(10):1342-51

III. *Rapid cortical reorganisation and improved sensitivity of the hand following cutaneous anaesthesia of the forearm*
Björkman A, Weibull A, Rosén B, Svensson J, Lundborg G.
Eur J Neurosci 2009; 29(4):837-44

IV. *Phantom digit somatotopy – a fMRI study in forearm amputees*
Björkman A, Weibull A, Olsrud J, Björkman-Burtscher I, Ehrsson H. H, Rosén B, Lundborg G.
Submitted to Brain

V. *Central nervous changes in dental technicians exposed to long-term high frequency vibrating tools: A fMRI study*
Björkman A, Weibull A, Svensson J, Balogh I, Rosén B.
Submitted to The Journal of Hand Surgery

VI. *Comparison of intrinsic motor networks using ICA and seed-based analysis to motor responses in task-based fMRI*
Weibull A, Mannfolk P, Björkman A, Olsrud J, Svensson J.
Manuscript

Published papers have been reproduced with kind permission from the following publishers:
Elsevier Inc. (paper I and II), Blackwell Publishing Ltd (paper III)

Preliminary reports were given at the following meetings:

i 23rd European Society for Magnetic Resonance in Medicine and Biology, Warsaw, Poland, September 21-23, 2006. Weibull et al. - *Investigation of partial volume effects in fMRI using artificial time series*, Weibull et al. - *A pneumatically driven stimuli system for fMRI mapping of somatosensory finger areas*.

ii The joint Annual Meeting of European Society for Magnetic Resonance in Medicine and Biology and International Society for Magnetic Resonance in Medicine, Berlin, Germany, May 19-25, 2007. Weibull et al. - *Investigation of partial volume effects in fMRI using artificial 3D time series*.

iii EUROHAND 2008, XIIIth Congress of the Federation of the European Societies for Surgery of the Hand and IXth Congress of the European Federation Societies for Hand Therapy, Lausanne, Switzerland, June 19–21, 2008. Lundborg et al. - *Rapid cortical reorganisation and improved sensibility as a result of cutaneous anaesthesia of the forearm*.

iv 63rd Annual Meeting of the American Society for Surgery of the Hand, Chicago, USA, September 18-20, 2008. Björkman et al. - *Central nervous changes in the hand-arm vibration syndrome: A FMRI study*.

v International Society for Magnetic Resonance in Medicine, Honolulu, Hawaii, USA, April 18-24, 2009. Weibull et al. - *Comparison of motor task responses in fMRI and intrinsic sensorimotor networks in ICA*.

Abbreviations

B_0	Magnetic field strength
CBF	Cerebral blood flow
CBV	Cerebral blood volume
CMR	Cerebral metabolic rate
$CMRO_2$	Cerebral metabolic rate for oxygen
CNR	Contrast-to-noise ratio
CSF	Cerebrospinal fluid
BOLD	Blood oxygen level dependent
EPI	Echo planar imaging
FDR	False discovery rate
fMRI	Functional magnetic resonance imaging
FN	False negative
FP	False positive
GLM	General linear model
Hb	Haemoglobin
ICA	Independent component analysis
M_0	Net magnetisation vector
M_t	Transverse magnetisation vector
MRI	Magnetic resonance imaging
PET	Positron emission tomography
pCO_2	Partial pressure of carbon dioxide
pO_2	Partial pressure of oxygen
S	Signal
S1	Primary somatosensory cortex
S2	Secondary somatosensory cortex
SMA	Supplementary motor areas
SNR	Signal-to-noise ratio
T1	Spin-lattice relaxation time
T2	Spin-spin relaxation time
T2*	Spin-spin relaxation time in a non-uniform field
TE	Echo time
TP	True positive
TR	Repetition time
tSNR	Temporal signal-to-noise ratio
ω	Angular precession frequency

Contents

1 Introduction

Since its beginning in 1973 (Lauterbur 1973), magnetic resonance imaging (MRI) has become a widely utilised imaging technique to visualise internal morphology and function of the human body. In 1982, Thulborn et al. (1982) observed that the transverse relaxation rate of water protons in blood was determined predominantly by the oxygenation state of the blood, later referred to as the MR signal being blood oxygen level dependent (BOLD). This gave great promise for the use of an endogenous contrast for imaging the oxygenation state of blood. However, it was not until the beginning of the 1990:s that this effect was used for monitoring human brain activity (Bandettini, et al. 1992; Belliveau, et al. 1991; Kwong, et al. 1992; Ogawa, et al. 1992). Since then, functional magnetic resonance imaging (fMRI) has been used for studying functional activity in various regions of the brain and the number of published studies has increased rapidly. Today, necessary equipment for performing fMRI is available in most larger hospitals.

The sensorimotor cortex of the brain is a frequently probed region and its functional properties and neural activation in response to externally applied stimulation are well characterised. Functional activation in this particular region may be achieved using simple and straightforward experimental designs. The primary somatosensory cortex (S1), where sensory signals from the body are processed, is situated in the post central gyrus. S1 is functionally divided into sub regions corresponding to a cortical map of the body surface, i.e. a somatotopic map (Penfield and Boldrey 1937). Thus, each part of the body surface is connected to a specific brain region. The size of these cortical sub regions does not reflect the actual body size but rather the magnitude of information processed. Body regions of exquisite sensory function such as the face and hand thus constitute the two largest cortical regions in S1.

The functional structure of these cortical maps are continuously changing as a response to our interaction with the outside world. This capacity to adapt, commonly referred to as brain plasticity (Elbert and Rockstroh 2004; Wall, et al. 2002), exists throughout the brain and is associated with e.g. experience and learning. However, brain plasticity could potentially also explain neurological symptoms experienced in various neural disorders, e.g. focal hand dystonia (Elbert, et al. 1998) or after nerve section (Merzenich, et al. 1984). On the contrary, effects following brain plasticity may potentially also be used for rehabilitation purposes after neural injury or pathology. In this case a chosen function could be promoted or strengthen by using

external manipulation of neural resources (Muellbacher, et al. 2002). To monitor these plastic effects a reliable mapping technique would be of great clinically value.

Although the cortical hand region is relatively large it is challenging to map individual fingers using fMRI. The limited sensitivity suggests that a rather low spatial resolution is advisable. However, the somatotopic map in this region is highly detailed and experiments using a low spatial resolution may suffer from partial volume effects (PVE), i.e. the imaging technique cannot resolve the anatomical or functional details of interest. This fine balance, between improving sensitivity and at the same time minimise partial volume effects, is crucial when monitoring plastic effects in the cortical hand region. Ultimately, a careful choice of spatial parameters is likely to increase the overall fMRI performance.

Recently, new ways to map various brain regions have also evolved, based on outlining networks which are connected functionally (Raichle and Snyder 2007). In this way it may be feasible to extract information from processes in the sensorimotor network that cannot be retrieved using conventional fMRI. The full potential for outlining brain function and neural networks when investigating plastic processes are however not yet known.

1.1 Objectives

The objectives of this thesis are:

- To optimise fMRI for mapping the primary somatosensory cortex during tactile stimulation of the hand (*chapter 2*). The impact of the choice of spatial parameters should be emphasised.

- To develop an easy to use, flexible, reproducible and MR compatible apparatus for tactile stimulation when mapping the primary somatosensory cortex (*chapter 2*).

- To study human plasticity in the primary somatosensory cortex in subjects where such effects are hypothesised (*chapter 3*).

- To explore novel methods for mapping the functional network of the sensorimotor cortex and compare the information retrieved to conventional fMRI (*chapter 4*).

2 fMRI performance

In fMRI, brain activation is studied by acquiring MR images sensitive to the physiological response following neural stimulation. Images acquired during a specific task are then compared to images acquired in absence of that task. Although the underlying principle is straightforward, the actual execution of the fMRI experiment as well as the properties of the measured signal are complex. Briefly, specific magnetic properties are imaged, reflecting haemodynamic variations due to changes in the underlying neural activity. This is performed in a highly dynamic and not easily controlled biological system, where small procedural changes could affect the outcome considerably. To increase fMRI performance, i.e. how well the activation map corresponds to the underlying neural activity, several steps may be optimised throughout the process. The choice of task/control state should be carefully considered to reflect the neuronal mechanisms of interest and comply to the specific hypothesis. Furthermore, the choice of imaging technique, including spatial and temporal resolution, signal-to-noise and contrast-to-noise, is of great importance to ensure high sensitivity as well as high specificity. Ultimately, the evaluation strategy of the often huge amount of data has a strong influence on the resulting brain activation map.

In this chapter the process of acquiring fMRI data is investigated in the sense of ensuring high fMRI performance when mapping S1. The underlying physiological mechanisms following neural activation, and how these mechanisms are used for imaging brain activity are discussed in *section 2.1*. In the subsequent sections, contributions regarding imaging technique, tactile stimulation and data evaluation are presented: In *section 2.2* the impact of spatial resolution and PVE is discussed and recommended spatial resolutions based on modelled data are presented (**paper I**). In *section 2.3*, a strategy for mapping different fingers in S1 is demonstrated (**paper II**). Furthermore, it is shown that the optimal magnitude of smoothing is intimately coupled to the image BOLD contrast-to-noise (**paper I and paper II**).

2.1 Imaging the BOLD contrast

2.1.1 Neural signalling

The basic unit for information processing and signalling in the brain is the neurone. The neurone consists of a soma, constituting the cell nucleus, and

an axon, a myelin sheeted fibre for conveying electrical signals to distant or nearby situated neurones (figure 2.1). This electrical signal is referred to as the action potential and it propagates along the axon by the opening and closing of specific ion channels and thereby depolarise and hyperpolarise the cell in an orderly fashion. The neurone also includes dendrites, making contacts to axon terminals of other neurones. The interconnection site between the axon terminal and the dendrite is called the synapse. Neuronal signals are typically transferred through these sites chemically, by pre-synapse released neurotransmitters (figure 2.1). These neurotransmitters (e.g. glutamate, γ-aminobutyric acid or dopamine), which act on post synaptic receptors, collectively either excite or inhibit the generation of a post synaptic potential and further propagation of the signal.

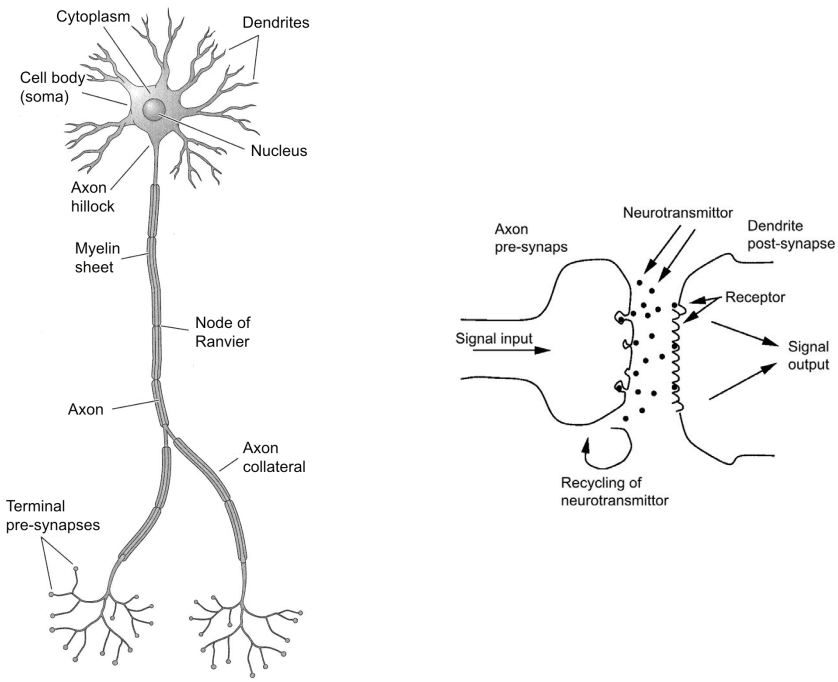

Figure 2.1 - The neurone consists of a soma, containing a nucleus, and an axon, a myelin sheeted fiber which convey electrical signals for the purpose of communication. The interconnection site between two neurones is called the synapse. Here, the electrical signals are transferred chemically by the release of neurotransmitters. Illustrations from http://www.neuropsychopathologie.fr

Processing signal information is a continuously ongoing activity in the brain. Whether we are awake or sleeping, responding to external stimulation (e.g. visual input or touch of a finger tip) or internal stimulation (e.g. planning or reasoning) or simply doing nothing, our brain is in some sense always active. Thus, the brain require oxygen and energy substrates at all times. The energy extracted is used predominantly for maintaining or restoring ion concentrations within the cytoplasm and releasing and recycling of neurotransmitters in the synaptic cleft (Logothetis and Pfeuffer 2004). Although the adult brain constitutes merely 2% of the body weight, it accounts for approximately 20% of the energy consumed, the major part being due to neuronal communication (Buzsaki, et al. 2007).

2.1.2 Neurovascular coupling

The total blood flow to the brain is about 750-1000 ml/min or approximately 15% of the cardiac output. (Kandel, et al. 2000). Since the brain has an ongoing demand for oxygen and energy substrates, it is not surprising that the brain and the vascular system is tightly connected. When the cerebral metabolic rate (CMR) suddenly increases in a region of the brain the demand for oxygen ($CMRO_2$) and energy increases swiftly as are the metabolic waste products (mainly CO_2 and water). This triggers the local arterioles and capillary sphincters to dilate and relax, providing the adjacent cells with well-oxygenated blood and an increased wash-out of CO_2 (figure 2.2). Surprisingly, the partial pressure of carbon dioxide (pCO_2) is a far more potent trigger of the haemodynamic response compared to pO_2 (Kandel, et al. 2000). Consequently, the haemodynamic response following neural activation, and thus increased $CMRO_2$, includes two major mechanisms: (i) An increase in regional cerebral blood flow (CBF) and (ii) an increase in regional cerebral blood volume (CBV).

These physiological responses do not occur instantly after neural activation. Although the neuronal firing delay after stimulation is in the order of 150 ms (Gerstein 1960), the haemodynamic response is much slower, showing dynamic features over a prolonged period of time. Initially after a momentary stimulus, the increase in $CMRO_2$ is assumed to deplete the well-oxygenated blood pool close to the activation site. One to two seconds later the CBF, and thus the CBV, increases rapidly and peak approximately five to eight seconds after the onset of neural activity (Buxton, et al. 2004). This auto-regulated response is far exceeding the tissue need resulting in oxygen saturation of the blood. This delayed effect is not particularly localised but

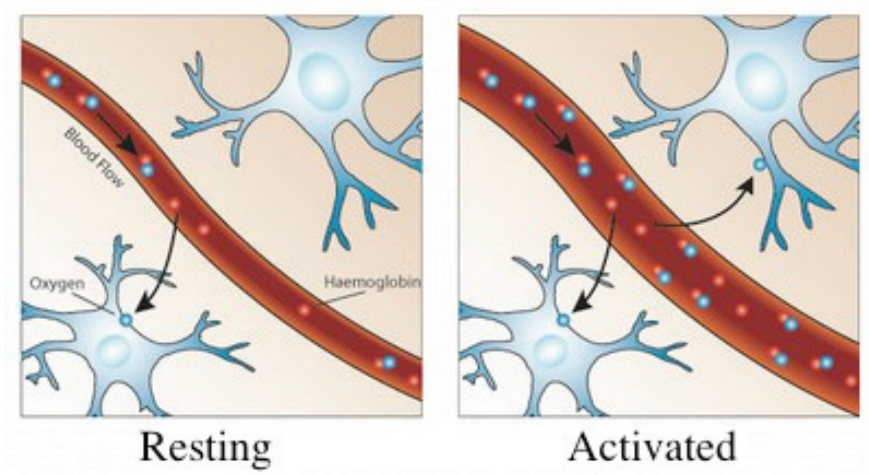

Figure 2.2 - During activation, the arterioles dilate in response to the growing concentration of metabolic waste products, resulting in an increased wash-out of deoxyHb. The local magnetic field becomes less distorted, ultimately increasing the MR signal. Courtesy of Stuart Clare, Oxford Centre for Functional MRI of the Brain

may include for example adjacent draining veins. The baseline return of CBV is slower compared to the baseline return of CBF (Buxton, et al. 2004) due to wall tension differences of arterioles and venules. Interestingly, recent investigations regarding the neural origin of the haemodynamic response suggest a correlation to the energetically expensive synaptic processes rather than to actual neurone firing (Logothetis, et al. 2001; Logothetis and Pfeuffer 2004).

2.1.3 Oxy- and deoxyhaemoglobin

When carried in blood, oxygen is almost exclusively bound to haemoglobin (Hb), a molecule complex abundant in the erythrocyte. Hb consists of four sub units, each containing an organic molecule (a heme group) tightly associated to a protein (globulin). The heme group includes an iron ion (Fe^{2+}) which functions as a site for oxygen binding, i.e. oxygenating Fe^{2+} to Fe^{3+}. The oxygen-rich blood leaving the lungs is close to fully saturated by oxygen, meaning that almost all Hb molecules are binding four O_2-molecules. This oxygen-rich state of Hb is commonly referred to as oxyHb.

When the blood reaches the tissue the oxygen binding capability decreases and oxygen is easily released, eventually entering the tissue by diffusion. In this state the Hb is saturated to a lesser degree, referred to as deoxyHb. Neural activation tends to lower the level of deoxyHb locally due to an increased CBF, although a counteracting effect from increased CBV exists. The ability to monitor changes of deoxyHb following neural activation using MRI is discussed next.

2.1.4 The BOLD effect

In MRI the origin of the intrinsic signal is the energy separation of the nuclear spin state in an externally applied magnetic field. This energy separation generates a slight dominance for proton spins oriented along the field (slightly lower energy state) compared to proton spins oriented against the field, due to the Boltzmann distribution of energy states. This equilibrium results in a net magnetisation vector (M_0) with an orientation along the external field and its magnitude being proportional to the magnetic field strength (B_0) and the number of protons. If electromagnetic energy, tuned to match the energy difference of the two states, is induced in the system the equilibrium is disturbed. In this way the orientation of M_0 is temporarily altered producing a transverse magnetic vector (M_t) proportional to M_0. This transversal spin precession is detectable by the system. The transverse proton spins gradually lose coherence due to spin-spin interaction, a process called T2 relaxation, resulting in a M_t signal loss. Moreover, the system also gradually loses energy approaching the equilibrium state, a process called T1 relaxation.

If the local magnetic field is non-uniform, the loss of coherence is more rapid because adjacent protons ”sense” different field strengths (T2* relaxation). This effect is typically seen due to magnetic susceptibility, a term describing the local contribution to magnetic flux density, induced by a substance in an externally applied magnetic field. Depending on the magnetic properties of the substance, this effect may be small or large and may enhance or counteract the local flux density, leading to local disturbances of magnetic field uniformity. Similar to water, oxyHb does not affect the local magnetic flux density extensively. However when the oxyHb releases oxygen, the complex will contain unpaired electrons contributing to the pronounced paramagnetic property of deoxyHb (Pauling and Coryell 1936). The result is a fast loss of MR signal in regions of deoxyHb, consequently referred to as the blood oxygen level dependent (BOLD)

effect. The T2* signal decay can be studied using imaging sequences sensitive to magnetic susceptibility, such as gradient echo techniques. The imaging technique of choice so far has been echo-planar imaging (EPI) (Mansfield 1977), which combines the possibility of T2* contrast and excellent temporal resolution. The accessible BOLD effect increases while increasing the field strength (van der Zwaag, et al. 2009), however, the T2* signal decay is faster and a shorter echo time (TE) is needed.

Susceptibility effects are not the only mechanisms that have been suggested to affect the T2* relaxation in BOLD fMRI. An increased level of oxygenation also alters the magnetic properties of blood, resulting in a decreased T2 relaxation. However, it seems as this contribution to the BOLD effect is less pronounced compared to the susceptibility effect (Hoogenraad, et al. 2001). Moreover, the T2 for blood is shortened at higher field strengths (Yacoub, et al. 2001) suggesting a smaller contribution to the BOLD signal in this case.

2.1.5 The fMRI experiment

To be able to monitor the BOLD effect, T2* weighted MR images acquired during a specific task are typically compared to some sort of control state. The brain volume is continuously imaged while alternating various tasks (e.g. sensory input or motor output) and periods of a preferred control state, for example eyes closed rest. In this manner image volumes are acquired over time resulting in a four-dimensional data set where each image volume corresponds to a single time point. In turn, each image volume comprises thousands of voxels (i.e. the smallest image volume element defining the spatial resolution of the image) resulting in time series of signal variations over time for each voxel region of the brain. These regional signal variations are potentially reflecting brain activity due to the BOLD effect. Note that, although eyes closed rest is a commonly used control state it may not be the most suitable in all experiments. For example, hippocampal activity has been shown to be higher during rest compared to simple cognitive tasks such as ”deciding whether a digit is odd or even” or ”deciding whether an arrow is pointing left or right” (Stark and Squire 2001).

Since the temporal design of the task application is known and the temporal characteristics of the haemodynamic response (see *section 2.1.2*) can be modelled, any BOLD activation is assumed to correlate to the temporal design convolved with the haemodynamic response (figure 2.3). Thus, statistical inferences of task induced brain activation can be made for each

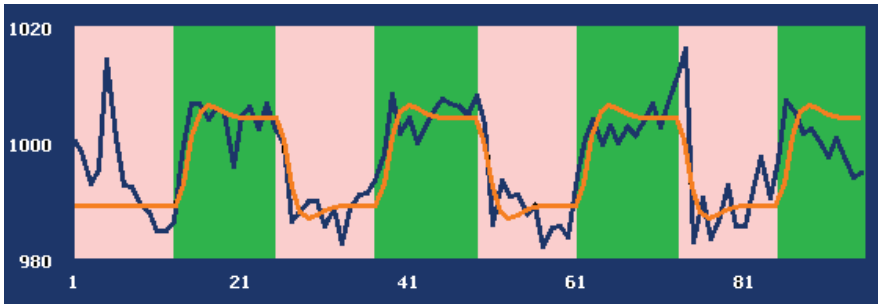

Figure 2.3 - A simple fMRI experiment of 96 time points where task periods (dark grey fields) alternate between rest periods (light grey fields). The dark grey curve represents the regional mean of the temporal signal from an activated brain region. Clearly this signal time series is highly correlated to the assumed BOLD response in light grey (i.e. the haemodynamic response function convolved with the rest-task design).

voxel time series based on correlation to this reference wave form (Bandettini, et al. 1993). This is commonly performed voxel wise by minimising the sum of the squared residuals $\sum \varepsilon^2$ in the general linear model (GLM (Friston, et al. 1995); Eq. 2.1), where $\boldsymbol{Y}$ is the measured signal time series, $\boldsymbol{X}$ is the design matrix and $\boldsymbol{\beta}$ is the weighting factors to be estimated.

$$Y = X\beta + \varepsilon \qquad \text{Eq. 2.1}$$

Before statistical evaluation the data is motion corrected, typically using a six parameter spatial transformation (assuming the brain being a rigid body). This is the single most important pre processing step during the data evaluation as head motion is recognised as the most severe and misleading confound in fMRI studies (Turner, et al. 1998). Furthermore, the time series are generally temporally filtered, using a high pass filter to correct for system drifts, and spatially smoothed (see *section 2.3.3*). In case of evaluating group data, each individual brain is conformed to a known co-ordinate system, e.g. the Talairach system (Talairach J. 1988).

Ultimately, functional brain activation images are constructed where colour-scaled statistical inferences are presented above a chosen statistical threshold, and subsequently overlaid on anatomical images for localisation purposes. Due to the extreme number of hypotheses in fMRI (one for each voxel), a statistical threshold based on controlling the amount of false

positives in the activated voxel cohort (false discovery rate; FDR) (Benjamini and Hochberg 1995) instead of controlling the number of false positives in the total cohort (all voxels) is generally but not always used in this thesis.

The choice of experimental design, spatial resolution and smoothing are seriously affecting the resulting activation image. The underlying mechanisms, recent progression and novel contributions to this specific field of fMRI optimisation are discussed and presented in the following section.

2.2 BOLD contrast-to-noise

2.2.1 Signal-to-noise in MRI

The measured MR signal (S) is proportional to the time derivative of the oscillating M_t, thus $S \propto \omega M_0$, where ω is the angular precession frequency of the spin vector (i.e. the Larmor frequency). Since both ω and M_0 are proportional to B_0, the intrinsic signal is proportional to B_0^2 and the number of protons in the sample volume studied. To measure this signal an antenna, or coil, tuned to match ω is used. However, the signal of interest is contaminated by various noise sources. Electrical noise in the receiver system as well as thermally generated, random currents in the sample contributes to the image noise. This type of noise is commonly referred to as thermal or white due to its typically flat power spectral characteristics. The magnitude of this noise is also proportional to B_0, resulting in a signal-to-noise ratio (SNR) being proportional to B_0 and the number of protons in the sample (Edelstein, et al. 1986). The thermal noise however, is independent of the sample volume or acquisition technique used. Since these oscillating signals are sampled over a time period, the SNR is also proportional to the square-root of the total sampling time (Edelstein, et al. 1986). Moreover, potential noise sources of more complex characteristics include system drift and imperfections in the RF, gradient and shim subsystems.

Since the MR signal is proportional to the number of protons in the sample and the magnitude of the thermal noise is not, the SNR is highly dependent on the voxel volume used. Since the BOLD contrast generally is low (typically 2 - 4% at 1.5 tesla (Turner, et al. 1998)) compared to the noise level, the image SNR is of critical importance in fMRI. Parrish et al. (2000) demonstrated that the SNR requirement for mapping BOLD induced signal changes increased rapidly when the expected BOLD contrast decreased. For small contrasts, $< 1\%$, a SNR > 70 was needed to be able to detect 50% of

the truly activated voxels. This suggests that a low spatial resolution should be used in order to ensure high SNR and activation sensitivity. However, as discussed next, SNR may not be the parameter of primary importance in fMRI experiments.

2.2.2 Temporal SNR

In fMRI, temporal BOLD signal variations originating from haemodynamic responses are measured over time and subsequently evaluated statistically, preferably by time-course correlation to a reference wave form. Since the statistical inferences are based on signal variations over time, the temporal SNR (tSNR), rather than SNR, is of primary importance. tSNR is not only dependent on thermal noise but also on periodic fluctuations, referred to as physiological noise (Biswal, et al. 1995; Hyde, et al. 2001; Kruger and Glover 2001). These can be of neural origin (spontaneous neural activity), affecting T2* or of non-neural origin (CSF fluctuation due to cardiac and respiratory functions), affecting the overall MR signal. In contrast to thermal noise, physiological noise has a typical power spectral dependence inversely proportional to the frequency, with additional peaks corresponding to fluctuations due to CSF pulsation and breathing (Turner, et al. 1998), and is predominantly seen in grey matter and CSF (Bodurka, et al. 2005). Physiological noise also contributes to the actual signal acquired, thus demonstrating a dependence of signal strength, λS. Kruger and Glover (2001) suggested that λ demonstrated a physical measure of SNR degradation by signal dependent fluctuations. The contribution of spontaneous neural activity was also shown to peak when TE ~ T2* (valid for BOLD imaging in general (Norris 2006)). Accordingly, it is the tSNR and not the SNR that is the limiting parameter in an fMRI experiment. It has now been shown that regardless of an increase in SNR, whether accomplished by increasing the magnetic field strength, using multichannel coils or lowering the spatial resolution, the tSNR tends to reach a plateau, theoretically described by Eq. 2.2 (Kruger and Glover 2001) and presented in figure 2.4, where further SNR improvement is of negligible benefit (Triantafyllou, et al. 2005).

$$tSNR = \frac{SNR}{\sqrt{1 + \lambda^2 SNR^2}} \qquad \text{Eq. 2.2}$$

For example, when the noise is predominantly thermal, i.e. SNR is poor, the plateau is not yet reached and tSNR may be increased, simply by increasing the SNR. However, as the magnitude of the physiological noise approaches the magnitude of the thermal noise, the tSNR gain diminishes. This is of great importance when deciding on what spatial resolution should be used. Bodurka et al. (2007) proposed a ”suggested” voxel volume where the total thermal and system related noise variance equals the physiological noise variance. The impact of tSNR has also been studied recently using various BOLD contrasts (Murphy, et al. 2007).

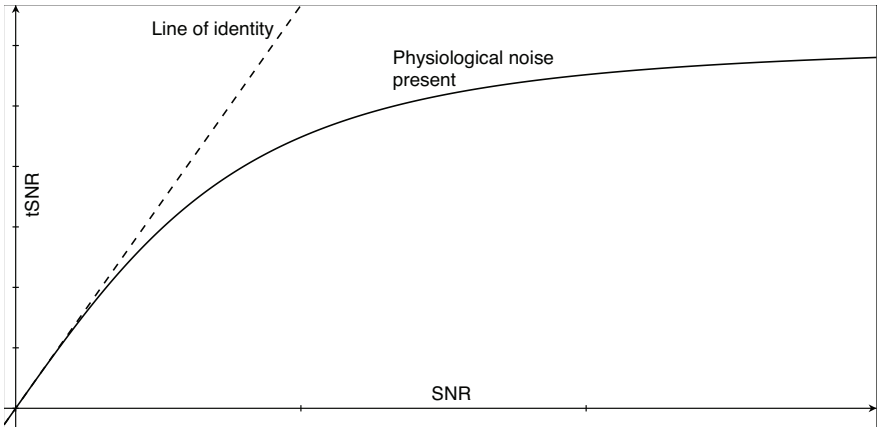

Figure 2.4 - The origin of the noise in fMRI is in part physiological. Since this noise contributes to the fMRI signal it is SNR dependent in contrast to thermal noise. Thus, in situations where the noise is predominantly physiological (e.g. high SNR), tSNR cannot be increased simply by increasing SNR.

tSNR is not the only parameter restricting fMRI sensitivity. As the voxel size increases, the risk of including both activated and non-activated tissue in a single voxel increases. This is commonly referred to as partial volume effects (PVE). In the next section the concept of PVE is discussed and in *section 2.2.4* results based on modelling the balance between tSNR and PVE (**paper I**) are presented, suggesting that the voxel volume of choice is highly dependent on the BOLD contrast at hand.

2.2.3 Partial volume effects

Insufficient image resolution may lead to mixing of different tissue types or activation states within a voxel. PVE have been thoroughly investigated in several MRI applications such as volumetric lesion estimations (Firbank, et al. 1999) and brain tissue segmentation (Zijdenbos and Dawant 1994). However, although several studies regarding the impact of functional resolution in fMRI exist (Bodurka, et al. 2007; Korvenoja, et al. 2006; Scouten, et al. 2006), PVE has rarely been considered. Since the spatial resolution in fMRI generally is poor (typically 3^3 mm^3) compared to the spatial characteristics of the tissues examined (e.g. the primary somatosensory cortex (Geyer, et al. 1999)), PVE may affect the outcome considerably, proposing the need for such studies.

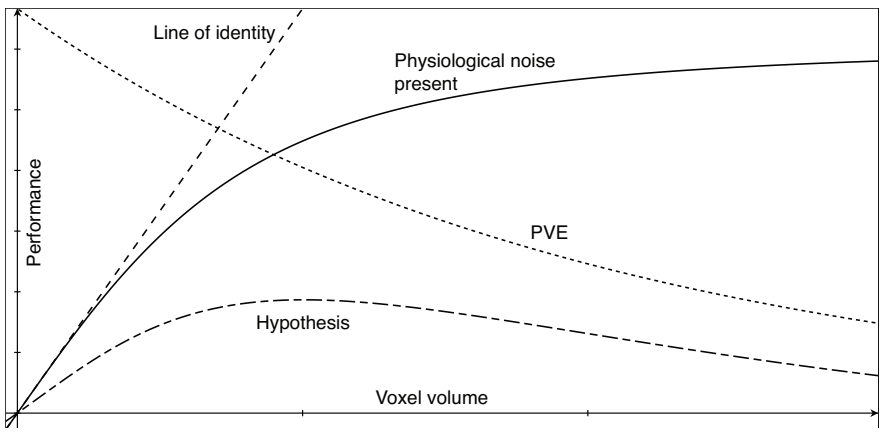

Figure 2.5 - Increasing the voxel volume does not necessarily result in an increased fMRI performance due to an increased contribution of physiological noise (solid). On the contrary, PVE (small dots; hypothetical feature) will deteriorate the performance, resulting in a peak performance (named hypothesis here) and thus an optimal voxel volume.

We will now return to figure 2.4, which presents the stagnating gain in tSNR as SNR increases. Here the label SNR could be switched to ”voxel volume” (see *section 2.2.1*). Furthermore, as tSNR is proportional to some sort of hypothetical fMRI performance the label tSNR could be switched to ”performance”. These changes will in turn enable some sort of imaginable effect from PVE: An infinitesimal voxel volume would minimise PVE and

thus maximise performance (if no noise was present). However, as the voxel volume increases, the contribution of PVE will increase, decreasing fMRI performance (hypothetically described in figure 2.5). fMRI performance would thus peak at some voxel volume where the balance between tSNR and PVE is optimal (labelled ”hypothesis” in figure 2.5). In fact, when examining the primary sensorimotor cortex, which is a region of high grey matter tortuosity (Scouten, et al. 2006), the overall fMRI performance drops rapidly at low spatial resolution, despite a favourable tSNR (**paper I**, see *section 2.2.4*). This suggests that the choice of spatial resolution is of utter importance when examining functional regions where small and localised activation is expected.

Using too high spatial resolution could potentially result in larger numbers of voxel activation beyond the actual site of neural activity. Kim et al. (2004) showed that the spatial correlation of the haemodynamic response to the underlying neural processes is less than 50% below 2.6^3 mm^3. This is surely a challenging issue when performing experiments of sub millimeter resolution.

2.2.4 Modelling fMRI performance

The thought of finding optimal voxel volumes in fMRI was encouraging. To investigate the impact of spatial resolution on fMRI performance the ”true” brain activation has to be known. This is however very difficult in *in vivo* fMRI studies. Fortunately there is always the possibility of investigating these properties in a model. Models for fMRI optimisation purposes have been sparse. Desco et al. (2001) studied the impact of spatial resolution, but this model did not account for physiological noise, and only one type of tissue was assumed throughout the whole brain. In **paper I** a model, based on high-resolution human data for studying fMRI performance, was presented which included thermal as well as physiological noise. Although the model can be used to assess the influence of various parameters, the impact of spatial resolution and smoothing is emphasised in this theses.

High-resolution (0.33^3 mm^3) cryo-sectional photographs of a representative female brain (The National Library of Medicine's Visible Human Project, http://www.nlm.nih.gov) were used to create artificial 3D time series of functional data, based on realistic and accurate information of the human brain anatomy (**paper I**). Thermal noise was subsequently added to the time series, with a variance magnitude corresponding to true SNR in various voxel volumes in the range of 1.3^3 mm^3 to 4.3^3 mm^3 (measured from actual

3^3 mm^3 MRI data assuming linear sample volume dependence). Because of the use of magnitude images in a typical fMRI setting, thermal noise in the image domain is not Gaussian but Rician distributed (Gudbjartsson and Patz 1995). This comes from the Gaussian distributed noise in the real and imaginary part of the quadrature receivers of the MR system being transformed during the creation of magnitude images. Rician distributed noise can be modelled according to Eq. 2.3, where S is the noisy voxel signal, S_0 is the noise-free signal and σ_R^2 and σ_I^2 are Gaussian distributed noise variances in the real and imaginary part of the quadrature receivers, respectively (Henkelman 1985).

$$S = \sqrt{(S_0 + \sigma_R)^2 + \sigma_I^2} \qquad \text{Eq. 2.3}$$

Furthermore, physiological noise was modelled from *in vivo* resting state time series in representative regions of grey matter, white matter and CSF. The time series were acquired at 3^3 mm^3 spatial resolution (3 tesla) to avoid major contributions of thermal noise to the overall noise (i.e. the majority of the noise was physiological in its origin). The physiological noise time series were motion corrected, their mean values were set to zero and they were low pass filtered to further minimise the thermal noise contribution. These physiological noise time series were scaled to match λS ($\lambda = 0.011$ in grey matter, $\lambda = 0.006$ in white matter (Kruger and Glover 2001) and 0.021 in CSF (Bodurka, et al. 2005)) and then randomly added to each voxel.

As no established definition of fMRI performance (P) is available we propose, in **paper I**, that the truly positive activation volume (TP), divided by the sum of the falsely activated (FP) and falsely inactivated (FN) activation volume (Eq. 2.4) reflect P - a straightforward, quantitative and single value measure, closely connected to the definition of sensitivity and specificity.

$$P = \frac{TP}{FP + FN} \qquad \text{Eq. 2.4}$$

fMRI performance was shown to be highly dependent on the choice of voxel volume. At very high spatial resolution, the poor tSNR (due to poor SNR) considerably decreases the sensitivity resulting in a low fMRI performance. Increasing the voxel volume initially improves the tSNR and the fMRI performance correspondingly. However, a turning point is

eventually reached where the stagnating benefit of increased SNR (i.e. as noise becomes dominated by physiological fluctuations and the gain in tSNR is negligible) is consumed by rapidly increasing PVE (figure 2.6). This turning point of maximal fMRI performance, which was hypothetically predicted in figure 2.5 (labelled ”hypothesis”), can be used for choosing the spatial resolution. It is easily seen that this optimal voxel volume is highly dependent on the intrinsic contrast-to-noise ratio (CNR), i.e. the magnitude of the BOLD effect compared to the underlying noise characteristics (defined in Eq. 2.5).

$$CNR = \frac{S_{active} - S_{rest}}{\sqrt{\sigma_R^2 + \sigma_I^2 + \lambda^2 S_{rest}^2}} \qquad \text{Eq. 2.5}$$

In cases with intrinsically higher CNR (e.g. in experiments performed at higher field strength and/or for stronger BOLD effects) a smaller voxel volume is of more value than for cases with lower CNR. Note that choosing too large voxel volume when CNR is high may actually deteriorate fMRI

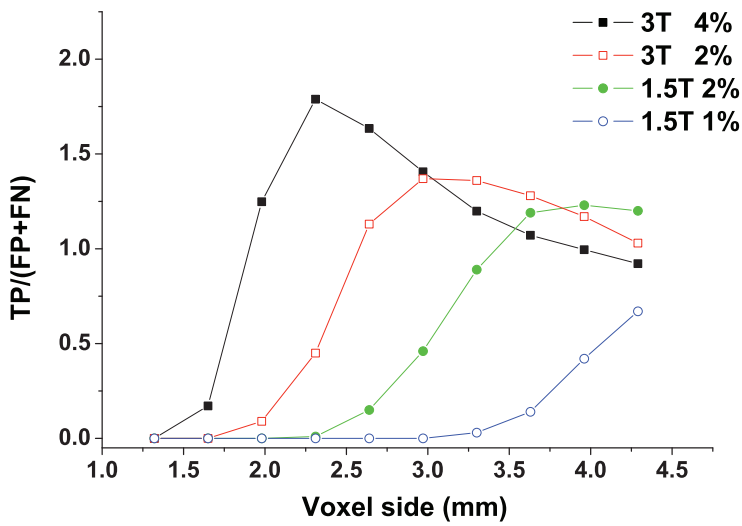

*Figure 2.6 - Modelled data of the impact of voxel volume on fMRI performance. At low voxel volumes the poor SNR results in low sensitivity. However, at too large voxel volume, fMRI performance decreases due to PVE. For each experiment CNR an optimal voxel volume can be found. (**Paper I**)*

performance compared to choosing the same voxel volume when the CNR is poorer (figure 2.6).

This fine balance between tSNR and PVE is indeed crucial for high fMRI performance. Since this balance is greatly dependent on the CNR, any choices of spatial matters should be performed with the expected experiment CNR in mind, if possible. Our results correspond well to results presented by other groups. Hyde et al. (2001) showed that 1.5^3 mm^3 voxel volume was preferable when using motor stimuli at 3 tesla, i.e. typically very high CNR. Bodurka et al. (2007) on the other hand, presented an optimal voxel volume of 1.8^3 mm^3 based on the concept of choosing a voxel volume that ensured the physiological and thermal noise to be equal.

2.3 Experimental design and post processing

2.3.1 Tactile stimulation

The theoretical and modelled results of the impact of spatial resolution inspired us to investigate this property *in vivo*. To do this, an unambiguous, straightforward and reproducible method for applying tactile stimulation was needed.

Several groups have been mapping the somatosensory finger regions using fMRI (Hansson and Brismar 1999; Hlushchuk and Hari 2006; Kurth, et al. 1998; Maldjian, et al. 1999; Stippich, et al. 1999; van Westen, et al. 2004; Wienbruch, et al. 2006). In **Paper II** we present an in-house built pneumatically driven and computer controlled system for tactile stimulation of the skin (figure 2.7), based on the principles presented by Wienbruch et al. (2006). The system allowed individual settings of pulse timing and frequency (< five Hz due to the compressive properties of air) for eight individual channels stimulating up to eight different skin areas.

The system was tested for mapping the small and localised functional regions of the S1, corresponding to the functional somatotopy of individual fingers. The BOLD activation of individual fingers was initially assumed to be small suggesting an optimal voxel volume around 3^3 mm^3, according to figure 2.6 (3 tesla and 2% BOLD contrast). However, it was found that the use of a higher spatial resolution was superior (**paper II**) to a more conventional spatial resolution. Cortical finger activation was found in 69%

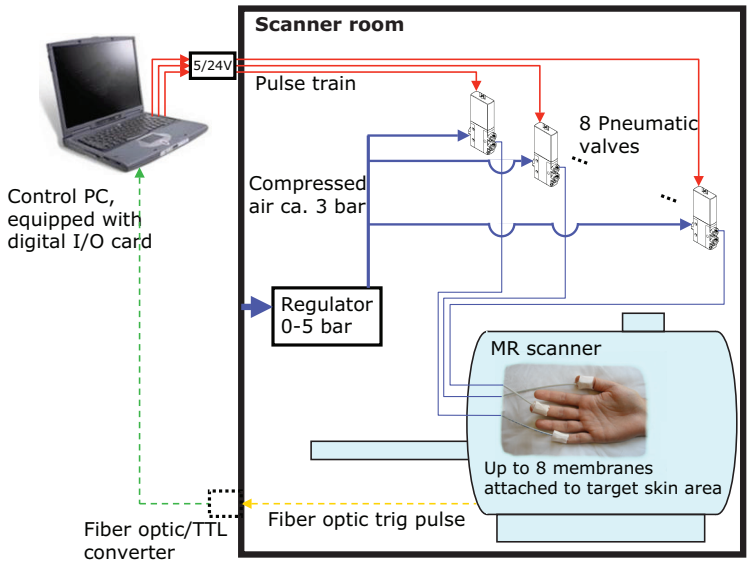

*Figure 2.7 - Schematic view of the tactile stimulation system. Eight membranes deliver individual tactile stimulation via computer controlled pneumatic valves. (**Paper II**)*

of the cases using 2^3 mm^3 compared to 57% using 3^3 mm^3. In fact cortical activation of the little finger was absent on group level for 3^3 mm^3 (figure 2.8). One explanation for the high resolution supremacy in this case could be that the experiment was performed using an eight channel coil, ensuring sufficient SNR despite the small voxel volume. Another explanation may be that the actual CNR was not as poor as initially assumed.

The short and long-term reproducibility of the S1 finger activation was also evaluated. Although complex methods for measuring the test-retest reliability in fMRI exists (Genovese, et al. 1997; Noll, et al. 1997) we merely compared the localisation, strength and volume of the BOLD activation over time for simplicity. One volunteer was scanned five consecutive days as well as two months after the initial experiment (**paper II**). The system showed remarkable reproducibility in localisation of the cortical regions (table 2.1 and figure 2.9) corresponding to different fingers (one standard deviation of the activated region centre-of-gravity was around 4 mm). The strength and extent of the BOLD activation varied more - properties which are known to be less reproducible (van Gelderen, et al. 2005) compared to localisation.

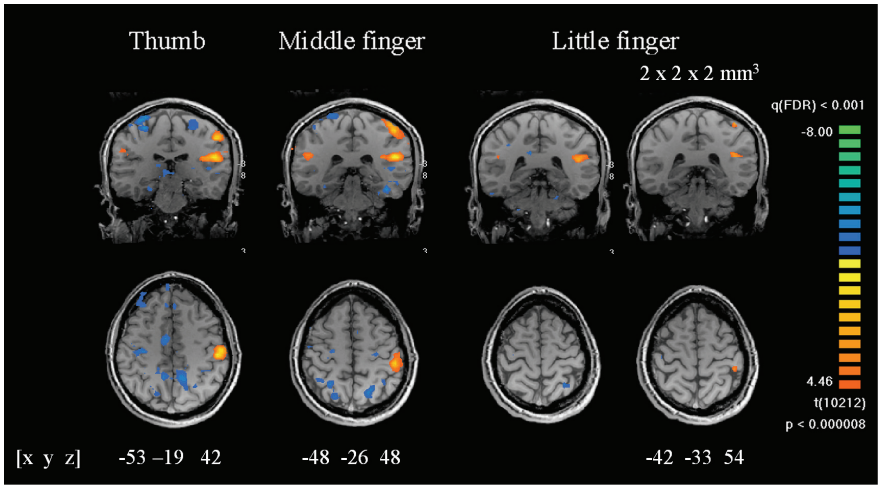

*Figure 2.8 - S1 and S2 activation during tactile stimulation of the thumb, middle and little finger. The results represent a group of 21 healthy volunteers. A separation of individual fingers according to the expected somatotopy in S1 can be seen. Interestingly, little finger activation was only found when increasing the spatial resolution to 2³ mm³. All other images here are acquired using 3³ mm³ spatial resolution. (**Paper II**)*

Table 2.1

Reproducibility of the centre-of-gravity and cluster sizes in a volunteer over two months.

Day	Thumb				Middle				Little			
	coordinates			cluster size	coordinates			cluster size	coordinates			cluster size
	x	y	z		x	y	z		x	y	z	
1	-50	-18	41	924	-43	-19	47	70	-42	-25	60	34
2	-51	-17	39	3552	-44	-20	49	4790	-42	-26	52	225
3	-52	-21	41	512	-44	-24	46	38	-43	-31	54	63
4	-54	-19	40	396	-44	-22	47	40**				
5	-48	-18	35	303	-43	-19	47	29	-42	-30	56	59**
66	-52	-18	42	1820	-44	-20	51	395*	-39	-27	55	1173
Mean	-51	-19	40	1251	-44	-21	48	1232	-42	-28	55	374
SD	2.0	1.4	2.5	1257	0.5	2.0	1.8	2372	1.5	2.6	3.0	539

*FDR < 0.05. * FDR < 0.01, ** FDR < 0.1. Co-ordinates* are given in Talairach space. 2 mm spatial *resolution and 4 mm smoothing kernel width are used. (**Paper II**)*

These results confirmed a sufficient sensitivity and reproducibility for tactile stimulation in clinical cohorts. Furthermore, we were convinced to use a relatively high spatial resolution in any subsequent project utilising tactile stimulation of the hand.

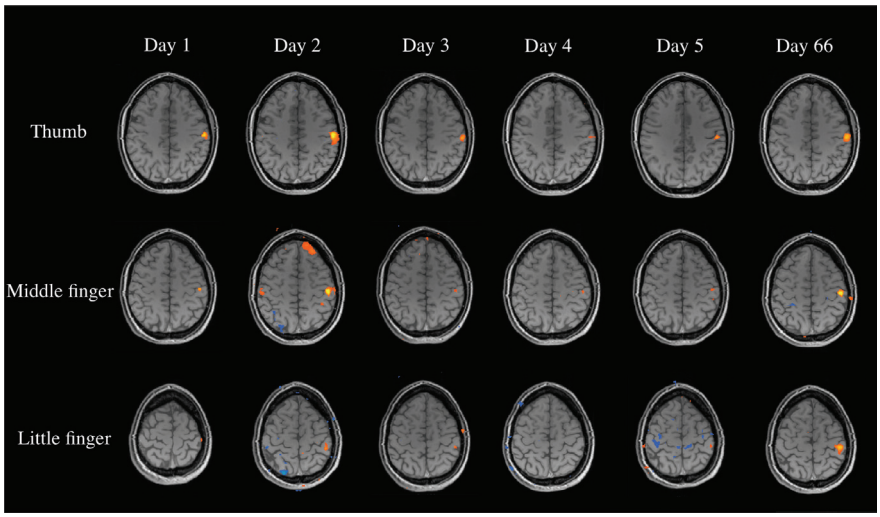

*Figure 2.9 - fMRI during tactile stimulation of the fingers was performed five consecutive days and two months after the initial scan in one volunteer. The localisation of the different fingers was highly reproducible. (**Paper II**)*

2.3.2 The choice of scan time

The most straightforward way to map any BOLD signal differences would naturally be to acquire one image volume during the active state and one image volume during the control state. However, this is not feasible for several reasons. First of all, the poor CNR necessitates signal averaging over a large number of time points to extract functional information. Moreover, as the scanner is susceptible to electronic drifts and shot-to-shot instabilities, the signal baseline is not necessarily maintained. Acquiring a large number of sample volumes makes it possible to correct for these types of linear or low frequency drifts. The impact of scan duration on detection sensitivity has been studied theoretically as well as experimentally (Murphy, et al. 2007). Notably, the scan duration required was shown to be proportional to $tSNR^{-2}$, suggesting the tSNR to be critical for experiment outcome.

However, estimating the required scan time based on expected tSNR is a delicate task. The human brain is an exceptionally dynamic system with a continuously ongoing perception of the external environment. This heavy information input would likely cause a system overflow if the brain was not able to distinguish important information from less important. In fMRI this process could be referred to as habituation effects, fatigue or loss of attention and is seriously hampering the fMRI performance. These effects are presumably more harmful when performing long session experiments, suggesting that an increase in scan time may not result in an expected improvement. In fact, this effect was unintentionally found (**paper II**), where the detection sensitivity after five minutes of tactile stimulation was decreased by ~20% regardless of the spatial resolution used.

Unfortunately minimising these effects is elusive. Session time could be reduced without hampering the tSNR if a high temporal resolution is used. However, high temporal resolution is often achieved at the expense of spatial resolution, SNR (due to limited T1 relaxation) or coverage. Keeping the experiment short using a simple design and a limited number of hypotheses may ultimately be the best approach. In **paper III**, **IV** and **V** a limited coverage (superior half of the brain) was used to maximise the temporal resolution, and thus minimising the length of the session.

2.3.3 Smoothing

Spatial smoothing of the functional data is normally used to improve SNR and to ensure a Gaussian distributed error in the GLM (Worsley and Friston 1995). The strategies of how to apply smoothing and to what extent has, however, been an area of discussion (Parrish, et al. 2000; Scouten, et al. 2006; Triantafyllou, et al. 2006). The choice of smoothing kernel width could in the end affect the resulting data considerably.

By smoothing the functional data it is possible to increase tSNR when the SNR is poor. However, when highly localised and spatially limited activation is expected, such as when mapping the cortical hand somatotopy, smoothing may critically deteriorate detection sensitivity (Geissler, et al. 2005). For example, sensory activation of the thumb, middle and little finger was found in one subject using little or no smoothing, but when applying a smoothing kernel size of 8 mm on the exact same data set, the activation of all fingers vanished (**paper II** ; figure 2.10).

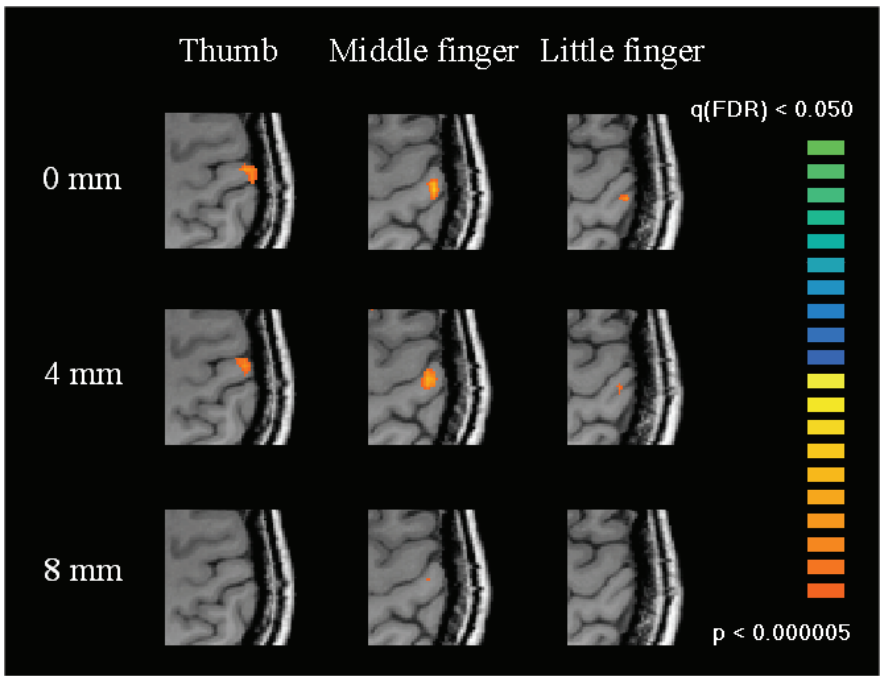

*Figure 2.10 - The potential negative effect of smoothing is illustrated. The choice of smoothing kernel widths can severely affect the resulting activation map although the exact same image set is used. Here, the use of an eight mm kernel (~2.5 times the voxel size) almost entirely erase the actual activation present. (**Paper II**)*

On the other hand smoothing may increase the number of FP activated voxels in situations where the original CNR is sufficient. This could also in part be due to the inclusion of draining veins or adjacent activation regions, ultimately decreasing the fMRI performance as FP increases (**paper I**). Evaluation of data sets after a commonly used smoothing kernel width (2.5 times the voxel side) shows a subtle increase in performance, but mainly in cases of poor CNR (figure 2.11 b). However, when the CNR is high, the choice of voxel volume is even more crucial, which is seen as a steeper decrease in performance at increasing voxel volumes compared to the unsmoothed data (figure 2.11 a).

Interestingly, Triantafyllou et al. (2006) showed that smoothing may improve SNR without affecting the magnitude of the physiological noise. This suggests that a high-resolution experiment could be beneficial even

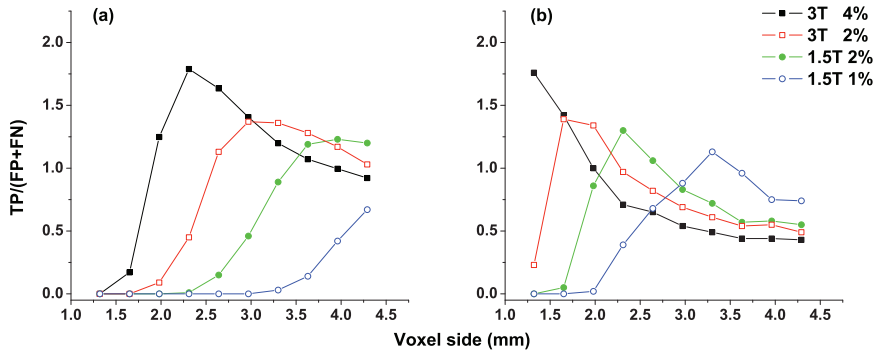

*Figure 2.11 - a) figure 2.6 for comparison (unsmoothed data), b) smoothed data. Smoothing (in this case ~2.5 times the voxel size) clearly affects the fMRI performance and the optimal choice of voxel volume. Smoothing may increase the performance but only when the original SNR is poor. Thus, in cases of high CNR, smoothing is only advisable when the voxel volume is very small. (**Paper I**)*

though a lower resolution is sufficient to answer a specific hypothesis. This effect is potentially seen in situations of high CNR (solid and open squares in figure 2.11); Applying a 4 mm smoothing kernel of the data acquired at 1.6^3 mm^3 results in increased performance (figure 2.11 b) compared to non-smoothed data acquired at 4^3 mm^3 (figure 2.11 a). Because of the limitation of voxel sizes investigated ($< 4.5^3$ mm^3) this effect is not seen in situations of poor CNR (solid and open circles), however it can still be anticipated.

Thus, choosing smoothing kernel size based on the voxel size, as commonly advised within the fMRI community, is clearly not a suitable solution (figure 2.11 b). In fact, the results presented in **paper I** suggest that the optimal magnitude of smoothing is highly dependent on the experiment CNR rather than the actual voxel size. By evaluating fMRI performance using various degrees of smoothing it was demonstrated that the optimal size of the smoothing kernel, normalised to voxel size, is highly dependent on CNR (figure 2.12). At CNR approximately larger than 1, smoothing kernel widths of the same magnitude as the voxel size (i.e. unsmoothed data in practice) maximised the performance. This suggests that the use of little or no smoothing is advantageous when the CNR is high.

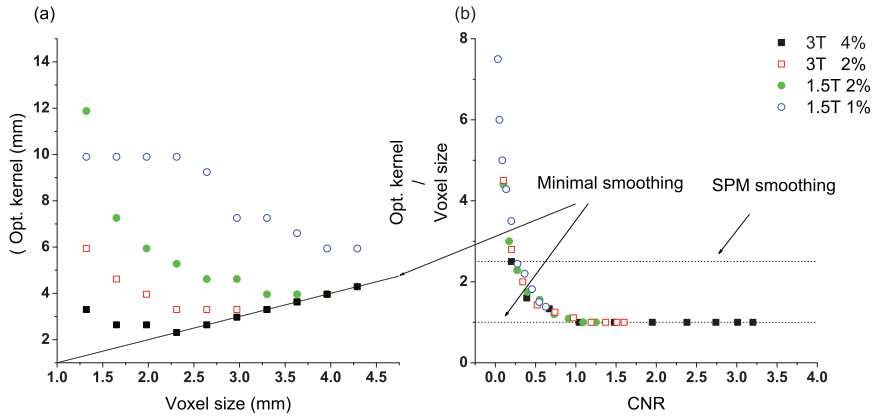

*Figure 2.12 - The need for smoothing is intimately coupled to the CNR (b) rather than to the voxel size (a). When the CNR is approximately larger than 1, little or no smoothing is preferable. (**Paper I**)*

3 Representation and reorganisation of the hand in somatosensory cortex

The world around us is perceived through our senses. We continuously receive and process a huge amount of information through our detection systems. Although connected to each other in a complex way, each detection system is independently functioning and related information is processed in separate regions of the brain. The structure of these cortical regions are further differentiated according to the detailed functionality of each such region. In the parietal lobe of the brain, where sensory stimulation is processed, a detailed map of the body exists that corresponds to the vast number of peripheral receptive fields of the body surface. This so called somatotopic map is not permanent. On the contrary, it is continuously changing due to experience and learning. This map may also change in response to an altered sensory input or in response to neuropathy. Knowledge of these processes may improve rehabilitation of patients where such changes exists (e.g. limb amputees, dystonia or neuropathy) (Lundborg 2003; Lundborg 2004).

In this chapter the cortical somatotopy of the human hand is initially overviewed and related to our results of mapping the hand in primary somatosensory cortex (S1). Subsequently, in *section 3.2.1*, the underlying mechanisms of cortical plasticity is briefly discussed. Plastic effects of S1 are studied by fMRI in three cohorts where reorganisational effects during sensory stimulation are hypothesised due to a cortical shift or re-routing of afferent nerve impulses: (i) In volunteers during cutaneous anaesthesia of the forearm (*section 3.2.2*), (ii) in hand amputees (*section 3.2.3*) and (iii) in subjects suffering from long-term exposure to vibrating tools (*section 3.2.4*). Here, evidence of cortical plasticity in all these cohorts by using fMRI are presented (**paper III, IV** and **V**). These results were achieved by utilising the optimised procedure for S1 mapping, presented in *section 2.2* and *section 2.3*.

3.1 Representation of the hand in S1

As first sensed by peripheral mechanoreceptors in the skin, touch sensation reaches the brain via the spinal cord. After synapsing in the thalamus the signal is projected to the contralateral S1 in the post central gyrus. This

results in a reversed somatosensory map where touch sensation in the right hand is predominantly processed in the left S1 and *vice versa*.

S1 contains four different areas, defined by their cytoarchitecture, namely Brodmann´s areas 1, 2, 3a and 3b (figure 3.1). The majority of the thalamic neurones project their axons to area 3a and 3b situated along the anterior bank of the post central gyrus. In turn, neurones in these areas project to area 1, situated in the most lateral part, and area 2, situated on the posterior bank, of the post central gyrus. Additionally, the right and left somatosensory cortex are interconnected through the *corpus callosum*. In turn, all these areas project to the higher-order secondary somatosensory cortex (S2), located on the superior bank of the lateral fissure, and associal areas in posterior parietal cortex (Purves, et al. 2004).

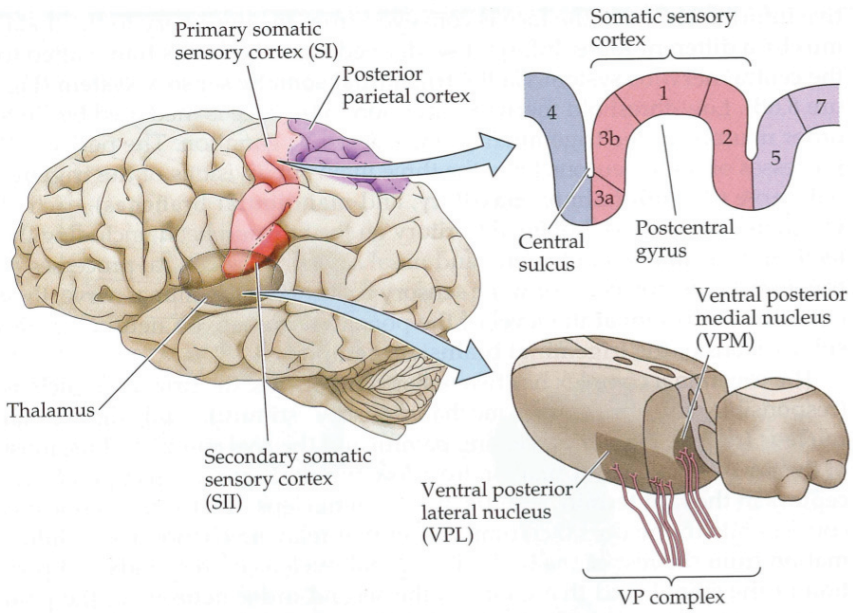

Figure 3.1 - Sensory information from the body surface is projected via the spinal cord and the thalamus to Brodmann's areas 1, 2, 3a and 3b of the primary somatosensory cortex (S1). S1 is bilaterally situated in the post central cortex, adjacent to the primary motor cortex in the pre central cortex and associal sensory cortex in the posterior parietal lobe. Illustrations from Purves et al., Neuroscience, third ed. Sinauer Associates, Inc.

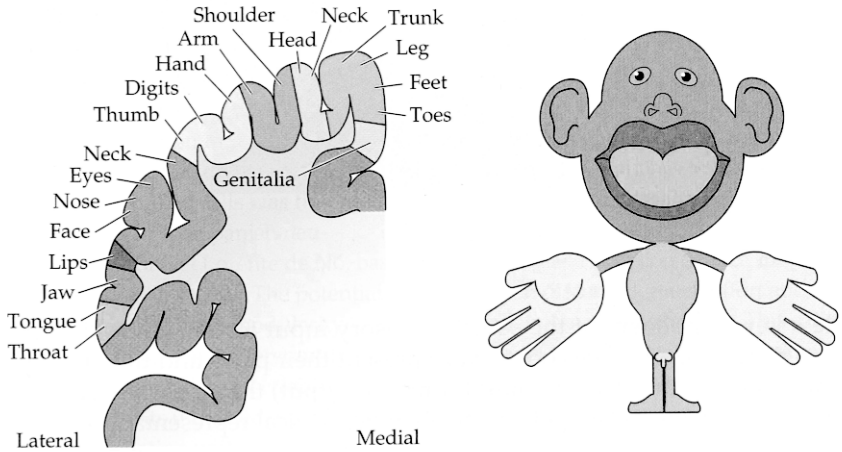

Figure 3.2 - S1 contains a complete map of the body surface. However, the map does not reflect the size of the body surface but rather the innervation density of the skin. Body regions of outstanding sensory function, such as the face and the hand, are thus unproportionally large in the cortex reflecting massive neural resources. This cortical representation of the body surface is commonly referred to as the homonculus. Illustrations from Purves et al., Neuroscience, third ed. Sinauer Associates, Inc.

Each of the four regions of the S1 contains a complete map of the body surface (Penfield and Boldrey 1937) (figure 3.2). This somatotopic map does not represent the body in its actual physical proportion. Instead each part of the body is represented in the brain in proportion to its relative significance to sensory perception. In fact, the map reflects the innervation density of the skin (Kandel, et al. 2000), suggesting that a large number of neurones result in an overall better sensitivity in that part of the body. Body parts with exquisite sensitivity, such as the hand and lips, are represented by the largest areas in S1 (figure 3.2) (Maldjian, et al. 1999; Stippich, et al. 1999), where the cortical grey matter mass per peripheral surface area is about 100 times larger compared to the abdomen (Kandel, et al. 2000).

Although the hand is represented by a comparably large area of S1, the distances between different fingers are only a few mm and the distance between the thumb and the little finger is approximately 20 mm (**paper II**). In order to map this detailed somatotopy, a computer controlled apparatus for tactile stimulation was used (see *section 2.3.1*). Preference for high-

resolution acquisition and limited smoothing was also concluded (see *section 2.2.4* and *section 2.3.3*).

Overall, the activation cluster localisation for the separate fingers corresponded well to the expected organisation in SI, i.e. the thumb, middle finger, and little finger were organised in an anterior-to-posterior, inferior-to-superior and, lateral-to-medial manner. The mean co-ordinates for the thumb, middle and little finger are shown in table 3.1. Although activation in area 3b is predominantly seen during tactile stimulation, activation in other areas is seen occasionally (figure 3.3).

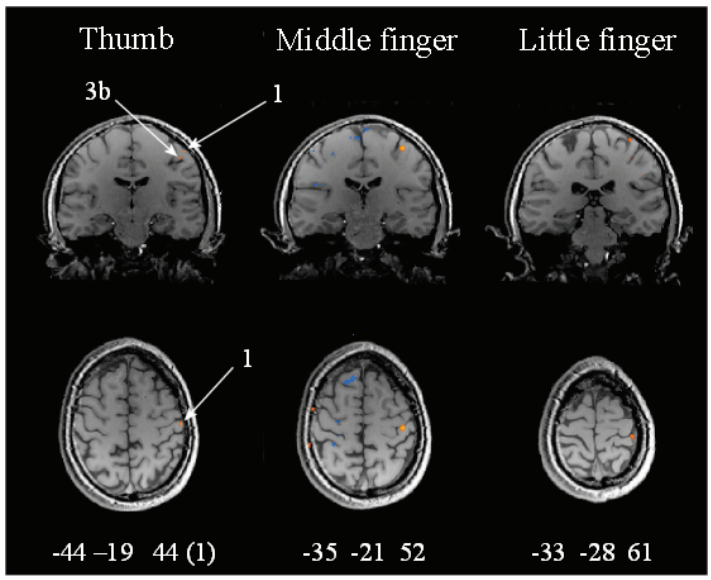

*Figure 3.3 - Tactile stimulation is often seen in S1 area 3b. In this subject additional activation on the crown of the post central gyrus (area 1) can be seen. (**Paper II**)*

Table 3.1

Individual Talairach co-ordinates at 2^3 mm^3 spatial resolution

Subject	Thumb				Middle finger				Little finger			
	Coordinates			Cluster size	Coordinates			Cluster size	Coordinates			Cluster size
	x	*y*	*z*		*x*	*y*	*z*		*x*	*y*	*z*	
1	-57	-16	37	<10**	-	-	-	0	-	-	-	0
2	-50	-19	46	218	-	-	-	0	-	-	-	0
3	-	-	-	0	-	-	-	0	-	-	-	0
4	-44	-19	44	15	-35	-21	52	146	-33	-28	61	27
5	-48	-13	49	<10**	-49	-25	50	614*	-42	-22	52	<10
6	-53	-20	42	55	-48	-29	52	<10**	-	-	-	0
7	-53	-15	43	<10**	-48	-23	52	185*	-42	-29	55	<10
8	-56	-22	44	418	-47	-31	52	54	-45	-29	51	616
9	-47	-21	41	595	-44	-25	48	356*	-42	-31	50	114*
10	-46	-14	46	472	-43	-24	53	153*	-35	-27	57	132
11	-	-	-	0	-	-	-	0	-	-	-	0
13	-53	-24	41	21	-	-	-	0	-	-	-	0
14	-49	-18	49	153	-	-	-	0	-37	-26	58	165**
15	-	-	-	0	-	-	-	0	-	-	-	0
16	-47	-28	42	42	-39	-26	53	34*	-40	-34	50	102*
17	-53	-17	41	1018	-49	-29	44	248*	-42	-31	46	47
18	-49	-16	44	877*	-	-	-	0	-	-	-	0
20	-52	-20	47	27	-	-	-	0	-	-	-	0
Mean	-50	-19	44		-45	-26	51		-40	-29	53	
S.D.	3.8	4.0	3.3		4.9	3.2	3.0		3.9	3.4	4.7	

*FDR < 0.05. * FDR < 0.01, ** FDR < 0.1. Volunteer 12, 19 and 21 are not included due to stimuli failure (volunteer 12) or compliance issues (volunteer 19 and 21). (**Paper II**)*

3.2 Brain plasticity

3.2.1 Synaptic and organisational mechanisms

The early brain development of the embryo is a product of genetic instructions and cell signalling and is thus activity independent. During this time neural circuits are abundantly established. As the brain mature these circuits are modified by patterns of neural activation, thus largely affected by incoming signals. In this way the functional systems of the brain develop under a strong influence of the surrounding environment admitting the brain to adapt to better respond to the demands from the outside world. This capacity to adapt is generally known as brain plasticity - a process closely associated to the concepts of experience, learning, conditioning and ability to store information. Although the majority of these processes are considered to become less effective in the adult brain, they persist throughout life in order to learn new skills or to store memories. Moreover, in situations where the perception of the outside world changes due to neural injury or pathology, brain plasticity may play an important role.

There is considerable evidence for plastic changes taking place in the mature synapse as moderation of the synapse strength. Depending on the underlying molecular alterations or potential changes in gene expression this moderation can be very short-lived or last for years (Kandel, et al. 2000). However, Merzenich et al. (1983) suggested that cortical reorganisation of existing functional networks also play a vital role. After section of the median nerve, i.e. silencing the cortical areas corresponding to the glabrous skin of the thumb, index and middle finger, these cortical areas momentarily responded to stimulation of the dorsal side of these fingers (normally covered by the radial nerve). Since this cortical ”unmasking” was seen immediately after nerve section, they concluded that the unmasked signal pathway must be present but heavily suppressed during normal circumstances. This second set of underlying pathway is suggested to exist in topographical areas of temporal firing pattern correlations, e.g. sensation of different fingers during grasp (Merzenich, et al. 1984). In this case these plastic changes are predominantly due to short-term reorganisation of existing networks rather than moderation of synapse strength. However, if this state persists, formerly suppressed axon tracts may be strengthened over time due to long-term synaptic alterations. Thus, the extension of these initially unmasked areas may increase over time.

This underlying circuitry may be detected in typical experiments, e.g. the experiment described in **paper II**. Here, stimulation of each finger did render slightly elevated activation in the cortical area corresponding to the other two fingers (figure 3.4). This could be due to such an underlying connection.

Although the molecular mechanisms of plasticity cannot be investigated using fMRI, the ability to monitor functional changes following plastic effects in S1 is promising. For example, long-term plasticity effects in S1 of chronic stroke patients was studied by Schaechter et al. (2006). In these patients an increased cortical thickness and functional activation of S1 areas were presented and suggested to originate from improved sensorimotor hand function. Short-term reorganisational effects due to immediate unmasking have also been observed in a few amputees (Borsook, et al. 1998; Grusser, et al. 2004).

In the following three sections, plastic changes due to reorganisation of existing networks and possibly long-term synaptic strengthening are examined in three cohorts where such effects are hypothesised. Although these plastic changes are by simplicity measured in S1, plasticity may also exist at sub cortical levels, such as in the thalamus and spinal cord.

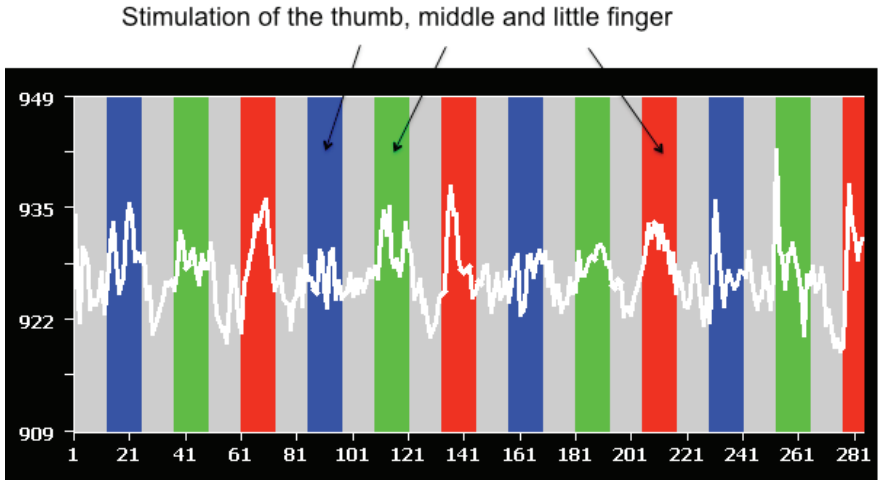

Figure 3.4 - An fMRI experiment showing the mean signal in the cortical region corresponding to the little finger (stimulation during the period in red). Clearly this region is activated during stimulation of the thumb (blue) and middle finger (green) as well, indicating substantial communication within these regions. Potentially, these second order connections can be unmasked if the direct path is restricted.

3.2.2 Cortical reorganisation of the hand following cutaneous anaesthesia of the forearm

Recently it was demonstrated that an inhibition of afferent nerve impulses from the forearm using cutaneous anaesthesia was improving sensory functions of the hand (Bjorkman, et al. 2004; Rosen, et al. 2006). The responsible mechanism was suggested to be a short-term cortical reorganisation resulting in more nerve cells supplying the hand. This guided plasticity is promising for promoting and improving weakened or lost sensory function (Muellbacher, et al. 2002). Intrigued by the robust and reproducible S1 activation presented in *section 2.3* (**paper II**), we wanted to confirm such cortical reorganisation during anaesthesia. Hypothetically, this silencing of forearm signals to S1 would thus lead to a reorganisation of adjacent cortical regions (see *section 3.2.1*), such as the hand.

Figure 3.5 - An anaesthetic cream was applied on the volar surface of the forearm to temporarily hinder sensation information from this region to reach S1.

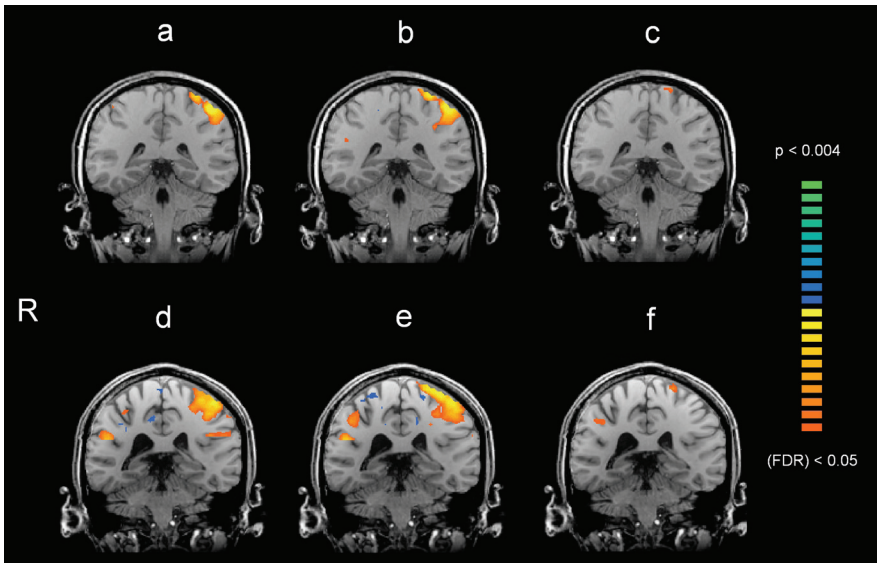

*Figure 3.6 - S1 activation after tactile stimulation of the right hand fingers in two volunteers before (a and d) and after (b and e) applying an anaesthetic cream to the forearm. Cortical activation expands cranially and medially after subcutaneous anaesthesia, thus including the cortical forearm region. The expansion is more clearly visualised by statistically comparing b to a (c) and e to d (f). (**Paper III**)*

To accomplish this, cutaneous sensation of the right volar forearm was temporarily inhibited in ten healthy volunteers, using an anaesthetic cream (figure 3.5). Tactile stimulation of the five right hand fingers was then examined using fMRI directly prior to and after 80 minutes of anaesthesia (**paper III**). Functional changes were subsequently correlated to potential improvements of the sensory function. It was shown that the cortical area representing the five fingers of the right hand expanded cranially, medially and posteriorly after forearm anaesthesia, suggesting an immediate reorganisation of receptive field inputs corresponding to the fingers, terminating in the forearm cortical area.

S1 activation during tactile stimulation was clearly apparent in all volunteers (see figure 3.6 a and d for two volunteers). The cortical finger representation expanded according to figure 3.6 b and e following forearm anaesthesia. In six out of ten subjects this functional reorganisation was statistically significant ($p < 0.004$; figure 3.6 c and f). Significantly increased activation was also seen in other regions, e.g. ipsi-lateral S1, posterior cingulate gyrus and superior parietal lobe, however, these activation clusters were less significant and smaller than 100 mm^3. Functional differences in the forearm region was also statistically significant in the group evaluation (FDR < 0.05), corresponding to the Talairach co-ordinates (-19, -33, 63). The sensory function of the hand was clinically tested by measuring the touch thresholds and two-point discrimination (the minimal distance between two points that can be distinguished and perceived as two) of the index and little finger.

The four volunteers that most clearly showed an expansion of finger activation into cortical forearm regions also improved finger sensitivity measured by tactile discrimination (marked by * in table 3.2). Such a plastic recruitment of neural resources could thus be coupled to improved functionality of cortically adjacent regions. A cortical expansion was not seen in all subjects. This could be due to the rather small cortical region corresponding to the forearm. In cases where nerve impulses from the hand are lost, a more pronounced fMRI effect is expected.

Table 3.2

Clinical improvement after EMLA® application in terms of tactile discrimination in tip of digit II and V and corresponding activation extension to cortical forearm regions

Subject	**Clinical improvement (2PD)**		**Significant activation**
	In percent and in mm (pre and post treatment raw data)		**of the forearm area**
			post/pre EMLA®
			contrast
	Digit II	Digit V	
6	39 (3.1-1.9)	48 (3.1-1.6)	
1	24 (2.5-1.9)	44 (3.4-1.9)	*
8	29 (3.1-2.2)	35 (3.4-2.2)	*
9	38 (1.6-1.0)	14 (2.2-1.9)	
5	11 (2.8-2.5)	38 (5.0-3.1)	***
3	24 (2.5-1.9)	24 (2.5-1.9)	*
7	36 (2.4-1.6)	11 (2.8-2.5)	
10	12 (2.5-2.2)	10 (3.1-2.8)	*
2	0 (2.5-2.5)	0 (2.8-2.8)	**
4	0 (2.5-2.5)	-14 (2.2-2.5)	

*Significant activation expansion to the forearm area in the S1 was seen in six subjects. *FDR < 0.05; ** p < 0.001, *** ipsilateral activation p < 0.001. The presented results are sorted by the best clinical improvement. (**Paper III**)*

3.2.3 Phantom hand somatotopy

After observing reorganisational effects following forearm anaesthesia we wanted to investigate whether any long-term reorganisations could be monitored in patients suffering from chronic blockage of afferent nerve impulses. This was performed in six unilateral hand amputees (**paper IV**). In these patients no neural connection between the hand and brain had been present for in average 12 years [range: 2 - 25].

Interestingly, these patients may experience phantom sensations of various fingers on the amputation stump, a feature that opens a promising approach for developing sensory feed-back in hand prostheses. The stump hand map could be explained by several mechanisms: Initially, an unmasking of underlying cortical pathways can explain such sensations in body parts which are cortically close to the hand (i.e. the face and forearm). Furthermore, the cut peripheral nerves undergo terminal swelling and regenerative sprouting following amputation, which may reinnervate stump skin regions. In this case the normal route for hand sensation is re-established and the cortical hand region is partly ”recaptured” (Bjorkman, et al. 2007) - a process not seen in the face hand-map. Variations in the reinnervation process could potentially explain the differences in the stump hand map.

The six patients in our study had a tactile finger map on the amputation stump, although in various degrees. These maps were individually outlined (figure 3.7) and subsequently used as receptive fields of phantom finger sensation in the fMRI experiment. The thumb, index and little finger map were outlined in all patients as well as three forearm control regions where no finger sensation was experienced.

Figure 3.7 - Forearm regions where the patient experienced sensation from the thumb, index and little finger are marked with I, II and V, respectively. Regions where no such finger sensation was perceived were marked as empty circles for control reasons.

Tactile stimulation was applied in nine regions: Three regions of the amputation stump, corresponding to thumb, index and little finger phantom sensation, three forearm regions with no such phantom finger sensation and finally the intact thumb, index and little finger of the opposite hand. The resulting cortical activation during stimulation of the phantom finger regions of the amputated stump was comparable to corresponding finger activation in a reference population of 20 healthy volunteers (figure 3.8).

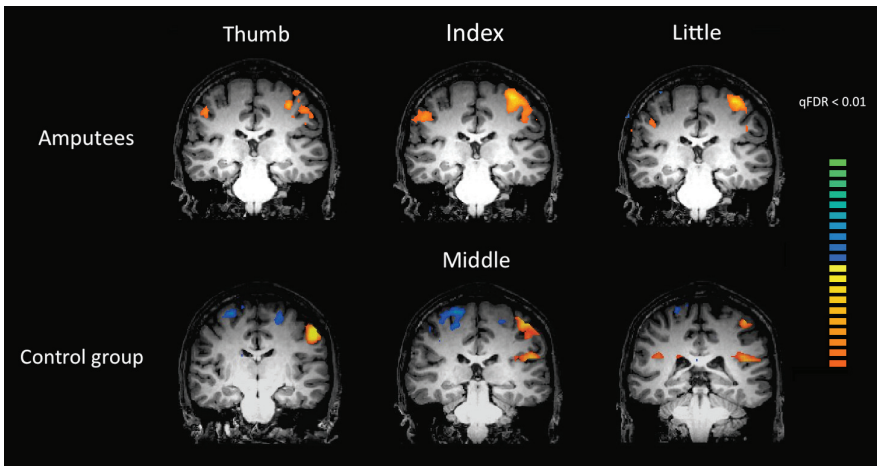

*Figure 3.8 - Tactile stimulation of the amputated stump skin regions corresponding to perceived sensation of the thumb, index and little finger in amputated hand patients (group results). Tactile stimulation of the right hand fingers in a control group are shown for comparison. (**Paper IV**)*

It is evident that stimulation of the amputated stump in these subjects activated cortical hand region. Furthermore, the location of the activated areas corresponded well to cortical finger representations of their healthy opposite hand (figure 3.9). However, activation of the amputated side was generally less distinct and the ipsilateral S1 was more robustly activated, suggesting an increased use of closely connected regions. Cortical activation corresponding to lost fingers was seen in three out of six subjects and after group evaluation. The contribution of nerve sprouting induced phantom sensation in these cases was unclear but could explain the large hand map diversity between subjects.

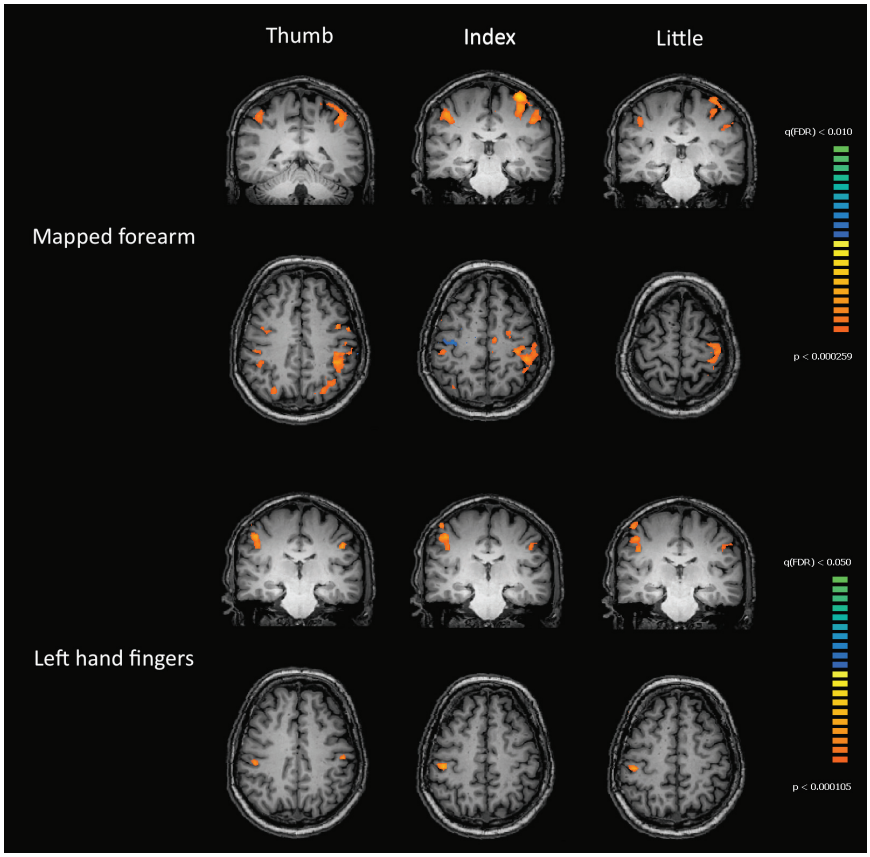

*Figure 3.9 - Cortical activation from tactile stimulation of the mapped amputated stump and the corresponding fingers of the healthy side. Stimulation of the amputated stump is activating cortical finger regions although activation is less distinct including more extensive ipsilateral activation. (**Paper IV**)*

An excellent phantom finger somatotopy of one patient is presented in figure 3.10. Stimulation of the forearm regions without phantom finger sensation did not result in focal activation or in most cases activation at all.

As the hand normally comprises a relatively large area of S1, a great loss of receptive fields potentially evokes a huge amount of neural resources. Resources which can be used momentarily by cortical reorganisation. Over time the original signalling route may be re-established as cut nerves may regenerate at the site of amputation leading to reinnervation of the forearm skin.

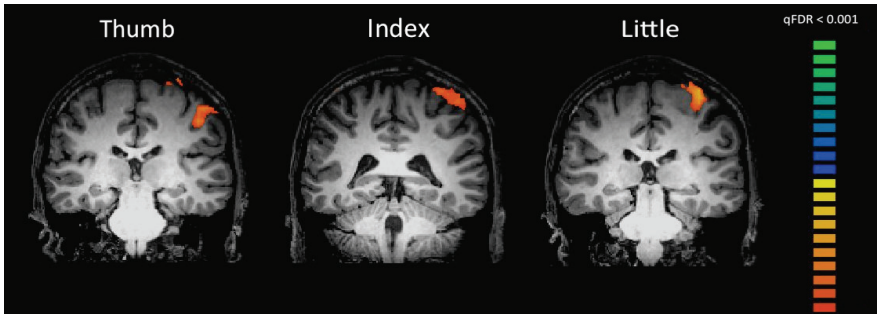

*Figure 3.10 - State-of-the-art activation during tactile stimulation of the mapped stump regions. A clear functional somatotopy corresponding to the thumb, index and little finger is seen. (**Paper IV**)*

3.2.4 Cortical expansion of the fingers in subjects suffering from long-term exposure to vibrating tools

It is well known that long-term exposure to vibrational hand-held tools could induce neurological symptoms, such as deteriorated sensory function, decreased fine motor ability and pain. These symptoms can in part be explained by injury to the peripheral nerve and mechanically induced muscle damage. However, central effects cannot be ruled out. Recently, Vidyasagar et al. (2009) showed cortical reorganisation of S1 after three hours of vibrotactile stimulation to the index and ring finger. Significant shifts of the cortical border areas of these two fingers were observed immediately following the vibrotactile stimulation, including an overlap of these regions and the cortical representation of the middle finger. Such plastic effects may in part explain symptoms seen in subjects suffering from vibration induced neuropathy. Knowledge of these processes can also improve existing treatment strategies.

To address this, reorganisation effects in S1 were studied in dental technicians who had been exposed to ~600 Hz hand vibration during 15 to 44 years (**paper V**). The subjects typically suffered from decreased finger sensitivity, fine motor ability and/or pain. Tactile stimulation of the thumb, middle and little finger was applied in these subjects and compared to a healthy control group. An increased overlap in cortical finger representations and a statistically significant ($p < 0.0005$) increase of activation in the regions corresponding to the thumb, middle and little finger

were found (figure 3.11). Furthermore, the activation volume was larger for all fingers in the group exposed to vibration, especially for the middle and little finger.

Similar cortical finger expansion has been presented before in musicians suffering from hand dystonia due to vigourous training (Elbert, et al. 1998). Indeed, strongly enhanced signalling pattern from vibrations may cause similar effects and eventually induce cortical deficits. Based on these reorganisations, individual rehabilitation programs may be custom designed.

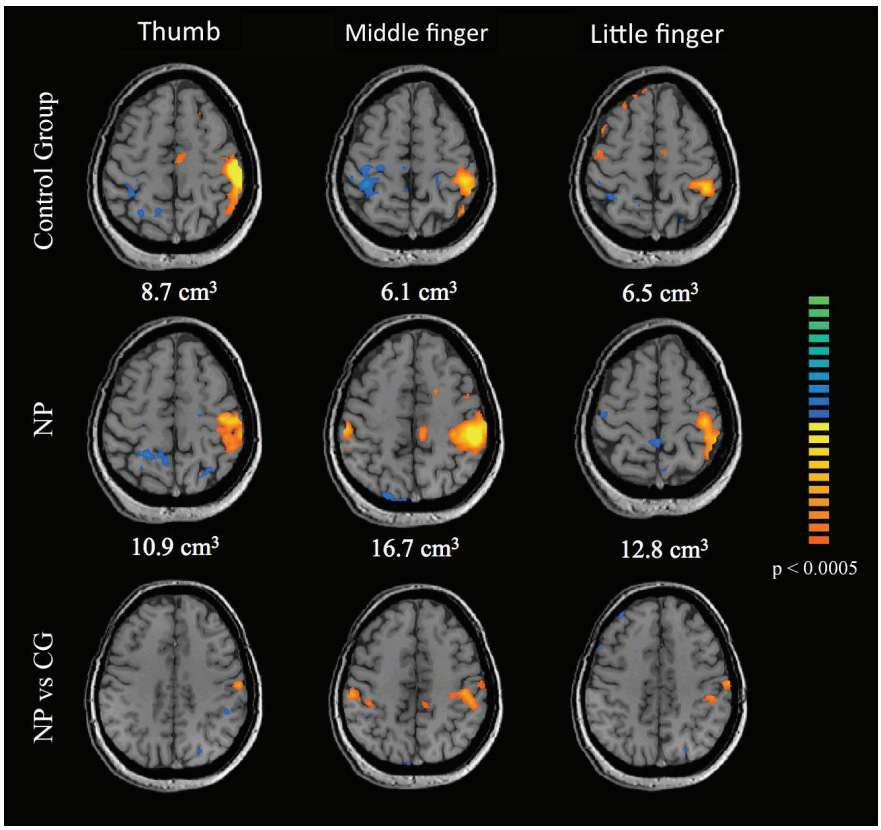

*Figure 3.11 - Tactile stimulation of patients suffering from neural pathology (NP) after long-term exposure to vibration, compared to a control group. An increased activation volume was seen in all fingers of NP subjects, suggesting that peripheral input may affect cortical function. (**Paper V**)*

4 fMRI of intrinsic brain activity

In conventional fMRI the normal approach is to compare functional images of a control state to functional images acquired during a specific task state. This type of experiment is generally referred to as task-based fMRI. However, 60-80% of the brain's energy budget is used to support intrinsic activity (Buzsaki, et al. 2007), i.e. activity not coupled to a specific task. In comparison, the energy burden from momentary demands may be as little as 0.5-1% of the total brain energy budget (Raichle and Mintun 2006). Thus, brain activity is mainly involving maintenance of information for interpreting, responding and predicting environmental demands (Raichle and Snyder 2007). This implies that most of our knowledge of brain function from fMRI is learned by studying a minor component of the brain function, i.e. reflexive responses to momentary demands. It is now possible to map brain function in absence of an external task by mapping functional brain regions of temporally correlated signal characteristics. These temporally correlated regions are commonly referred to as functional networks.

How well do these networks correspond to activation maps during task-based fMRI? Could such a network map potentially offer additional information when investigating plastic processes in the sensorimotor cortex? The first question is of interest when using fMRI for pre-surgical planning, i.e. mapping vital brain regions close to brain tumours (Vlieger, et al. 2004). In patients unable to perform tasks in a controlled manner (children or patients suffering from cognitive impairment or paresis), a task-free mapping method would be advantageous. The second question addresses the reorganisational effects investigated in this thesis. Are plastic changes restricted within each functional network or can these reorganisational effects cross functional boundaries?

In this chapter the properties of brain activity in absence of a task is discussed and how these properties can be used to map the sensorimotor cortex. Finally, in *section 4.2.3*, I address the first question by comparing the activation map from conventional task-based fMRI to the intrinsic network of the sensorimotor cortex (**paper VI**). The second question is not addressed in this thesis, however, it is considered important and will be investigated in the near future.

4.1 Intrinsic activity of the brain

4.1.1 Spontaneous neural firing

In the beginning of the 1990:s the introduction of BOLD fMRI resulted in an escalation of studies for mapping brain function. However, it was soon discovered that some regions of the brain showed negative signal responses in certain circumstances (Raichle, et al. 1994; Shulman, et al. 1997). This was a peculiar finding since the rest state was simply thought of as a baseline of neuronal activity. Using positron emission tomography (PET) it was quantitatively found that these regions had a decreased activity during goal directed tasks, rather than increased activity during rest (Raichle, et al. 2001). Such negative responses were consequently labelled "deactivations". The intrinsic brain activity was considered to be physiological fluctuations of the BOLD signal and was later named physiological noise (Kruger and Glover 2001). This noise included hemodynamic and CSF fluctuations, due to breathing and heart activity, as well as poorly characterised low-frequency fluctuations (< 0.1 Hz (Biswal, et al. 1995)). These fluctuations are roughly twice as large in grey matter compared to white matter (Bodurka, et al. 2005; Kruger and Glover 2001).

These low-frequency fluctuations are now assumed to reflect metabolic fluctuations due to spontaneous neuronal firing, a continuously ongoing neural process which was first investigated in the human brain some 50 years ago (Gerstein 1960). These processes are not likely induced from spontaneous behavior of the subject (e.g. day-dreaming) because of its presence throughout the whole brain (compared to task-based activity) and its consistency between different subjects. Furthermore, ongoing activation in form of spontaneous neural firing is present at all times, e.g during external stimulation (Fox and Raichle 2007), during anaesthesia (Vincent, et al. 2007) and also in the infant brain (Fransson, et al. 2007).

4.1.2 Functional networks

Biswal et al. (1995), who studied correlations of the BOLD response in sensorimotor regions in absence of a task, was the first to find signal correlations within the left and right primary motor cortex, including supplementary motor areas (SMA). Such correlations are now suggested to reflect considerable axonal connections revealing potential functional networks within the brain (Fox and Raichle 2007). Since then, several

functional networks have been found (Damoiseaux, et al. 2006; De Luca, et al. 2006). The functional network perhaps most frequently studied is the so called default network. The default network is unique in its responsiveness to cognitive tasks. Activation suppression during cognitive tasks cause the regional deactivations often encountered during task-based fMRI. Since these deactivations almost always include some specific regions of the brain, such as the ventral anterior and posterior cingulate cortex (Fransson 2005), the thought of a basal network, somehow connected to the underlying brain function has been suggested (Raichle, et al. 2001). This default network has been investigated by several groups (Biswal, et al. 1995; De Luca, et al. 2006; Fransson 2005), These networks have been studied in various types of neural dysfunctions, such as attention deficit hyperactivity disorder (ADHD) (Zang, et al. 2007) and Alzheimer's disease (Wang, et al. 2007).

4.2 Imaging strategies for mapping functional networks

The two most commonly used methods for mapping intrinsic networks are based on finding functional connectivity through signal correlations, although the specific approaches differ somewhat. Both methods have advantages and drawbacks. In order to more easily understand the experiment addressing the first question above, a short introduction to these imaging strategies for mapping connectivity is needed. It should be noted that the physiological "noise" from spontaneous neural firing is the signal of interest when mapping functional networks. Thus, a substantially larger voxel volume is used in this particular case to ensure a large contribution of physiological noise compared to thermal noise (see *section 2.2.2*). Preprocessing strategies which are commonly used in both intrinsic and task-based fMRI (see *section 2.1.5*) are not discussed in detail here.

4.2.1 Seed-based intrinsic fMRI

A correlation analysis to identify functional connectivity can be performed using time courses from so called seed regions. Seed regions are chosen based on an assumed functional relevancy to the network of interest. Thus, these regions can be chosen from anatomical information (e.g. pre-scanned images) or from functional information (e.g. task-based fMRI). The seed-based technique is limited to applications where there is an *a priori* expectation of an existing functional network.

In seed-based correlation analysis, the mean signal time course of the seed region is representing the temporal signal characteristic of interest, similar to what the modelled haemodynamic response is representing in task-based fMRI. This signal time course, or regressor, is then correlated to all other voxel time courses of the functional data in order to map regions of similar temporal BOLD response. However, the temporal BOLD response is generally contaminated as several potential noise sources are affecting the signal. These noise sources should be controlled to be able to avoid any non-neural correlations, such as head motion, CSF and brain tissue pulsations and global signal changes. This is typically done using head motion correction, correction for mean global signal and temporal filtering of the data to reject fluctuations outside the region of interest (i.e. above 0.1 Hz). Furthermore, potential physiological confounds may be modelled in the GLM by modelling additional regressors reflecting the signal time courses in the white matter and the ventricles (CSF) (Cordes, et al. 2000; Vincent, et al. 2006). Temporal characteristics originating from these sources can thus ultimately be rejected instead of included. Functional network maps are finally created based on a chosen correlation threshold.

4.2.2 Independent component analysis

When using independent component analysis (ICA) to find regional connectivity, neither seed regions nor the use of a hypothetical reference function are required. It is thus possible to characterise several types of fluctuations without the constraints of prior assumptions. On the other hand the resulting amount of data is often huge and it may be elusive to separate the underlying sources of information.

ICA is based on the assumption that neural signal time courses from different functional networks are independent and that acquired functional information is a mixture of these independent sources. In practice ICA works in a reversed fashion, splitting the acquired temporal information into statistically independent components, thus outlining different functional networks. Although the mathematical details are elaborate and an extensive presentation is beyond the scope of this thesis, the underlying principles are to separate components so that 1) independence between components is maximised, 2) complexity of the data is minimised (data from one single functional network is always less complex than data from several functional networks) and 3) minimise normality (data from one single functional

network is always less Gaussian than data from several functional networks). For a full tutorial, I recommend Stone (2004).

As multiple components are found, there is a need to determine the ones of interest. This could be a difficult task since components may be associated to not only spontaneous neural activity but also various noise components. Spontaneous fluctuations are certainly separated in frequency from non-neural haemodynamic noise sources, such as CSF and brain tissue pulsation. However, the temporal resolution of the acquired functional data is generally around 2 seconds and thus, signal fluctuations above 0.25 Hz cannot be accurately measured (according to the Nyquist-Shannon sampling theorem). This ultimately leads to temporal aliasing of higher frequency components, such as cardiac pulsation and respiration cycle (De Luca, et al. 2006), contaminating the low-frequency data if the EPI repetition time (TR) is not lowered. To better distinguish between different noise sources, an ICA "finger print technique" has been suggested (De Martino, et al. 2007). This method utilise the possibility to characterise the source components beyond their frequency components. Several additional component characteristics can be analysed, such as degree of clustering, skewness of the data, kurtosis and temporal and spatial entropy. As BOLD signals of neural origin typically has a high degree of clustering, skewness and entropy and low kurtosis it is possible to distinguish them from typical EPI artefacts, e.g. susceptibility effects, residual motion artefacts, vessel-induced BOLD signals or cardiac pulsations (De Martino, et al. 2007).

4.3 Comparing intrinsic network maps to task-based activation maps

How well do these networks correspond to activation maps during task-based fMRI? The consistency of functional brain networks has previously been evaluated using various approaches. For example, these networks have been shown to be consistent across healthy subjects (Damoiseaux, et al. 2006) and the intra subject test-retest precision using ICA was presented to be similar to conventional task-based methods (Nybakken, et al. 2002). Furthermore, ICA has proved to give results comparable to conventional fMRI when examining task-based data sets from auditory stimulation and language tasks (Quigley, et al. 2002) and from sensorimotor stimulation (Moritz, et al. 2000; Quigley, et al. 2002). Similar results have been presented for seed-based analysis (Quigley, et al. 2001).

However, in these studies information based on functional mapping prior to the experiment have been used, making such comparisons less useful in situations where no task-based information will be available (e.g. fMRI aided pre-surgical planning of patients unable to perform tasks). Recently, Kokkonen et al. (2009) compared intrinsic state data and finger-tapping data using ICA in patients with brain tumour, concluding that it was possible to localise sensorimotor areas from rest data using ICA without using any *a priori* acquired information. In the same manner, Liu et al. (2009) showed that activation maps from seed-based correlations was quite similar to both motor task activation and direct cortical stimulation in patients with tumour and epileptic foci close to the primary motor cortex. Unfortunately, these results were not evaluated using a quantitative approach making any comparisons difficult.

To fully cover the question asked, we wanted to contribute with a quantitative approach, using no a priori functional information (**paper VI**). The sensorimotor cortex was examined using seed-based analysis and ICA (fastICA) (Hyvarinen and Oja 2000) of rest data, according to *section 4.2.1 and 4.2.2*, and using finger tapping fMRI (motor and sensory stimulation). The intrinsic network maps found were individually compared to the task-based activation map utilising a quantitative definition of concurrence ratio (c ; Eq. 4.1), introduced by Quigley et al. (2001).

$$c = \frac{V_{ica,s} \cap V_t}{mean\,[V_{ica,s}, V_t]} \qquad \text{Eq. 4.1}$$

Here, V is the mapped volume using ICA (ica), seed-based analysis (s) and task-based fMRI (t). Thus if the mapped brain volumes (using different approaches) are largely shared, compared to the size of the maps, c will be large.

Ten subjects were included in the study and bilateral activation of the primary motor cortex and SMA were generally seen in all three methods. Although the motor networks found using ICA and seed-based correlation analysis were qualitatively comparable to the activated regions during the motor task, these areas were only partly overlapping in most subjects. This is shown in figure 4.1 and 4.2 where activation maps from task-based fMRI in blue, seed-based correlation analysis (figure 4.1) and ICA (figure 4.2) in yellow and their intersect in green are presented. This non-perfect correspondence is expected due to several reasons: Finger-tapping activates regions corresponding to the hand solely, while network maps likely include

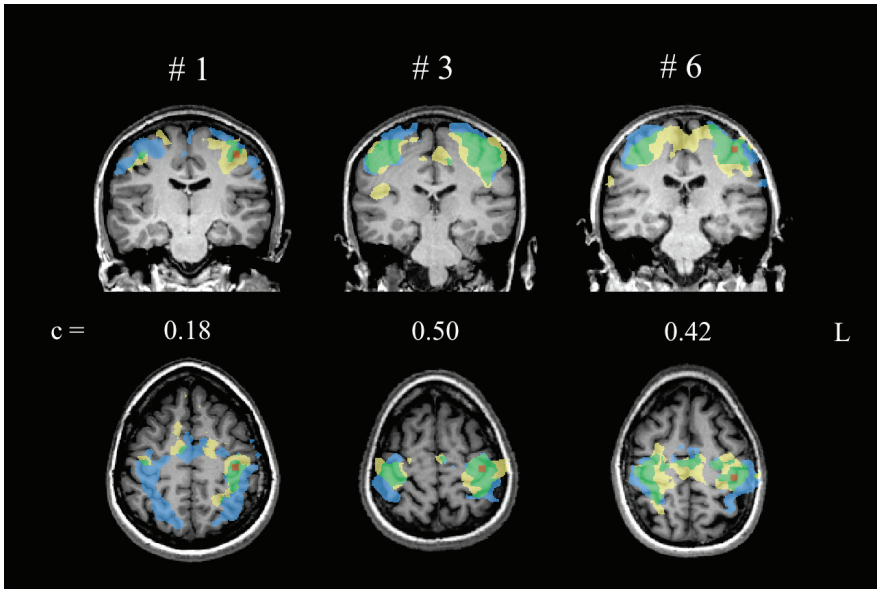

*Figure 4.1 - The intrinsic sensorimotor network found using a seed situated in the left pre central gyrus compared to bilateral motor-task fMRI. The intrinsic sensorimotor network is shown in yellow, the task-based activation is shown in blue and regions activated using both methods are shown in green. The seed region is shown in red. Corresponding concurrence ratios (c) for three representative subjects are shown. (**Paper VI**)*

functional regions corresponding to the whole body. These differences probably also reflect the methods inherently different sensitivity characteristics and noise susceptibility. Furthermore, the use of different statistics makes it difficult to choose specific thresholds. Finally, the extent and magnitude of all BOLD responses are continuously fluctuating from time to time. For example, the task-based map typically includes parietal activation such as the primary and secondary somatosensory cortex. In addition the posterior parietal cortex is intimately coupled to sensory initiation and guidance of movement of the performing hand (Kandel, et al. 2000). These regions were occasionally also mapped in ICA, perhaps due to inclusion of additional inseparable components of the network found, such as components of sensory basis, however, using the seed-based analysis these parietal regions were occasionally missed.

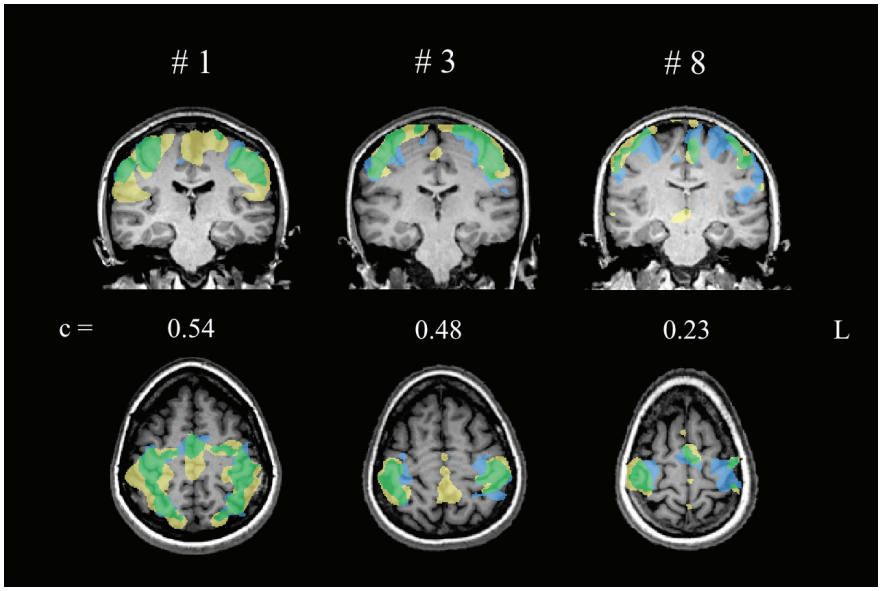

*Figure 4.2 - The intrinsic sensorimotor network found using ICA compared to bilateral motor-task fMRI. The component of interest was chosen based on two criteria: The component was largely situated around the central sulcus and the data characteristics suggested a neural origin (see section 4.2.2). The sensorimotor network is shown in yellow, the task-based activation is shown in blue and regions activated using both methods are shown in green. Corresponding concurrence ratios (c) for three representative subjects are shown. (**Paper VI**)*

When comparing the motor networks found using ICA to the bilateral motor task activation, an average c of 0.35 [0.19 - 0.54] was obtained. This could be compared to the slightly lower c of 0.26 [0.07 – 0.50] in the case of seed-based analysis. In general the maximal c were obtained at low to moderate statistical thresholds suggesting that the regions of most significant activation in the resulting ICA and seed-based maps overlapped poorly to the highly significant motor task activation. This proposes that lower statistical thresholds are preferable when using these alternative approaches, as the most strongly activated regions may not overlap at all.

Hence, both regional overlap and mismatches between intrinsic sensorimotor networks and conventional finger-tapping fMRI were found. Generally, the regions presenting highly pronounced activation differed substantially between techniques. Both seed-based analysis and ICA have

potential for intrinsic network mapping and both methods present similar concurrence ratios. Because of the huge amount of information received in ICA, potentially leading to difficulties when choosing components of interest, I recommend the seed-based method in situations where the warranted network is known. This generally applies in pre surgery planning of patients unable to perform tasks. This may also be the case when reorganisational effects in primary somatosensory cortex are to be studied.

5 Conclusions and future aspects

In this thesis, functional mapping of the primary somatosensory cortex (S1) using fMRI was investigated. fMRI performance in this region was evaluated in theory by modelling BOLD responses based on the underlying mechanisms of neural activation (**paper I**). Using a computer controlled apparatus for tactile stimulation, fMRI performance was further examined *in vivo* (**paper II**). In these studies, it was shown that both the optimal voxel volume and amount of smoothing applied are highly dependent on experiment's CNR. Furthermore, the use of robustly applied and computer controlled tactile stimulation ensured precise and reproducible finger activation. The results presented in these two papers encouraged us to continue and study plastic S1 reorganisation in subjects with sensory dysfunction.

Reorganisational effects due to brain plasticity in S1 were investigated in volunteers (**paper III**), in hand amputees (**paper IV**) and in subjects exposed to vibrating tools (**paper V**). Activation of the cortical forearm area was found during finger stimulation if the forearm skin surface was anaesthetised. This was coupled to a clinically improved sensory function, suggesting that an increased amount of neural resources was provided for the hand. Furthermore, phantom hand somatotopy was studied in hand amputees. It was shown that the cortical region corresponding to the missing hand was activated during tactile stimulation of specific areas of the amputated stump where phantom finger sensation was perceived. Finally, cortical activation of the hand area was proven to be increased and enlarged in subjects suffering from long-term exposure to vibration tools. Hence, evidence of reorganisational effects due to brain plasticity in S1 was seen in several types of sensory dysfunction using fMRI.

Recently proposed methods (ICA and seed-based approach) for mapping S1 in absence of a specific task were evaluated. The intrinsic network of sensorimotor cortex found using these techniques was quantitatively evaluated and compared to S1 activation during task-based fMRI (**paper VI**). The networks found were roughly overlapping the task-based activation map. However, supplementary information reflecting the whole somatotopic body region is retrieved, which may offer an additional view of plastic processes in this region.

For future projects in this field I suggest:

- Investigations of various acquisition and evaluation parameters in fMRI using the theoretical model presented here. For example, an evaluation of how to choose an appropriate statistical threshold in task-based fMRI, would be of great interest.

- Further development of a tactile stimulation system to increase fMRI sensitivity.

- Complementary studies of subjects suffering from neural disorders, such as diabetic feet patients and subjects exposed to long-term low-frequent vibrating tools.

- Examinations of reorganisational effects due to S1 plasticity in subjects suffering from neural hand disorders using intrinsic state network mapping.

6 Acknowledgements

This work was supported by grants from Lund University, Malmö University Hospital, the SMARThand EU-project (contract no NMP4-CT-2006-0033423) and the Swedish Council for Working Life and Social Sciences.

- - - - - - -

Jag skulle främst vilja tacka mina huvudhandledare, Jonas Svensson och Sören Mattsson. Jonas, även om du har låtit mig utforska mina egna idéer så har du alltid funnits som ett stöd när det har behövts som bäst. Våra diskussioner har varit givande och alltid fokuserade och effektiva. Du är noggrann och professionell - en riktig vetenskapsman! Sören, du har verkligen en förmåga att se möjligheter och vara positiv. Även om våra forskningsområden skiljer sig åt något har du alltid visat stort intresse för mig och min forskning. Du var även väldigt positiv när jag bestämde mig för att börja läsa medicin och därmed gå ner på halvtid.

Jag vill även tacka mina medarbetare på handkirurgen, Göran Lundborg, Birgitta Rosén och Anders Björkman. Er otroliga kunskap, förmåga att samarbeta och era intressanta idéer gjorde dessa år roligare och lättare. Jag är glad att våra vägar korsades och jag ser fram emot ett fortsatt samarbete!

Under åren har jag även haft glädjen att arbeta tillsammans med många andra duktiga människor. Särskilt tack till Karin Johansson, Ann-Cathrine Johansson, Håkan Brorson, Kasim, Pia och Pavel, Jonatan, Peter och Johan i Lund och Siegbert. Tack till Kjell, som tillsammans med Sören introducerade mig till forskarvärlden. Tack även till alla på Diagnostiskt Centrum och särskilt de på Neuroradiologen. Kramar till Lena och Eva på Sonatan och till Maria!

Det är verkligen roligt att arbeta med alla doktorandvänner och medarbetare på Medicinsk strålningsfysik, Radiofysik och i MR-gruppen. Tack till mina trevliga ”roomies”, Anna (master roomie), Marie och Marcus och till Helen för alla mysiga luncher - hoppas du trivs i Australien. Till mina vänner på läkarprogrammet - jag ser fram emot att bli er kollega.

Tack till alla mina släktingar, till familjerna Jannesson och Wickander och mina allra närmsta vänner (ni vet alla vem ni är). Ni betyder mycket för mig!

Till sist vill jag tacka min familj. Ingenting hade kunnat genomföras utan er. Caroline, mamma och pappa, mormor, Sarah och Mattias.

7 References

Bandettini PA, Jesmanowicz A, Wong EC, Hyde JS. 1993. Processing strategies for time-course data sets in functional MRI of the human brain. Magn Reson Med 30(2):161-73.

Bandettini PA, Wong EC, Hinks RS, Tikofsky RS, Hyde JS. 1992. Time course EPI of human brain function during task activation. Magn Reson Med 25(2):390-7.

Belliveau JW, Kennedy DN, Jr., McKinstry RC, Buchbinder BR, Weisskoff RM, Cohen MS, Vevea JM, Brady TJ, Rosen BR. 1991. Functional mapping of the human visual cortex by magnetic resonance imaging. Science 254(5032):716-9.

Benjamini Y, Hochberg Y. 1995. Controlling the False Discovery Rate: A Practical and Powerful Approach to Multiple Testing. Journal of the Royal Statistical Society 57(1):289-300.

Biswal B, Yetkin FZ, Haughton VM, Hyde JS. 1995. Functional connectivity in the motor cortex of resting human brain using echo-planar MRI. Magn Reson Med 34(4):537-41.

Bjorkman A, Rosen B, Lundborg G. 2004. Acute improvement of hand sensibility after selective ipsilateral cutaneous forearm anaesthesia. Eur J Neurosci 20(10):2733-6.

Bjorkman A, Waites A, Rosen B, Lundborg G, Larsson EM. 2007. Cortical sensory and motor response in a patient whose hand has been replanted: one-year follow up with functional magnetic resonance imaging. Scand J Plast Reconstr Surg Hand Surg 41(2):70-6.

Bodurka J, Ye F, Petridou N, Bandettini PA. Determination of the Brain Tissue-Specific Temporal Signal to Noise Limit of 3T BOLD-weighted Time Course Data; 2005; Miami, USA. p p. 1554.

Bodurka J, Ye F, Petridou N, Murphy K, Bandettini PA. 2007. Mapping the MRI voxel volume in which thermal noise matches physiological noise--implications for fMRI. Neuroimage 34(2):542-9.

Borsook D, Becerra L, Fishman S, Edwards A, Jennings CL, Stojanovic M, Papinicolas L, Ramachandran VS, Gonzalez RG, Breiter H. 1998. Acute plasticity in the human somatosensory cortex following amputation. Neuroreport 9(6):1013-7.

Buxton RB, Uludag K, Dubowitz DJ, Liu TT. 2004. Modeling the hemodynamic response to brain activation. Neuroimage 23 Suppl 1:S220-33.

Buzsaki G, Kaila K, Raichle M. 2007. Inhibition and brain work. Neuron 56(5):771-83.

Cordes D, Haughton VM, Arfanakis K, Wendt GJ, Turski PA, Moritz CH, Quigley MA, Meyerand ME. 2000. Mapping functionally related regions of brain with functional connectivity MR imaging. AJNR Am J Neuroradiol 21(9):1636-44.

Damoiseaux JS, Rombouts SA, Barkhof F, Scheltens P, Stam CJ, Smith SM, Beckmann CF. 2006. Consistent resting-state networks across healthy subjects. Proc Natl Acad Sci U S A 103(37):13848-53.

De Luca M, Beckmann CF, De Stefano N, Matthews PM, Smith SM. 2006. fMRI resting state networks define distinct modes of long-distance interactions in the human brain. Neuroimage 29(4):1359-67.

De Martino F, Gentile F, Esposito F, Balsi M, Di Salle F, Goebel R, Formisano E. 2007. Classification of fMRI independent components using IC-fingerprints and support vector machine classifiers. Neuroimage 34(1):177-94.

Desco M, Hernandez JA, Santos A, Brammer M. 2001. Multiresolution analysis in fMRI: sensitivity and specificity in the detection of brain activation. Hum Brain Mapp 14(1):16-27.

Edelstein WA, Glover GH, Hardy CJ, Redington RW. 1986. The intrinsic signal-to-noise ratio in NMR imaging. Magn Reson Med 3(4): 604-18.

Elbert T, Candia V, Altenmuller E, Rau H, Sterr A, Rockstroh B, Pantev C, Taub E. 1998. Alteration of digital representations in somatosensory cortex in focal hand dystonia. Neuroreport 9(16):3571-5.

Elbert T, Rockstroh B. 2004. Reorganization of human cerebral cortex: the range of changes following use and injury. Neuroscientist 10(2): 129-41.

Firbank MJ, Coulthard A, Harrison RM, Williams ED. 1999. Partial volume effects in MRI studies of multiple sclerosis. Magn Reson Imaging 17(4):593-601.

Fox MD, Raichle ME. 2007. Spontaneous fluctuations in brain activity observed with functional magnetic resonance imaging. Nat Rev Neurosci 8(9):700-11.

Fransson P. 2005. Spontaneous low-frequency BOLD signal fluctuations: an fMRI investigation of the resting-state default mode of brain function hypothesis. Hum Brain Mapp 26(1):15-29.

Fransson P, Skiold B, Horsch S, Nordell A, Blennow M, Lagercrantz H, Aden U. 2007. Resting-state networks in the infant brain. Proc Natl Acad Sci U S A 104(39):15531-6.

Friston K, Holmes AP, Worsley KP, Poline J, D. FC, Frackowiak RS. 1995. Statistical parametric maps in functional imaging: a general linear approach. Hum Brain Mapp 2:189-210.

Geissler A, Lanzenberger R, Barth M, Tahamtan AR, Milakara D, Gartus A, Beisteiner R. 2005. Influence of fMRI smoothing procedures on replicability of fine scale motor localization. Neuroimage 24(2): 323-31.

Genovese CR, Noll DC, Eddy WF. 1997. Estimating test-retest reliability in functional MR imaging. I: Statistical methodology. Magn Reson Med 38(3):497-507.

Gerstein GL. 1960. Analysis of Firing Pafferns in Single Neurons. Science 131(3416):1811-1812.

Geyer S, Schleicher A, Zilles K. 1999. Areas 3a, 3b, and 1 of human primary somatosensory cortex. Neuroimage 10(1):63-83.

Grusser SM, Muhlnickel W, Schaefer M, Villringer K, Christmann C, Koeppe C, Flor H. 2004. Remote activation of referred phantom sensation and cortical reorganization in human upper extremity amputees. Exp Brain Res 154(1):97-102.

Gudbjartsson H, Patz S. 1995. The Rician distribution of noisy MRI data. Magn Reson Med 34(6):910-4.

Hansson T, Brismar T. 1999. Tactile stimulation of the hand causes bilateral cortical activation: a functional magnetic resonance study in humans. Neurosci Lett 271(1):29-32.

Henkelman RM. 1985. Measurement of signal intensities in the presence of noise in MR images. Med Phys 12(2):232-3.

Hlushchuk Y, Hari R. 2006. Transient suppression of ipsilateral primary somatosensory cortex during tactile finger stimulation. J Neurosci 26(21):5819-24.

Hoogenraad FG, Pouwels PJ, Hofman MB, Reichenbach JR, Sprenger M, Haacke EM. 2001. Quantitative differentiation between BOLD models in fMRI. Magn Reson Med 45(2):233-46.

Hyde JS, Biswal BB, Jesmanowicz A. 2001. High-resolution fMRI using multislice partial k-space GR-EPI with cubic voxels. Magn Reson Med 46(1):114-25.

Hyvarinen A, Oja E. 2000. Independent component analysis: algorithms and applications. Neural Netw 13(4-5):411-30.

Kandel ER, Schwartz JH, Jessell TM, editors. 2000. Principles of neural science. 4 ed: McGraw-Hill.

Kim DS, Ronen I, Olman C, Kim SG, Ugurbil K, Toth LJ. 2004. Spatial relationship between neuronal activity and BOLD functional MRI. Neuroimage 21(3):876-85.

Kokkonen S-M, Nikkinen J, Remes J, Kantola J, TStarck T, Haapea M, Tuominen J, Tervonen O, Kiviniemi V. 2009. Preoperative localization of the sensorimotor area using independent

component analysis of resting-state fMRI Magnetic Resonance Imaging.
Korvenoja A, Kirveskari E, Aronen HJ, Avikainen S, Brander A, Huttunen J, Ilmoniemi RJ, Jaaskelainen JE, Kovala T, Makela JP and others. 2006. Sensorimotor cortex localization: comparison of magnetoencephalography, functional MR imaging, and intraoperative cortical mapping. Radiology 241(1):213-22.
Kruger G, Glover GH. 2001. Physiological noise in oxygenation-sensitive magnetic resonance imaging. Magn Reson Med 46(4):631-7.
Kurth R, Villringer K, Mackert BM, Schwiemann J, Braun J, Curio G, Villringer A, Wolf KJ. 1998. fMRI assessment of somatotopy in human Brodmann area 3b by electrical finger stimulation. Neuroreport 9(2):207-12.
Kwong KK, Belliveau JW, Chesler DA, Goldberg IE, Weisskoff RM, Poncelet BP, Kennedy DN, Hoppel BE, Cohen MS, Turner R and others. 1992. Dynamic magnetic resonance imaging of human brain activity during primary sensory stimulation. Proc Natl Acad Sci U S A 89(12):5675-9.
Lauterbur PC. 1973. Image Formation by Induced Local Interactions: Examples of Employing Nuclear Magnetic Resonance. Nature 242:190-191.
Liu H, Buckner RL, Talukdar T, Tanaka N, Madsen JR, Stufflebeam SM. 2009. Task-free presurgical mapping using functional magnetic resonance imaging intrinsic activity. J Neurosurg.
Logothetis NK, Pauls J, Augath M, Trinath T, Oeltermann A. 2001. Neurophysiological investigation of the basis of the fMRI signal. Nature 412(6843):150-7.
Logothetis NK, Pfeuffer J. 2004. On the nature of the BOLD fMRI contrast mechanism. Magn Reson Imaging 22(10):1517-31.
Lundborg G. 2003. Richard P. Bunge memorial lecture. Nerve injury and repair--a challenge to the plastic brain. J Peripher Nerv Syst 8(4): 209-26.
Lundborg G, editor. 2004. Nerve injury and repair. Regeneration, reconstruction and cortical remodelling. 2nd ed ed. Philadelphia: Elsevier.
Maldjian JA, Gottschalk A, Patel RS, Detre JA, Alsop DC. 1999. The sensory somatotopic map of the human hand demonstrated at 4 Tesla. Neuroimage 10(1):55-62.
Mansfield P. 1977. Multiplanar image formation using NMR spin echoes. J Phys C 10:55-58.
Merzenich MM, Kaas JH, Wall JT, Sur M, Nelson RJ, Felleman DJ. 1983. Progression of change following median nerve section in the

cortical representation of the hand in areas 3b and 1 in adult owl and squirrel monkeys. Neuroscience 10(3):639-65.

Merzenich MM, Nelson RJ, Stryker MP, Cynader MS, Schoppmann A, Zook JM. 1984. Somatosensory cortical map changes following digit amputation in adult monkeys. J Comp Neurol 224(4):591-605.

Moritz CH, Haughton VM, Cordes D, Quigley M, Meyerand ME. 2000. Whole-brain functional MR imaging activation from a finger-tapping task examined with independent component analysis. AJNR Am J Neuroradiol 21(9):1629-35.

Muellbacher W, Richards C, Ziemann U, Wittenberg G, Weltz D, Boroojerdi B, Cohen L, Hallett M. 2002. Improving hand function in chronic stroke. Arch Neurol 59(8):1278-82.

Murphy K, Bodurka J, Bandettini PA. 2007. How long to scan? The relationship between fMRI temporal signal to noise ratio and necessary scan duration. Neuroimage 34(2):565-74.

Noll DC, Genovese CR, Nystrom LE, Vazquez AL, Forman SD, Eddy WF, Cohen JD. 1997. Estimating test-retest reliability in functional MR imaging. II: Application to motor and cognitive activation studies. Magn Reson Med 38(3):508-17.

Norris DG. 2006. Principles of magnetic resonance assessment of brain function. J Magn Reson Imaging 23(6):794-807.

Nybakken GE, Quigley MA, Moritz CH, Cordes D, Haughton VM, Meyerand ME. 2002. Test-retest precision of functional magnetic resonance imaging processed with independent component analysis. Neuroradiology 44(5):403-6.

Ogawa S, Tank DW, Menon R, Ellermann JM, Kim SG, Merkle H, Ugurbil K. 1992. Intrinsic signal changes accompanying sensory stimulation: functional brain mapping with magnetic resonance imaging. Proc Natl Acad Sci U S A 89(13):5951-5.

Parrish TB, Gitelman DR, LaBar KS, Mesulam MM. 2000. Impact of signal-to-noise on functional MRI. Magn Reson Med 44(6):925-32.

Pauling L, Coryell CD. 1936. The Magnetic Properties and Structure of Hemoglobin, Oxyhemoglobin and Carbonmonoxyhemoglobin. Proc Natl Acad Sci U S A 22(4):210-6.

Penfield W, Boldrey E. 1937. Somatic motor and sensory representation in the cerebral cortex of man as studied by electrical stimulation. Brain 60:389-443.

Purves D, Augustine GJ, Fitzpatrick D, Katz LC, LaMantia A, McNamara JO, editors. 2004. Neuroscience. Sunderland: Sinauer Associates, Inc. 147-163 p.

Quigley M, Cordes D, Wendt G, Turski P, Moritz C, Haughton V, Meyerand ME. 2001. Effect of focal and nonfocal cerebral lesions on functional connectivity studied with MR imaging. AJNR Am J Neuroradiol 22(2):294-300.

Quigley MA, Haughton VM, Carew J, Cordes D, Moritz CH, Meyerand ME. 2002. Comparison of independent component analysis and conventional hypothesis-driven analysis for clinical functional MR image processing. AJNR Am J Neuroradiol 23(1):49-58.

Raichle M, Mintun M. 2006. Brain work and brain imaging. Annu. Rev. Neurosci. 29:449-476.

Raichle ME, Fiez JA, Videen TO, MacLeod AM, Pardo JV, Fox PT, Petersen SE. 1994. Practice-related changes in human brain functional anatomy during nonmotor learning. Cereb Cortex 4(1): 8-26.

Raichle ME, MacLeod AM, Snyder AZ, Powers WJ, Gusnard DA, Shulman GL. 2001. A default mode of brain function. Proc Natl Acad Sci U S A 98(2):676-82.

Raichle ME, Snyder AZ. 2007. A default mode of brain function: a brief history of an evolving idea. Neuroimage 37(4):1083-90; discussion 1097-9.

Rosen B, Bjorkman A, Lundborg G. 2006. Improved sensory relearning after nerve repair induced by selective temporary anaesthesia - a new concept in hand rehabilitation. J Hand Surg Br 31(2):126-32.

Schaechter JD, Moore CI, Connell BD, Rosen BR, Dijkhuizen RM. 2006. Structural and functional plasticity in the somatosensory cortex of chronic stroke patients. Brain 129(Pt 10):2722-33.

Scouten A, Papademetris X, Constable RT. 2006. Spatial resolution, signal-to-noise ratio, and smoothing in multi-subject functional MRI studies. Neuroimage 30(3):787-93.

Shulman GL, Fiez JA, al. e. 1997. Common blood flow changes across visual tasks: II. Deacreses in cerebral cortex. J. Cogn. Neurosci. 9(5):648-663.

Stark CE, Squire LR. 2001. When zero is not zero: the problem of ambiguous baseline conditions in fMRI. Proc Natl Acad Sci U S A 98(22):12760-6.

Stippich C, Hofmann R, Kapfer D, Hempel E, Heiland S, Jansen O, Sartor K. 1999. Somatotopic mapping of the human primary somatosensory cortex by fully automated tactile stimulation using functional magnetic resonance imaging. Neurosci Lett 277(1):25-8.

Stone JV. 2004. Independent component analysis - A tutorial introduction. London: The MIT press.

Talairach J. TP. 1988. Co-planar stereotaxic atlas of the Human Brain: 3-Dimensional Proportional System: An approach to Cerebral Imaging. Thieme Medical, New York.

Thulborn KR, Waterton JC, Matthews PM, Radda GK. 1982. Oxygenation dependence of the transverse relaxation time of water protons in whole blood at high field. Biochim Biophys Acta 714(2):265-70.

Triantafyllou C, Hoge RD, Krueger G, Wiggins CJ, Potthast A, Wiggins GC, Wald LL. 2005. Comparison of physiological noise at 1.5 T, 3 T and 7 T and optimization of fMRI acquisition parameters. Neuroimage 26(1):243-50.

Triantafyllou C, Hoge RD, Wald LL. 2006. Effect of spatial smoothing on physiological noise in high-resolution fMRI. Neuroimage 32(2): 551-7.

Turner R, Howseman A, Rees GE, Josephs O, Friston K. 1998. Functional magnetic resonance imaging of the human brain: data acquisition and analysis. Exp Brain Res 123(1-2):5-12.

Wall JT, Xu J, Wang X. 2002. Human brain plasticity: an emerging view of the multiple substrates and mechanisms that cause cortical changes and related sensory dysfunctions after injuries of sensory inputs from the body. Brain Res Brain Res Rev 39(2-3):181-215.

van der Zwaag W, Francis S, Head K, Peters A, Gowland P, Morris P, Bowtell R. 2009. fMRI at 1.5, 3 and 7 T: characterising BOLD signal changes. Neuroimage 47(4):1425-34.

van Gelderen P, C WHW, de Zwart JA, Cohen L, Hallett M, Duyn JH. 2005. Resolution and reproducibility of BOLD and perfusion functional MRI at 3.0 Tesla. Magn Reson Med 54(3):569-76.

van Westen D, Fransson P, Olsrud J, Rosen B, Lundborg G, Larsson EM. 2004. Fingersomatotopy in area 3b: an fMRI-study. BMC Neurosci 5:28.

Wang K, Liang M, Wang L, Tian L, Zhang X, Li K, Jiang T. 2007. Altered functional connectivity in early Alzheimer's disease: a resting-state fMRI study. Hum Brain Mapp 28(10):967-78.

Vidyasagar R, Parkes L. An FMRI Study of Induced Plasticity in S1 in the Human Brain; 2009; Honolulu.

Wienbruch C, Candia V, Svensson J, Kleiser R, Kollias SS. 2006. A portable and low-cost fMRI compatible pneumatic system for the investigation of the somatosensensory system in clinical and research environments. Neurosci Lett 398(3):183-8.

Vincent JL, Patel GH, Fox MD, Snyder AZ, Baker JT, Van Essen DC, Zempel JM, Snyder LH, Corbetta M, Raichle ME. 2007. Intrinsic

functional architecture in the anaesthetized monkey brain. Nature 447(7140):83-6.

Vincent JL, Snyder AZ, Fox MD, Shannon BJ, Andrews JR, Raichle ME, Buckner RL. 2006. Coherent spontaneous activity identifies a hippocampal-parietal memory network. J Neurophysiol 96(6): 3517-31.

Vlieger EJ, Majoie CB, Leenstra S, Den Heeten GJ. 2004. Functional magnetic resonance imaging for neurosurgical planning in neurooncology. Eur Radiol 14(7):1143-53.

Worsley KJ, Friston KJ. 1995. Analysis of fMRI time-series revisited--again. Neuroimage 2(3):173-81.

Yacoub E, Shmuel A, Pfeuffer J, Van De Moortele PF, Adriany G, Andersen P, Vaughan JT, Merkle H, Ugurbil K, Hu X. 2001. Imaging brain function in humans at 7 Tesla. Magn Reson Med 45(4):588-94.

Zang YF, He Y, Zhu CZ, Cao QJ, Sui MQ, Liang M, Tian LX, Jiang TZ, Wang YF. 2007. Altered baseline brain activity in children with ADHD revealed by resting-state functional MRI. Brain Dev 29(2): 83-91.

Zijdenbos AP, Dawant BM. 1994. Brain segmentation and white matter lesion detection in MR images. Crit Rev Biomed Eng 22(5-6): 401-65.

Paper I

ELSEVIER

NeuroImage

www.elsevier.com/locate/ynimg
NeuroImage 41 (2008) 346–353

Investigation of spatial resolution, partial volume effects and smoothing in functional MRI using artificial 3D time series

A. Weibull,[a,*] H. Gustavsson,[a,b] S. Mattsson,[a] and J. Svensson[a]

[a]*Department of Medical Radiation Physics, Lund University, SE-205 02 Malmö, Sweden*
[b]*Siemens Medical Solutions, Malmö, Sweden*

Received 3 July 2007; revised 20 December 2007; accepted 11 February 2008
Available online 10 March 2008

This work addresses the balance between temporal signal-to-noise ratio (tSNR) and partial volume effects (PVE) in functional magnetic resonance imaging (fMRI) and investigates the impact of the choice of spatial resolution and smoothing. In fMRI, since physiological time courses are monitored, tSNR is of greater importance than image SNR. Improving SNR by an increase in voxel volume may be of negligible benefit when physiological fluctuations dominate the noise. Furthermore, at large voxel volumes, PVE are more pronounced, leading to an overall loss in performance. Artificial fMRI time series, based on high-resolution anatomical data, were used to simulate BOLD activation in a controlled manner. The performance was subsequently quantified as a measure of how well the resulted activation matched the simulated activation. The performance was highly dependent on the spatial resolution. At high contrast-to-noise ratio (CNR), the optimal voxel volume was small, i.e. in the region of 2^3 mm^3. It was also shown that using a substantially larger voxel volume in this case could potentially negate the CNR benefits. The optimal smoothing kernel width was dependent on the CNR, being larger at poor CNR. At CNR > 1, little or no smoothing proved advantageous. The use of artificial time series gave an opportunity to quantitatively investigate the effects of partial volume and smoothing in single subject fMRI. It was shown that a proper choice of spatial resolution and smoothing kernel width is important for fMRI performance.
© 2008 Elsevier Inc. All rights reserved.

Introduction

In functional magnetic resonance imaging (fMRI), the resulting activation map is a statistical map of hemodynamic response originating from neuronal activity. The hemodynamic responses can be monitored by acquiring blood oxygen level dependent (BOLD) contrast weighted MR-images (Bandettini et al., 1992; Kwong et al., 1992; Ogawa et al., 1992). The BOLD effect is generally small compared to the noise level in fMRI (Turner et al., 1998), suggesting that a low spatial resolution of the functional image should be used in order to increase the signal-to-noise ratio (SNR). Furthermore, the fMRI technique requires high temporal resolution, which generally necessitates a relatively poor spatial resolution, i.e. 3^3 mm^3 or lower. The large voxel volume often used makes fMRI prone to partial volume effects (PVE) that may be critical when mapping brain regions with a well-defined and detailed functional topography, e.g. somatosensory (Geyer et al., 1999) and motor cortex (Geissler et al., 2005).

Spatial smoothing of the functional data is normally used to further improve SNR and to ensure a Gaussian distributed error in the general linear model (GLM) (Worsley and Friston, 1995). The strategies of how to apply smoothing and to what extent has, however, been an area of discussion (Scouten et al., 2006; Triantafyllou et al., 2006; Parrish et al., 2000). The choice of spatial resolution and smoothing kernel width is expected to affect the obtained data in several ways.

Since the statistical inferences in fMRI are based on signal variations over time, the temporal SNR (tSNR) is of primary importance. tSNR is not only dependent on thermal noise but also on hemodynamic and metabolic fluctuations, referred to as physiological noise (Biswal et al., 1995; Hyde et al., 2001; Kruger and Glover, 2001), predominantly seen in gray matter (GM) and cerebrospinal fluid (CSF) (Bodurka et al., 2005). Although the origin of physiological noise is not fully understood, Kruger and Glover (2001) suggest that it demonstrates a dependence of signal strength, in contrast to thermal noise, which is mainly determined by coil loading. It has been shown that, regardless of an increase in signal-to-noise ratio, accomplished by increasing the magnetic field strength, using multichannel coils or lowering the spatial resolution, the tSNR tends to reach a plateau, where further SNR improvement is of negligible benefit (Triantafyllou et al., 2005).

The impact of tSNR at various BOLD contrasts has been studied recently (Murphy et al., 2007). Since the spatial resolution generally is poor, it is also important to investigate the combined impact of tSNR and PVE in an fMRI experiment. This is a delicate task since in vivo studies lack the opportunity to assess a quantitative measure of

* Corresponding author. Fax: +46 40 963185.
E-mail address: andreas.weibull@med.lu.se (A. Weibull).
Available online on ScienceDirect (www.sciencedirect.com).

1053-8119/$ - see front matter © 2008 Elsevier Inc. All rights reserved.
doi:10.1016/j.neuroimage.2008.02.015

performance as the size and localization of activation in the human brain are unknown. Although several studies regarding the impact of functional resolution and spatial localization in fMRI exist (Korvenoja et al., 2006; Scouten et al., 2006; Bodurka et al., 2007), PVE are often not considered. PVE have, however, thoroughly been investigated in other MR applications as volumetric lesion estimations (Firbank et al., 1999) and brain tissue segmentation (Zijdenbos and Dawant, 1994). For fMRI, one group used a modeled activation response to investigate the impact of different spatial resolutions in various multiresolution wavelet approaches (Desco et al., 2001). In this way it was possible to know the true activation a priori, but this model did not account for physiological noise. Also, only one type of tissue was assumed throughout the whole brain.

The purpose of this study is to investigate how the choice of spatial resolution and smoothing kernel width affects the performance in single-subject fMRI. We present a model based on a high-resolution anatomical template that simulates artificial fMRI time series under the influence of temporal signal to noise and partial volume effects. The model is used to examine fMRI performance over a broad range of spatial resolutions, using different smoothing kernel widths.

Materials and methods

Creation of artificial time series

High-resolution (0.33^3 mm^3) cryosectional photographs of a representative female cadaver (The National Library of Medicine's Visible Human Project, http://www.nlm.nih.gov) were used as a basic anatomical map of the human brain. One hundred images were used to represent a $75\times75\times33$ mm^3 volume of the cerebrum. The images were segmented into white matter (WM), GM, and CSF volumes using signal thresholding. The contrast in the images was altered to resemble echo-planar imaging (EPI) contrast. Representative signal values for the different tissues were obtained from volunteer measurements at a whole body 3 T scanner (Siemens Medical Solutions, Erlangen, Germany) using an EPI BOLD sequence with TE/TR=30/2660 ms, bandwidth=2442 Hz/pixel and spatial resolution=3^3 mm^3. The measured signal levels for CSF, GM and WM were approximately 2900, 1900 and 1700, respectively. These values were magnified proportionally to avoid any quantum noise effects in the further processing of the data.

The 3D volume was replicated into 4×12 "rest" and 4×12 "active" volumes in order to create a block designed artificial fMRI time series. Within the active volumes, activation was created as a signal increase in the GM in a selected ellipsoid-shaped region (hereafter referred to as true activation), using typical BOLD contrasts, see section Contrast-to-noise ratio. The spatial scale, where the hemodynamic responses correlate to neuronal activity, is a few millimeters (Kim et al., 2004; Ugurbil et al., 2003). Thus, to more accurately model the spatial extension of the hemodynamic response due to neural activity, a 3 mm diameter sphere was used to spatially dilate the activation. However, activation was always constricted to tissue regions (i.e. not dilated into CSF). Activated regions were simulated in the region of primary somatosensory and motor cortex.

Modeling and applying noise

In MR BOLD imaging, several sources of undesired signal variances may occur. In this study only the thermal noise and the physiological noise were included in the model. Furthermore, the term SNR refers to the image signal-to-noise ratio (i.e. signal divided by the standard deviation of the thermal noise), while tSNR includes additional temporal noise originating from physiological fluctuations. The investigation of intersubject variability and motion-induced noise was beyond the scope of this study, and shot-to-shot electronic instabilities were neglected since they only comprise a small fraction of the in vivo time series noise (Triantafyllou et al., 2005).

It has been shown that thermal noise in a magnitude MR image is Rician distributed (Gudbjartsson and Patz, 1995). This distribution arises from Gaussian distributed noise in the quadrature receiver of the MR system. Rician distributed noise can be modeled according to Eq. (1) where S is the noisy voxel signal, S_0 is the noise free signal and σ_R^2 and σ_I^2 are Gaussian distributed noise variances in the real and imaginary part of the quadrature receivers, respectively (Henkelman, 1985).

$$S = \sqrt{[S_0 + \sigma_R]^2 + \sigma_I^2} \tag{1}$$

To obtain a start value for σ_R^2 and σ_I^2, the standard deviation of the thermal noise was measured in a tissue-free region in the same head scans used to determine EPI-BOLD contrast (3^3 mm^3 voxel size) and corrected by a factor 0.655^{-1} to get the standard deviation $\sigma_R=\sigma_I$ of the intrinsic Gaussian distributed noise (Henkelman, 1985).

Image volumes with ten different spatial resolutions were then generated by resampling the high-resolution images into coarser voxel resolutions of 1.3^3, 1.7^3, 2.0^3, 2.4^3, 2.7^3, 3.0^3, 3.3^3, 3.6^3, 4.0^3 and 4.3^3 mm^3 (multiples of the original resolution of 0.33^3 mm^3). Each low-resolution voxel signal was thus calculated as the mean signal of the corresponding high-resolution voxels. Rician distributed noise was modeled using Eq. (1) and applied in the generated images of different resolutions so that the SNR was proportional to the voxel volume, using the measured SNR for 3^3 mm^3 voxel volume as a reference. Different resolutions were simulated keeping the field-of-view constant.

Physiological noise is typically signal fluctuations that are spatially and temporally correlated (Biswal et al., 1995). Noise due to metabolic fluctuations has a typical frequency below 0.1 Hz while breathing and heart activity induces colored noise at higher frequencies. However, these higher frequencies are often aliased in fMRI due to insufficient sampling speed and appear as lower frequency contributions below the Nyquist frequency (0.5 TR^{-1}=0.2 Hz in this case). The temporal standard deviation of the physiological noise has been shown to be proportional to the signal itself, λS, where the proportionality constant λ has been empirically determined to 0.011 in GM, 0.006 in WM (Kruger and Glover, 2001) and 0.021 in CSF (Bodurka et al., 2005). Furthermore, λ is comparable at different field strengths (Triantafyllou et al., 2005).

To model the temporal characteristics of the physiological noise, in vivo resting-state time series were used (the same head scans used to determine EPI-BOLD contrast). 3 T and 3^3 mm^3 voxel size were used to assure that the majority of the noise was physiological in its origin (Bodurka et al., 2007). 100 GM, 100 WM and 100 CSF voxel time series from different parts of the brain were chosen to represent a selection of different physiological time series. The time series were motion corrected (BrainVoyager), and their mean values were set to zero. Finally, the time series were low pass filtered using a

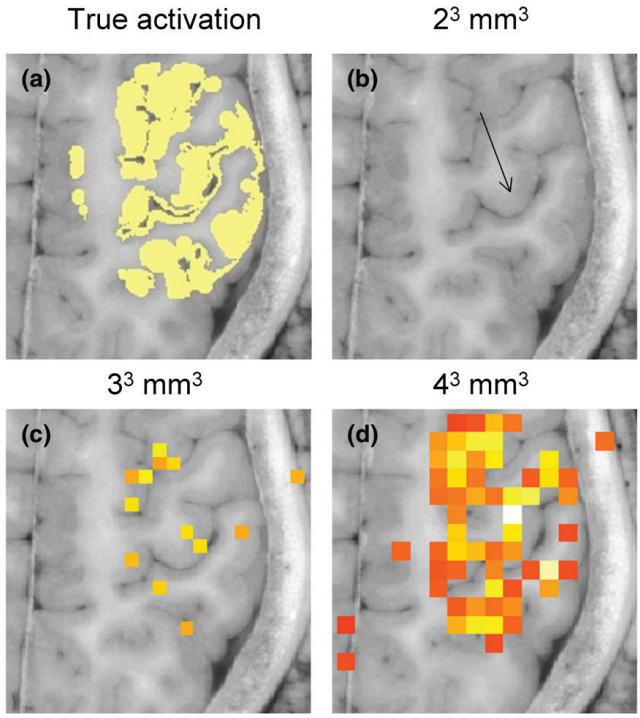

Fig. 1. 2D activation patterns from an unsmoothed data set (1.5 T and 2% activation contrast) on an anatomical background, i.e. cryosectional photographs of a representative female cadaver. The slice position was chosen so that the central sulcus (arrow), between motor cortex and primary somatosensory cortex, was visible. a) True high-resolution activation pattern, b–d) FDR-corrected statistical parametric maps $q(\mathrm{FDR}) < 0.05$. 2^3 mm^3, 3^3 mm^3 and 4^3 mm^3 spatial resolution, respectively.

Butterworth filter (cutoff=0.2 Hz) to minimize the thermal noise contribution. Subsequently, temporally correlated and tissue-specific physiological noise was applied, i.e. a random (out of 100) physiological time series was added to each voxel, and scaled to match λS.

Contrast-to-noise ratio

In fMRI, statistical inferences are based on signal changes, i.e. activation contrast, over time in a noisy environment, making the activation contrast-to-noise ratio (CNR) an important and interesting

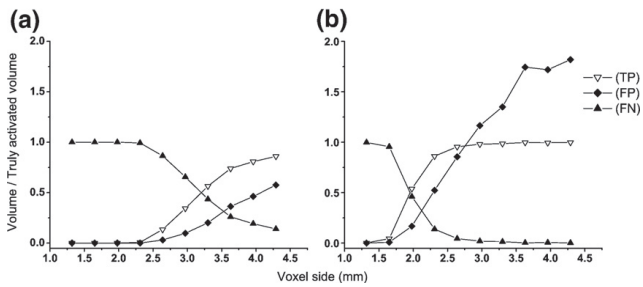

Fig. 2. True positive (TP), false positive (FP) and false negative (FN) volumes normalized to the truly activated volume. The *x* axis represents the length of the cubic voxel side in mm. (a) No smoothing, (b) smoothing with a kernel filter width of 2.5 times the voxel volume. An increase in TP activated volume after smoothing is seen mainly at high resolution, when the initial tSNR is poor. At larger voxel volumes, the FP activated volume increases rapidly.

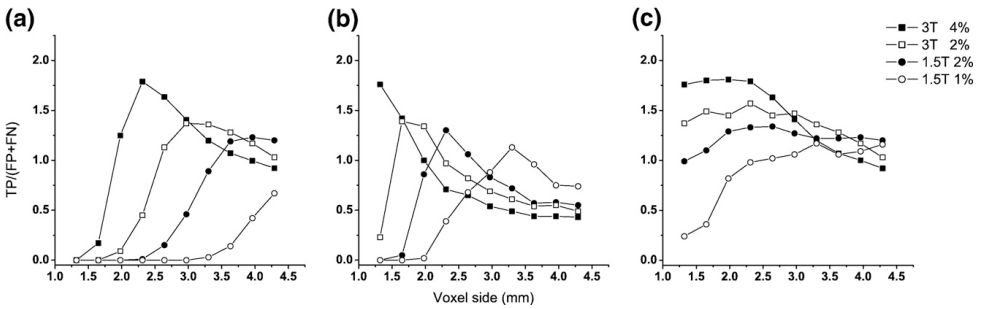

Fig. 3. The TP/(FP+FN) ratio versus spatial resolutions for different smoothing kernel widths. Hypothetical experiments at 1.5 T (circles) and 3 T (squares) are shown as well as small hemodynamic response (open characters) and larger (doubled) hemodynamic response (solid characters). (a) Unsmoothed data sets, (b) data sets smoothed using a kernel width of 2.5 times the voxel side, and (c) data sets smoothed at an optimal kernel width maximizing performance at each voxel volume.

parameter to consider. In this work the CNR was defined as the difference between the activated and non-activated voxel signal divided by the standard deviation of the total applied noise (Eq. 2), where $S_{\text{active}}/S_{\text{rest}}-1$ corresponds to the BOLD contrast.

$$\text{CNR} = \frac{S_{\text{active}} - S_{\text{rest}}}{\sqrt{\sigma_R^2 + \sigma_I^2 + \lambda^2 S_{\text{rest}}^2}} \quad (2)$$

Four hypothetical fMRI experiments were modeled using typical BOLD contrasts (Kwong et al., 1992). The BOLD effect was assumed being roughly proportional to the field strength (Turner et al., 1998). Hence, in the first two experiments, a hemodynamic response corresponding to a BOLD contrast of 1% at 1.5 T and 2% at 3 T was assumed. In the second two experiments, a stronger hemodynamic response with a BOLD contrast of 2% at 1.5 T and 4% at 3 T was used.

SPM processing

The artificial time series were analyzed using SPM5 (Statistical Parametric Mapping 5, http://www.fil.ion.ucl.ac.uk/spm). Motion correction was not applied since patient motion was not modeled. Each time series was high pass filtered (cutoff=3 cycles/modeled session), and the effect of spatial smoothing was studied by evaluating the data sets using several different Gaussian smoothing kernel widths (i.e. full width at half maximum) ranging from 0 mm, i.e. no smoothing, to several times the voxel volume. The hemodynamic response function was expressed as a simple step function, being zero during rest and one during activation, to match the simplified model of response. Serial correlations were corrected for using autoregressive characterization of the first order, AR(1), in the GLM (Friston et al., 2000). The resulting parametric map was overlaid on the corresponding high-resolution anatomical image (see Fig. 1). A statistical threshold corrected for false discovery rate of $q(\text{FDR})<0.05$ (Benjamini and Hochberg, 1995) was used.

Evaluation

The resulting activation map at the given threshold was compared voxel-by-voxel to the true activation data in the high-resolution key map. Since the key map and the resulting activation map were of

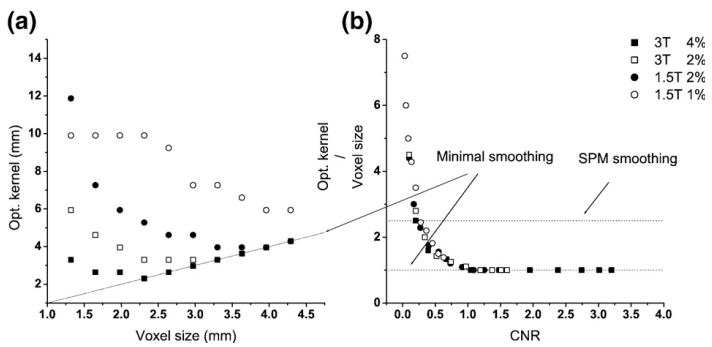

Fig. 4. Scatter plots of optimal smoothing kernel widths that maximize the performance. (a) Optimal kernel widths versus voxel volume. The dashed line represents virtually no smoothing (the kernel size is the same as the voxel side leading to negligible smoothing effects). (b) Optimal kernel width/voxel side versus CNR. The lower dashed line represents virtually no smoothing, suggesting that little or no smoothing should be used at CNR >1. The upper dashed line represents a smoothing kernel width based on 2.5 times the voxel size.

different resolutions, the data in the activation map were resampled using a resolution corresponding to the key map data. Each voxel in the resulting high-resolution key map was regarded as either 'activated' or 'non-activated', i.e. neglecting specific *t*-values, and subsequently labeled as a true positive (TP), true negative (TN), false positive (FP) or false negative (FN). As a measure of performance, the ratio TP/(FP+FN) was used. When comparing activation maps using various spatial resolutions and smoothing kernel widths, values maximizing this ratio were considered optimal.

Results

The resulting activation map is highly dependent on the spatial resolution (Fig. 1). For example, at high resolution, poor tSNR lowers the possibility to detect significant activation. Increasing the voxel volume increases tSNR initially and improves sensitivity, although the specificity decreases due to PVE and the increasing contribution of physiological noise. This relationship is evaluated quantitatively by calculating the TP, FP and FN activated volumes. At high resolution, the resulting activation map has large volumes of FN activation, also seen as small volumes of TP activation as these parameters are coupled with the relationship TP=1−FN (Fig. 2a). When increasing the voxel volume (decreasing the spatial resolution), TP activation increases rapidly, and at large voxel volumes, the TP activation is stable and close to the truly activated volume. However, the volume of FP activation also increases slowly with increasing voxel volume.

By smoothing the time series spatially, it is possible to gain tSNR. This leads to an increase in the TP activated volume, especially for higher spatial resolutions (Fig. 2b) where the original tSNR is poor. However, smoothing also increases the amount of FP activated volume.

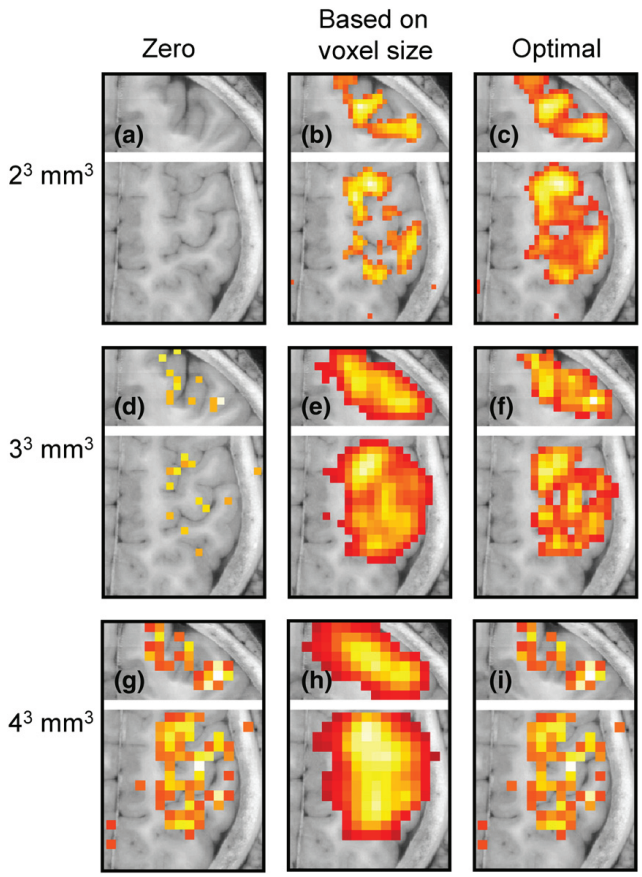

Fig. 5. Coronal and axial activation maps, at 1.5 T and 2% BOLD contrast (solid circles in Figs. 3 and 4), in and around the region of motor cortex and primary somatosensory cortex. The images are presented in radiological convention. Activation maps are FDR corrected with a statistical threshold, $q(\mathrm{FDR})<0.05$. Three frequently used spatial resolutions (2^3 mm^3 (a, b and c), 3^3 mm^3 (d, e and f), and 4^3 mm^3 (g, h and i)) at different smoothing kernels are presented. No smoothing was used in (a), (d) and (g). (b), (e) and (h) were smoothed using a kernel width 2.5 times the voxel volume, and (c), (f) and (i) were smoothed using a kernel width maximizing the performance. Note that zero smoothing was optimal for 4^3 mm^3 (g, i).

As a measure of performance, the ratio TP/(FP+FN) was used. This ratio is small at high resolution due to the small volume of TP activation and large volume of FN activation. Increasing the voxel volume, and consequently also the tSNR, will make the system more sensitive for detecting activation and hence the TP/FN ratio increases. Continuing to increase the voxel volume will eventually reduce the ratio as the volume of FP activation grows due to increased PVE. The performance is plotted for four hypothetical experiments in Fig. 3. High tSNR and large BOLD contrast, i.e. high CNR, are generally beneficial, but the choice of spatial resolution is important (Fig. 3a). The optimal voxel volume is smaller when the CNR is high. Using a large voxel volume in this case may even negate the benefit of high CNR. This is visualized in Fig. 3a, where the performance of high CNR data (solid squares) drops below the performance of lower CNR data (open squares and solid circles) at large voxel volumes. Evaluation of the data sets that were spatially smoothed with a kernel width of 2.5 times the voxel side (Fig. 3b) shows an increase in performance, but mainly in cases of poor CNR. However, when the CNR is high, the choice of voxel volume is even more crucial, which is seen as a steeper decrease in performance at increasing voxel volumes (Fig. 3b) compared to the unsmoothed data (Fig. 3a). The performance was further evaluated using a broad range of smoothing kernel widths (not shown). In this way, it was possible to maximize performance, i.e. maximizing the ratio TP/(FP+FN), for all voxel volumes using optimal kernel widths (Fig. 3c). The optimal size of the smoothing kernel width is not directly related to the voxel volume (Fig. 4a). However, the optimal size of the smoothing kernel, normalized to voxel size, is highly dependent on CNR (Fig. 4b). At CNR approximately larger than 1, smoothing kernel widths of the same magnitude as the voxel size or smaller (resulting in the same activation pattern as unsmoothed data in practice) maximized the performance, suggesting the use of little or no smoothing. To visualize the performance result, activation maps at 1.5 T and 2% BOLD contrast (solid circles in Figs. 3 and 4) are shown in axial and coronal orientation for 2^3, 3^3 and 4^3 mm^3 voxel volumes (Fig. 5). When the CNR is low or moderate (a–f), smoothing the images is favorable, yet too much (e) may lower the specificity. At high CNR (g–i), little or no smoothing is advantageous. For this specific case (1.5 T and 2% BOLD contrast) the optimal smoothing kernel width was 6 mm at 2^3 mm^3, 5 mm at 3^3 mm^3 and 4 mm (equivalent to zero smoothing) at 4^3 mm^3 voxel volume.

Discussion

It is feasible to simultaneously investigate the impact of different spatial resolutions, partial volume effects and smoothing in fMRI by simulating activation patterns using high-resolution templates. The access to "true" activation maps in this study made it possible to quantitatively investigate the TP, TN, FP and FN activation, which would be impossible to do using in vivo data. It is also helpful to be able to investigate these effects over a broad range of CNRs since fMRI experiments may be performed in various ways. The use of high-resolution photographs as anatomical and functional maps minimizes induced errors coupled to the MR modality itself.

The choice of spatial resolution in fMRI is highly dependent on tSNR and BOLD response. At very high spatial resolution, the poor SNR makes it difficult to distinguish activated tissue from non-activated. Increasing the voxel volume ensures better SNR, however, additional increase in SNR will not affect the tSNR proportionally, due to physiological noise (Triantafyllou et al., 2005). Continuing increasing voxel volume will therefore eventually result in only a negligible gain in statistical power as the noise becomes dominated by the physiological fluctuations. At a specific voxel volume, the benefit from high tSNR is counterbalanced by the escalating PVE, especially due to increased FP activated volumes (Fig. 2a). In cases with intrinsically higher CNR (e.g. in experiments performed at higher field strength and/or for stronger BOLD effects) a smaller voxel volume is of more value than for cases with lower CNR (Fig. 3a). A way of increasing CNR for noisy data is to apply smoothing, but this also leads to increased amounts of FP activation. Depending on the situation, smoothing could thus be of different value. For low CNR cases, it might be the difference between detecting and not detecting activation at all, whereas for high CNR situations, smoothing hampers the result by large amounts of FP activation. Although difficult in practice, adjustment of the smoothing kernel width in relation to the specific CNR of each experiment (Fig. 4b), rather than in relation to the voxel side used (which is normally the case), would be of great value. However, to take advantage of high-field fMRI and high-quality coils, when available, it seems disadvantageous to use larger voxel volumes than 3^3 mm^3 (Fig. 3c).

Smoothing strategies in fMRI have been discussed in many studies (Parrish et al., 2000, Scouten et al., 2006, Triantafyllou et al., 2006). Scouten et al. argued for a relatively large functional voxel volume rather than a smaller functional voxel volume combined with a large smoothing kernel width due to the irreversible SNR loss when averaging high-resolution data in MRI (Edelstein et al., 1986). However, the noise in fMRI also includes physiological noise, which is proportional to the voxel volume. It has been suggested that, in some cases, it could be beneficial to use a higher resolution to minimize the effect of the physiological noise and then smooth to regain SNR (Triantafyllou et al., 2006). An example of this is seen in Fig. 3, where the high CNR data sets (solid squares) benefit from smoothing at high spatial resolution (Fig. 3b, 1.3^3 mm^3 and 1.7^3 mm^3 smoothed using 3.3 mm and 4.0 mm smoothing kernel width respectively) rather than using a low spatial resolution from the beginning (Fig. 3a, 3.3^3 mm^3 and 4.0^3 mm^3 voxel size).

The optimal voxel volume has been investigated by other groups (Bodurka et al., 2007; Hyde et al., 2001). Hyde et al. showed that 1.5^3 mm^3 voxel volume was preferable when using motor stimuli at 3 T, i.e. typically very high CNR. Bodurka et al. presented an optimal voxel volume of 1.8^3 mm^3 based on the concept of choosing a voxel volume that ensured the physiological and thermal noise to be equal. Although the smoothing strategies used in these studies are not clearly stated, their results agree fairly well with the results presented in this study. However, it is evident that the actual CNR and smoothing used play vital roles. Furthermore, the choice of statistical threshold is likely to affect the optimal voxel sizes in general.

Regions with high surface-to-volume ratio, such as the primary somatosensory and motor cortex modeled in this study, are more prone to PVE because of the high tortuosity in these regions (Scouten et al., 2006). In a real fMRI experiment, the usually high and robust activation due to motor stimuli may suggest the use of higher spatial resolution. However, in the sensory cortex, where more subtle activation contrast is expected, a lower spatial resolution may be preferable. On the other hand, using large voxel volumes and smoothing in these anatomically and functionally detailed regions may combine adjacent activations or draining vessels from neighboring tissue (Geissler et al., 2005).

This study shows that the choice of spatial resolution and smoothing strategy is important. The choice is highly dependent on the CNR, and in the end, it is a matter of the required sensitivity and specificity. In studies requiring detailed localization and quantification of small activation clusters, high resolution and limited

smoothing kernel may be the way to go. However, when expecting large volumes of activation or when an actual finding rather than the precision of it is important, lower resolution and smoothing may be used more generously.

The performance was here estimated as the ratio TP/(FP+FN) simply because a large volume of TP activation is preferable, as are limited volumes of FP and FN activation. There are undoubtedly several ways to estimate the performance in an fMRI experiment; however, there is to our knowledge no standardized method. The best type of method used likely depends on what one is trying to study. By choosing TP/(FP+FN) as a measure of performance, we emphasize on giving a true depiction of the BOLD effect in a highly tortuous region with highly detailed and well-defined activation. Nevertheless, it is not unlikely that the results presented in this study would be somewhat different depending on the performance estimation method chosen.

Physiological noise is difficult to model due to its complex characteristics, e.g. spatial correlations (Biswal et al., 1995), potential phase propagations throughout the brain, and temporal aliasing due to insufficient sampling time. It has been modeled mathematically for regression purposes to improve the GLM model (Glover et al., 2000). In this study, a model based on measured resting-state data was used; however, the physiological noise was not implemented as spatially correlated. In a real experiment, where spatial correlations may be present, smoothing could amplify the effect of physiological noise in neighboring voxels, within the range of the smoothing kernel. This could potentially hamper the efficiency of the correction for serial correlations, AR(1). We also evaluated applying the physiological noise as a pure increase of the standard deviation of the white Gaussian noise $\sigma^2=[\sigma_0^2+\lambda^2 S^2]^{1/2}$ (Kruger and Glover, 2001). The results obtained (not presented here) were very similar to the results presented in this paper, suggesting that the use of AR(1) in the GLM to whiten the noise was efficient in this case.

The change of voxel dimensions in this study was simulated solely as a change in the matrix size. The SNR gain due to increased sampling time of a larger *k*-space was not considered, resulting in a potential underestimation of SNR at high spatial resolution. On the other hand, a high spatial resolution may force the use of longer TE due to increased sampling time. This could result in a decreased BOLD effect. In addition, increased sampling time also induces blurring due to more pronounced T2* decay and susceptibility effects during longer read out time. In practice, it may even not be feasible to increase the spatial resolution beyond 2^3 mm^3, at least not using typical EPI sequences for covering the whole brain, due to insufficient gradient performance. In addition, the slice profile was modeled as perfectly rectangular. This approximation is less valid at high through-plane resolution as a rectangular slice profile is more difficult to achieve when slices are thin. For higher spatial resolution acquisitions, the use of partial *k*-space GR-EPI (Hyde et al., 2001) or 3D fMRI based on balanced steady-state techniques (Miller et al., 2006) could be an alternative.

The "true" activation was created as a homogenous signal increase throughout the gray tissue within an ellipsoid-shaped region. Although this is an approximation, it should not affect the investigation of PVE and smoothing effects considerably. Draining veins are important when discussing the specificity of the experiment. However, activation from draining veins was not considered in this study, although they often can contribute as false activated voxels.

In this study, fMRI in a single subject was emphasized, where smoothing mainly is applied to increase SNR and to prevent a non-Gaussian error distribution in the analysis. The latter may have a larger importance in vivo as head motion and physiological fluctuations result in spatially correlated changes in image intensity, which evoke non-Gaussian error distributions (Turner et al., 1998). In group studies, smoothing also makes it possible to account for anatomical diversity and functional discrepancies, introducing another dimension of the role of smoothing in these cases.

Depending on the choice of statistical threshold, different combinations of sensitivity and specificity are achieved, suggesting interpretation differences of any outcome. One way to take these differences into consideration is to use a receiver operating characteristics (ROC) analysis (Metz, 2000) which has been used before in the field of fMRI (Skudlarski et al., 1999). An investigation of the impact of changing the statistical threshold on fMRI performance would be an interesting future study.

In conclusion, this study introduces a novel way to simultaneously investigate how different spatial resolutions are affected by partial volume effects and smoothing strategies in fMRI experiments. The use of a high-resolution anatomical template made it possible to apply artificial activation in an anatomically correct way. Knowledge of the true activation a priori made it possible to investigate the performance quantitatively. The simultaneous evaluation of temporal signal-to-noise and partial volume effects over a broad range of spatial resolutions suggested that the choice of spatial resolution is important in order to maximize the performance. The results also illustrate that the optimal width of the smoothing kernel depends on the experiment CNR rather than the voxel volume.

Acknowledgment

The authors would like to thank The National Library of Medicine's Visible Human Project for providing the Visible Human data set used in this study.

References

Bandettini, P.A., Wong, E.C., Hinks, R.S., Tikofsky, R.S., Hyde, J.S., 1992. Time course EPI of human brain function during task activation. Magn. Reson. Med. 25, 390–397.

Benjamini, Y., Hochberg, Y., 1995. Controlling the false discovery rate: a practical and powerful approach to multiple testing. J.R. Stat. Soc. 57, 289–300.

Biswal, B., Yetkin, F.Z., Haughton, V.M., Hyde, J.S., 1995. Functional connectivity in the motor cortex of resting human brain using echo-planar MRI. Magn. Reson. Med. 34, 537–541.

Bodurka, J., Ye, F., Petridou, N., Bandettini, P.A., 2005. Determination of the brain tissue-specific temporal signal to noise limit of 3 T BOLD-weighted time course data. XIII International Society of Magnetic Resonance in Medicine. Miami, USA.

Bodurka, J., Ye, F., Petridou, N., Murphy, K., Bandettini, P.A., 2007. Mapping the MRI voxel volume in which thermal noise matches physiological noise—implications for fMRI. NeuroImage 34, 542–549.

Desco, M., Hernandez, J.A., Santos, A., Brammer, M., 2001. Multi-resolution analysis in fMRI: sensitivity and specificity in the detection of brain activation. Hum. Brain. Mapp. 14, 16–27.

Edelstein, W.A., Glover, G.H., Hardy, C.J., Redington, R.W., 1986. The intrinsic signal-to-noise ratio in NMR imaging. Magn. Reson. Med. 3, 604–618.

Firbank, M.J., Coulthard, A., Harrison, R.M., Williams, E.D., 1999. Partial volume effects in MRI studies of multiple sclerosis. Magn. Reson. Imaging 17, 593–601.

Friston, K.J., Josephs, O., Zarahn, E., Holmes, S.P., Rouquette, S., Poline, J., 2000. To smooth or not to smooth? Bias and efficiency in fMRI time-series analysis. NeuroImage 12, 196–208.

Geissler, A., Lanzenberger, R., Barth, M., Tahamtan, A.R., Milakara, D., Gartus, A., Beisteiner, R., 2005. Influence of fMRI smoothing procedures on replicability of fine scale motor localization. NeuroImage 24, 323–331.

Geyer, S., Schleicher, A., Zilles, K., 1999. Areas 3a, 3b, and 1 of human primary somatosensory cortex. NeuroImage 10, 63–83.

Glover, G.H., Li, T.Q., Ress, D., 2000. Image-based method for retrospective correction of physiological motion effects in fMRI: RETROICOR. Magn. Reson. Med. 44, 162–167.

Gudbjartsson, H., Patz, S., 1995. The Rician distribution of noisy MRI data. Magn. Reson. Med. 34, 910–914.

Henkelman, R.M., 1985. Measurement of signal intensities in the presence of noise in MR images. Med. Phys. 12, 232–233.

Hyde, J.S., Biswal, B.B., Jesmanowicz, A., 2001. High-resolution fMRI using multislice partial *k*-space GR-EPI with cubic voxels. Magn. Reson. Med. 46, 114–125.

Kim, D.S., Ronen, I., Olman, C., Kim, S.G., Ugurbil, K., Toth, L.J., 2004. Spatial relationship between neuronal activity and BOLD functional MRI. NeuroImage 21, 876–885.

Korvenoja, A., Kirveskari, E., Aronen, H.J., Avikainen, S., Brander, A., Huttunen, J., Ilmoniemi, R.J., Jaaskelainen, J.E., Kovala, T., Makela, J.P., Salli, E., Seppa, M., 2006. Sensorimotor cortex localization: comparison of magnetoencephalography, functional MR imaging, and intraoperative cortical mapping. Radiology 241, 213–222.

Kruger, G., Glover, G.H., 2001. Physiological noise in oxygenation-sensitive magnetic resonance imaging. Magn. Reson. Med. 46, 631–637.

Kwong, K.K., Belliveau, J.W., Chesler, D.A., Goldberg, I.E., Weisskoff, R.M., Poncelet, B.P., Kennedy, D.N., Hoppel, B.E., Cohen, M.S., Turner, R., et al., 1992. Dynamic magnetic resonance imaging of human brain activity during primary sensory stimulation. Proc. Natl. Acad. Sci. U. S. A. 89, 5675–5679.

Metz, C.E., 2000. Fundamental ROC analysis. In: Beutel H.L.K., Jacob, Van Metter, Richard L. (Eds.), Handbook of Medical Imaging. SPIE Press, Bellingham.

Miller, K.L., Smith, S.M., Jezzard, P., Pauly, J.M., 2006. High-resolution FMRI at 1.5 T using balanced SSFP. Magn. Reson. Med. 55, 161–170.

Murphy, K., Bodurka, J., Bandettini, P.A., 2007. How long to scan? The relationship between fMRI temporal signal to noise ratio and necessary scan duration. Neuroimage 34, 565–574.

Ogawa, S., Tank, D.W., Menon, R., Ellermann, J.M., Kim, S.G., Merkle, H., Ugurbil, K., 1992. Intrinsic signal changes accompanying sensory stimulation: functional brain mapping with magnetic resonance imaging. Proc Natl Acad Sci U S A 89, 5951–5955.

Parrish, T.B., Gitelman, D.R., Labar, K.S., Mesulam, M.M., 2000. Impact of signal-to-noise on functional MRI. Magn. Reson. Med. 44, 925–932.

Scouten, A., Papademetris, X., Constable, R.T., 2006. Spatial resolution, signal-to-noise ratio, and smoothing in multi-subject functional MRI studies. Neuroimage 30, 787–793.

Skudlarski, P., Constable, R.T., Gore, J.C., 1999. ROC analysis of statistical methods used in functional MRI: individual subjects. Neuroimage 9, 311–329.

Triantafyllou, C., Hoge, R.D., Krueger, G., Wiggins, C.J., Potthast, A., Wiggins, G.C., Wald, L.L., 2005. Comparison of physiological noise at 1.5 T, 3 T and 7 T and optimization of fMRI acquisition parameters. Neuroimage 26, 243–250.

Triantafyllou, C., Hoge, R.D., Wald, L.L., 2006. Effect of spatial smoothing on physiological noise in high-resolution fMRI. Neuroimage 32, 551–557.

Turner, R., Howseman, A., Rees, G.E., Josephs, O., Friston, K., 1998. Functional magnetic resonance imaging of the human brain: data acquisition and analysis. Exp Brain Res 123, 5–12.

Ugurbil, K., Toth, L., Kim, D.S., 2003. How accurate is magnetic resonance imaging of brain function? Trends Neurosci. 26, 108–114.

Worsley, K.J., Friston, K.J., 1995. Analysis of fMRI time-series revisited—again. Neuroimage 2, 173–181.

Zijdenbos, A.P., Dawant, B.M., 1994. Brain segmentation and white matter lesion detection in MR images. Crit Rev Biomed Eng 22, 401–465.

Paper II

Available online at www.sciencedirect.com
ScienceDirect
Magnetic Resonance Imaging 26 (2008) 1342–1351
MAGNETIC RESONANCE IMAGING

Optimizing the mapping of finger areas in primary somatosensory cortex using functional MRI

Andreas Weibull[a,*], Anders Björkman[b], Henrik Hall[c], Birgitta Rosén[b], Göran Lundborg[b], Jonas Svensson[a]

[a]*Department of Medical Radiation Physics, Lund University, 205 02 Malmö, Sweden*
[b]*Department of Hand Surgery, Lund University, 205 02 Malmö, Sweden*
[c]*Department of Biomedical Engineering, Lund University, 205 02 Malmö, Sweden*

Received 19 November 2007; revised 15 April 2008; accepted 19 April 2008

Abstract

Functional magnetic resonance imaging mapping of the finger somatotopy in the primary somatosensory cortex requires a reproducible and precise stimulation. The highly detailed functional architecture in this region of the brain also requires careful consideration in choice of spatial resolution and postprocessing parameters. The purpose of this study is therefore to investigate the impact of spatial resolution and level of smoothing during tactile stimulation using a precise stimuli system. Twenty-one volunteers were scanned using 2^3 mm^3 and 3^3 mm^3 voxel volume and subsequently evaluated using three different smoothing kernel widths. The overall activation reproducibility was also evaluated. Using a high spatial resolution proved advantageous for all fingers. At 2^3 mm^3 voxel volume, activation of the thumb, middle finger and little finger areas was seen in 89%, 67% and 50% of the volunteers, compared to 78%, 61% and 33% at 3^3 mm^3, respectively. The sensitivity was comparable for nonsmoothed and slightly smoothed (4 mm kernel width) data; however, increasing the smoothing kernel width from 4 to 8 mm resulted in a critical decrease (~50%) in sensitivity. In repeated measurements of the same subject at six different days, the localization reproducibility of all fingers was within 4 mm (1 S.D. of the mean). The precise computer-controlled stimulus, together with data acquisition at high spatial resolution and with only minor smoothing during evaluation, could be a very useful strategy in studies of brain plasticity and rehabilitation strategies in hand and finger disorders and injuries.
© 2008 Elsevier Inc. All rights reserved.

Keywords: fMRI; Spatial resolution; Spatial smoothing; Tactile stimulation

1. Introduction

Precise spatial mapping of finger areas in the primary somatosensory cortex (SI) is interesting for several different applications. Studies of functional changes in the brain after hand injuries and studies of neurological disturbances like focal hand dystonia and vibration-induced neuropathy could benefit from a reliable mapping method. The ability to monitor functional changes in the SI over time could contribute to optimisation of rehabilitation strategies [1,2]. It would also be an important tool when investigating the brain–hand neuronal network principles for sensory feedback in the growing field of intelligent hand prosthesis [1,2].

Functional magnetic resonance imaging (fMRI) has proved to be a valuable tool for studies of cortical activation in vivo [3,4]. However, due to the highly detailed somatotopic architecture of the hand and fingers in cortex [5], fMRI using standard (3^3 mm^3 or lower) spatial resolution may be inadequate for mapping purposes. When using very poor spatial resolution, the separation of closely localized and confined sensory finger regions could be hampered. An enhanced risk of falsely activated or nonactivated voxels is also present due to partial volume effects [6]; that is, mixed activated and nonactivated tissue in a single voxel is interpreted as homogeneous. Furthermore, using large smoothing kernel widths during postprocessing of the data may combine activations from functionally separated brain regions or draining veins [7]. However, as the cortical blood-oxygen-level-dependent (BOLD) response of pure tactile stimulation is typically

* Corresponding author.
E-mail address: andreas.weibull@med.lu.se (A. Weibull).

0730-725X/$ – see front matter © 2008 Elsevier Inc. All rights reserved.
doi:10.1016/j.mri.2008.04.007

less than 2% [8], the contrast-to-noise ratio may be too poor when using nonsmoothed high-resolution data. These aspects suggest that the choice of spatial resolution and smoothing kernel width could be crucial when mapping highly detailed and localized tactile activation in SI. Finally, the diverse population of cutaneous and subcutaneous receptors at the fingertip [9] makes it important to stimulate the skin in a controlled and known manner.

Several groups have investigated stimuli systems for mapping the finger somatotopy in SI [10–14]. One group investigated area 3b with a manually applied brushing stimuli and reported activation of all cortical finger areas in 94% of the volunteers investigated, although an intraexaminer error of 18% was reported [11]. This study showed a somatotopic relationship on group level that was comparable to results from earlier studies performed on different modalities of functional neuroimaging. Another group used a low-cost and computer-controlled pneumatic stimuli system to show that 1 Hz stimulation frequency resulted in the largest BOLD activation contrast in the low-frequency range (1–5 Hz) when stimulating the thumb [12]. In some studies, a well-organized somatotopy has been shown on a group level only [11,14]. However, when investigating sensory feedback in the field of prosthesis development and monitoring patient rehabilitation after hand injuries, information of the individual somatotopy would be beneficial.

Reproducible, accurate and easy-to-use in vivo mapping methods of SI finger areas are a prerequisite for studies of brain plasticity and functional changes in neurological disturbances and hand rehabilitation. Although various stimulation procedures have been tested, the impact of different spatial resolutions and level of smoothing has, to our knowledge, not been investigated for this application.

The aim of this study was to optimize the choice of spatial resolution and smoothing kernel width in fMRI finger mapping of SI. To achieve reproducible and unambiguous stimulation, we used a pneumatically driven and computer-controlled system for tactile stimuli of targeted skin areas. Somatosensory fMRI data were acquired in healthy volunteers at two different spatial resolutions, and the data were subsequently evaluated using different smoothing kernel widths to find an optimized set of acquisition and evaluation parameters.

2. Subjects and methods

2.1. Subjects

fMRI was performed on 22 healthy, right-handed volunteers (12 females) with a mean age of 39 years (age range, 19–56 years). Written informed consent was obtained from each volunteer and the local ethics committee approved the study. Three volunteers were excluded from the study: Volunteer 12 was excluded due to an electrical error in the power amplifier during stimulation. The amplifier was repaired before the next volunteer, and the specific error did not recur during the project. Volunteer 19 was not able to complete the scanning session due to claustrophobia-related problems, and Volunteer 21 was excluded due to extreme head motion, which was not possible to correct for by postprocessing techniques.

2.2. Stimuli system

The stimuli system is pneumatically driven and electronically controlled (Fig. 1), based on the same principle as presented by Wienbruch et al [12]. It has eight separate channels that can be individually controlled. Each channel consists of a pneumatic valve (Festo, Germany, 525146) connected with a plastic tube (length, 4.5 m; inner radius, 1 mm) to a membrane (4-D Neuroimaging; area, ca. 0.8 cm^2). The membrane can be attached to the target skin area using tape, and when the valve is alternately opened and closed, compressed air (1–5 bars) delivers tactile stimuli through the membrane. It is important that the length/radius ratio of the plastic tubes is small enough to deliver distinct stimuli, due to the compressive properties of air and potential tube compliance. The time-dependent air pressure at the site of the membranes was not measured; however, distinct, periodic and minimally delayed membrane pressure was empirically ensured prior to each examination. The permanently installed air supply in the scanner room was used.

The pneumatic valves are electronically controlled using an ordinary laptop PC equipped with a 24-channel digital I/O PCMCIA card (National Instruments, 776912-01) and a custom written LabVIEW software. The software allows individual setting of the desired pulse timings and frequencies for each separate channel. The pulse signals are amplified from 5 to 24 V using an in-house-built power amplifier.

All pneumatic equipment is placed inside the scanner room, whereas the electronic control equipment is placed outside, in the control room. All electronic communication to the scanner room is transferred through a filter plate, minimizing radiofrequency noise penetration from outside.

2.3. fMRI experiments

fMRI was performed using a whole-body 3-T scanner (Siemens Medical Solutions, Erlangen, Germany) equipped with an eight-channel head coil. All volunteers were asked to lay still with their eyes closed during the experiment, and the head was stabilized with cushions and foam pads. Three membranes were attached, by tape, to the tips of the thumb, middle finger and little finger of the right hand. In this manner, the function of both the medianus (thumb and middle finger) and ulnaris (little finger) nerve was addressed. Each volunteer was instructed to position both arm and hand in the most comfortable way with the help of cushions and other support material to ensure patient comfort and to minimize induced errors due to motion or fatigue.

Two fMRI experiments were conducted in the study. Volunteers 1 through 21 participated in the main experiment where two BOLD data sets with different spatial resolution were acquired during each session (2^3 mm^3 and 3^3 mm^3

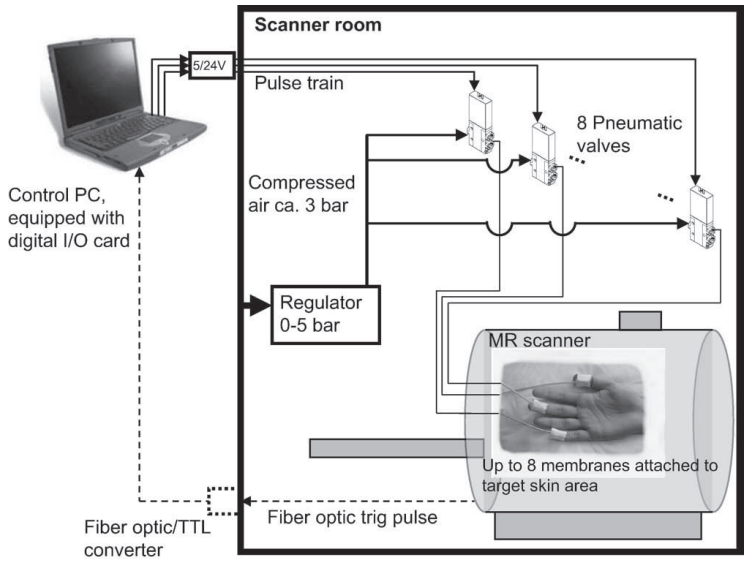

Fig. 1. Schematic view of the stimuli system setup. Eight easily attachable plastic membranes deliver tactile stimulation using pressurised air. Eight pneumatic valves, electronically controlled by an in-house-built LabVIEW program, manage the air pressure delivery. The eight independent stimulation channels may be varied with regard to frequency, amplitude and duration.

cubic voxels). The second experiment was a repeated acquisition over several days on Volunteer 22, to evaluate the reproducibility of the measurement.

Before functional imaging, a high-resolution anatomical scan was acquired (3D-FLASH, TE/TR=4.9/11 ms, flip angle=15°, resolution=1×1×1 mm^3, 176 oblique transversal slices oriented to form a plane through the anterior–posterior commissures). Functional BOLD imaging was then performed using a gradient-echo echo-planar imaging (GE-EPI) pulse sequence with TE/TR=30/2660 ms, flip angle=90° and 288 functional 3D volumes. The functional scans were in the same orientation as the anatomical scan, and the most superior slice was matched to precisely cover the most superior part of the brain in all experiments. The 3^3-mm^3 spatial resolution [64×64 matrix size, 192×192 mm^2 field of view (FOV), 36 slices, 2440 Hz/pixel] was applied first in 11 subjects, whereas the 2^3-mm^3 spatial resolution (128×128 matrix size, 256×256 mm^2 FOV, 23 slices, 1502 Hz/pixel, 6/8 partial *k*-space acquisition) was applied first in 10 subjects. In the case of 2^3 mm^3 spatial resolution, the use of 6/8 partial *k*-space acquisition was necessary to maintain TE at 30 ms. The theoretical SNR difference for the two measurements was $SNR_{3\ mm}/SNR_{2\ mm}$=2.2 [15]. In addition, when using 2^3 mm^3 spatial resolution, the maximal slice coverage within one TR was reduced, and for this reason, only the superior part of the brain, that is, the secondary somatosensory cortex and above, was covered.

During the functional acquisition, tactile stimuli of the three fingers [pulse frequency=1 Hz, pulse width=100 ms, 2.5 bars (pressure)] were separately applied in a semirandom block design (the order of finger stimuli was continuously changing between volunteers) alternating between rest conditions of no stimuli. The operator started the stimulation protocol and the GR-EPI sequence simultaneously. Any delay differences were assumed to be below 100 ms and insignificant to the final result, due to the use of block design. The block length was 31.92 s, that is, 12 TR, and the experiment started with a rest condition.

The second experiment was performed to investigate the reproducibility of the main experiment. Volunteer 22 (male, 30 years old) was scanned on five consecutive days (Day 1–Day 5) and on Day 66, using 2^3 mm^3 resolution. The parameters were exactly the same as in the main experiment when the 2^3-mm^3 resolution was used.

After the scanning session, each volunteer was asked if any complications had occurred, to ensure the use of proper data and the possibility to exclude data on reasonable grounds.

2.4. Evaluation

Evaluation of the data was performed using BrainVoyager QX 1.8 software (Brain Innovation B.V., The Netherlands). The functional data series were preprocessed and coregistered to the anatomical data. The data sets were subsequently normalized to Talairach space using a fit of the anatomical data to a Talairach template (coordinate grid). Preprocessing

included motion correction by means of trilinear interpolation, high-pass filtering to suppress low-frequency modulation (limited to three cycles) and spatial smoothing using a 0-mm (nonsmoothed), 4-mm and 8-mm smoothing kernel width, respectively. In the second experiment, that is, the reproducibility investigation, a smoothing kernel width of 4 mm was used.

Separate activation maps for the three different fingers, that is, each finger was individually contrasted to rest, were created using the general linear model (GLM). Serial correlations were corrected for by using autoregressive characterization of the first order, AR(1), in the GLM [16]. A false discovery rate (FDR; [17])-corrected statistical threshold of q(FDR)<.05 was used as default for individual subjects. In the absence of activation, a less conservative threshold, q(FDR)<.1, was tested. If SI activation appeared at this lowered threshold without inducing large or scattered activation in other regions, the activation was considered true and above noise threshold. In case of large combined activation regions, a threshold of q(FDR)<.01 was used. All spatial coordinates were determined as center of gravity of the clusters. If more than one activation cluster was visible within the SI, here anatomically defined as the postcentral gyrus, the coordinates of the cluster that had the highest t-value average were used. In cases of potential motion artefacts, that is, large activation regions close to the skull or to tissue borders or motion corrections in excess of 1 mm or 1°, the motion correction estimates were also included as regressors in the GLM. Data were evaluated for single volunteers as well as on a group level. The mean value and standard deviation of the Talairach coordinates were calculated in both experiments.

3. Results

In general, contralateral activation of SI was more often seen in the high-resolution 2^3-mm^3 functional maps, compared to the 3^3-mm^3 maps, when using a 4-mm smoothing kernel width (Tables 1 and 2). The statistical threshold was carefully lowered to q(FDR)<.1 (marked with ** in Tables 1 and 2) to increase the sensitivity in cases of absent activation at q(FDR)<.05. This resulted in contralaterally activated SI regions of the thumb, middle finger and little finger areas in 83%, 50% and 50% of the volunteers, respectively, at 2^3 mm^3 (Table 1). In comparison, only 50%, 44% and 22% of the volunteers showed activated regions in SI at 3^3 mm^3 at equivalent threshold (Table 2). When evaluating only one of the two spatial resolutions, that is, either 2^3 mm^3 or 3^3 mm^3, conducted first in each session, the sensitivity was improved further. First-session SI activation of the thumb, middle finger and little finger was seen in 89%, 67% and 50% of the volunteers at 2^3 mm^3 and in 78%, 61% and 33% of the volunteers at 3^3 mm^3, respectively. Images from Volunteer 4, with activation in all three fingers, are shown in Fig. 2. In this specific case, activation was present in both Brodmann area 1 and area 3b. All individual Talairach coordinates are presented in Tables 1 and 2

Table 1
Individual Talairach coordinates at 2^3 mm^3 spatial resolution

Subject	Thumb				Middle finger				Little finger			
	Coordinates			Cluster size	Coordinates			Cluster size	Coordinates			Cluster size
	x	*y*	*z*		*x*	*y*	*z*		*x*	*y*	*z*	
1	−57	−16	37	<10 **								
2	−50	−19	46	218								
3												
4	−44	−19	44	15	−35	−21	52	146	−33	−28	61	27
5	−48	−13	49	<10 **	−49	−25	50	614 *	−42	−22	52	<10
6	−53	−20	42	55	−48	−29	52	<10 **				
7	−53	−15	43	<10 **	−48	−23	52	185 *	−42	−29	55	<10
8	−56	−22	44	418	−47	−31	52	54	−45	−29	51	616
9	−47	−21	41	595	−44	−25	48	356 *	−42	−31	50	114 *
10	−46	−14	46	472	−43	−24	53	153 *	−35	−27	57	132
11												
13	−53	−24	41	21								
14	−49	−18	49	153					−37	−26	58	165 **
15												
16	−47	−28	42	42	−39	−26	53	34 *	−40	−34	50	102 *
17	−53	−17	41	1018	−49	−29	44	248 *	−42	−31	46	47
18	−49	−16	44	877 *								
20	−52	−20	47	27								
Mean	−50	−19	44		−45	−26	51		−40	−29	53	
S.D.	3.8	4.0	3.3		4.9	3.2	3.0		3.9	3.4	4.7	

q(FDR)<.05. Volunteers 12, 19 and 21 are not included due to stimuli failure (Volunteer 12) or compliance issues (Volunteers 19 and 21). Cluster sizes in mm^3.
* q(FDR)<.01.
** q(FDR)<.1.

Table 2
Individual Talairach coordinates at 3^3 mm^3 spatial resolution

Subject	Thumb				Middle finger				Little finger			
	Coordinates			Cluster size	Coordinates			Cluster size	Coordinates			Cluster size
	x	*y*	*z*		*x*	*y*	*z*		*x*	*y*	*z*	
1	−56	−15	39	181	−48	−21	45	237	−45	−25	49	<10
2					−42	−22	53	<10				
3												
4					−35	−20	53	28 *				
5	−52	−12	50	56 **								
6												
7												
8	−55	−19	41	1337	−44	−18	49	313 *	−42	−26	49	86
9												
10	−48	−16	40	<10 **								
11												
13	−52	−22	43	289								
14	−54	−16	46	11 **								
15					−46	−30	50	56				
16	−49	−25	42	42 *	−42	−31	49	<10	−30	−32	54	<10
17	−54	−19	35	178	−48	−27	42	114				
18												
20	−49	−23	44	318	−45	−32	51	782 *	−44	−34	53	<10
Mean	−52	−19	42		−44	−25	49		−40	−29	51	
S.D.	2.9	4.2	4.3		4.2	5.5	3.8		6.9	4.4	2.6	

q(FDR)<.05. Volunteers 12, 19 and 21 are not included due to stimuli failure (Volunteer 12) or compliance issues (Volunteers 19 and 21). Cluster sizes in mm^3.
* q(FDR)<.01.
** q(FDR)<.1.

including the group mean and standard deviation (1 S.D.) of all fingers. Overall, the activation cluster localization for the separate fingers corresponded well to the expected organization in SI; that is, the thumb, middle finger and little finger were organized in an anterior-to-posterior, inferior-to-superior and lateral-to-medial manner.

The individual fMRI data were also evaluated using three different smoothing kernel widths (0, 4 and 8 mm), as shown for Volunteer 1 in Fig. 3. When using spatially nonsmoothed data (0 mm smoothing kernel width), finger activation was seen in three additional cases of little finger stimulation when using 3^3 mm^3 spatial resolution. However, at 2^3 mm^3 spatial resolution, the use of nonsmoothed data resulted in a complete loss of SI activation in five sessions, all showing activation when using a 4-mm smoothing kernel width. Using an 8-mm smoothing kernel width resulted in a major decrease of sensitivity to finger activation in SI regardless of spatial resolution used. Here, only 22%, 28% and 6% (2^3 mm^3) and 44%, 39% and 22% (3^3 mm^3) of the volunteers showed activation of the thumb, middle finger and little finger areas, respectively.

A group analysis of the 3^3-mm^3 data, that is, including all volunteers in the GLM, yielded SI activation at q(FDR)<.001 for the thumb and middle finger only (Fig. 4). Even at more conventional thresholds, that is, q(FDR)<.05, no little finger SI activation was seen. At 2^3 mm^3, however, all three fingers showed SI activation in the group analysis, q(FDR)<.001.

The reproducibility study of Volunteer 22 generated activation in the thumb, middle finger and little finger areas in all cases except for little finger activation on Day 4 (Fig. 5). The mean Talairach coordinates from the six experiments for the three fingers were (−51±2.0, −19±1.4, 40±2.5), (−44±0.5, −21±2.0, 48±1.8) and (−42±1.5, −28±1.5, 55±3.0) for the thumb, middle finger and little finger, respectively (Table 3).

4. Discussion

In individuals in general, the activation cluster localization for the separate fingers corresponded well to the expected organization in SI [18] (Tables 1 and 2); that is, the thumb, middle finger and little finger were organized in an anterior-to-posterior, inferior-to-superior and lateral-to-medial manner. In some individuals, however (Volunteers 8 and 20), the distributed somatotopy of the middle finger and the little finger was not found. This is likely to be due to overlap in sensory distribution of different fingers [19]. High-resolution (2^3 mm^3) BOLD imaging proved to be more sensitive compared to BOLD imaging at 3^3 mm^3 spatial resolution. This was also seen at group level (Fig. 4), where group activation of the little finger was absent at 3^3 mm^3 resolution. The advantage of using a high spatial resolution could be due to the detailed functional somatotopy in SI [5]. This specific region may also be more prone to partial volume effects due to the highly tortuous anatomy, that is, large surface-to-volume ratio [20]. Although the BOLD response from tactile stimulation is expected to be rather low, the use of high field strength and multichannel coils

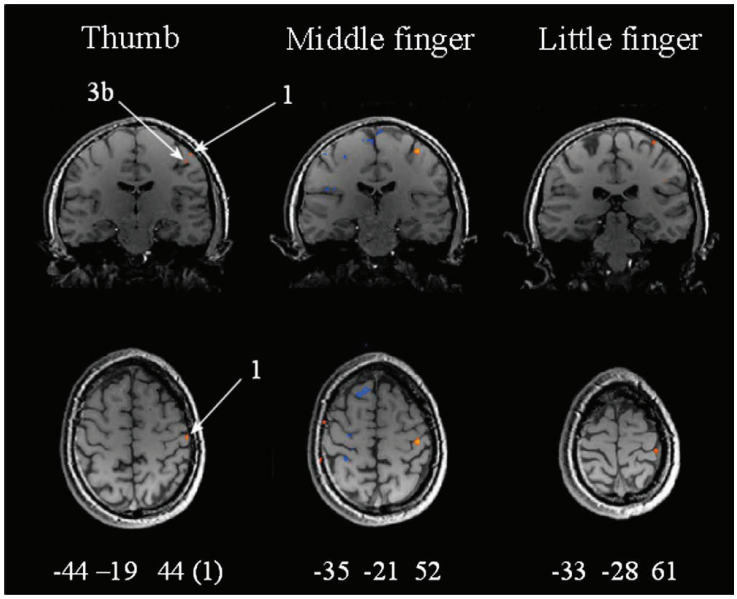

Fig. 2. Single volunteer (Volunteer 4) activation in primary somatosensory cortex from tactile stimuli of thumb, middle finger and little finger tips at 2^3 mm^3 spatial resolution. Coordinates are given in Talairach space. The resulting activation shows well-separated finger somatotopy and clusters do not overlap. In case of multiple significant clusters in SI (here, thumb activation in Brodmann areas 1 and 3b), the cluster containing the most significant voxel was evaluated (here, Brodmann area 1).

increases the contrast-to-noise ratio, which, in turn, favors the use of high spatial resolution [6].

Since 2^3 mm^3 spatial resolution required a 128×128 matrix, the comparison between 2^3 mm^3 and 3^3 mm^3 spatial resolution was not straightforward. Partial *k*-space acquisition (6/8) was necessary to be able to maintain TE at 30 ms. Overall, the theoretical SNR for the 3^3-mm^3 spatial resolution session was 2.2-fold increased compared to the 2^3-mm^3 spatial resolution session. If all parameters, except for voxel volume, would have been identical, this factor had been expected to be 3.4. It would have been possible to carry out the experiments using equal theoretical SNR, by increasing the bandwidth to more than what was needed in the case of 2^3 mm^3 spatial resolution. However, the use of optimized protocols was considered important, rather than having equal acquisition parameters. In the end, the use of 3^3 mm^3 spatial resolution resulted in a poorer outcome despite more than twice as high SNR compared to the use of 2^3 mm^3 spatial resolution.

The choice of smoothing kernel width proved to be crucial when investigating small, localized and highly detailed functional regions such as the finger areas in SI. Our results in this article show that using a large smoothing kernel width when mapping the SI in individual subjects was disadvantageous. The decrease in sensitivity was either due to a combination of activation and draining veins, making it impossible to distinguish the finger activation, or due to activation loss (Fig. 3; 8 mm smoothing kernel width). The sensitivity was improved when smoothing the high-resolution data using a 4-mm smoothing kernel width, although this was not seen in the low-resolution data. This could be due to an inherent need for smoothing high-resolution data as SNR might be too poor [6,21]. Although nonsmoothed data resulted in good sensitivity, some smoothing is advisable to avoid non-Gaussian error in the GLM [22]. In a group study, there may also be a need for additional smoothing due to anatomical and functional variations within a group [23].

The sensitivity of finger activation in SI was improved when evaluating the acquisition parameter set (either 2^3 mm^3 or 3^3 mm^3 spatial resolution) used first in each experiment. A possible explanation is that volunteers suffer from habituation effects, loss of attention and/or fatigue during the experiment, which are likely to increase over time. This suggests a less sensitive activation result for the specific acquisition parameter set applied last in the experiment. Activation during the first session, regardless of spatial resolution used, was seen in 23% more cases, implying an improvement when only one resolution is used. Thus, the improved statistical inference of a long session, that is, a large number of time points, could be counterbalanced with a potential decrease in sensitivity over time.

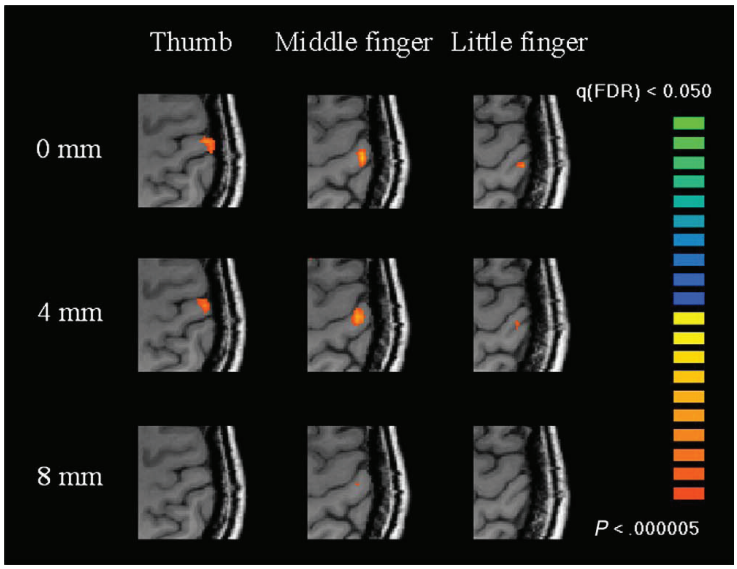

Fig. 3. Visualization of smoothing effects in Volunteer 1 at 3^3 mm^3 spatial resolution. At 8 mm smoothing kernel width (2.5 times the voxel size), the sensitivity to tactile finger activation is critically hampered.

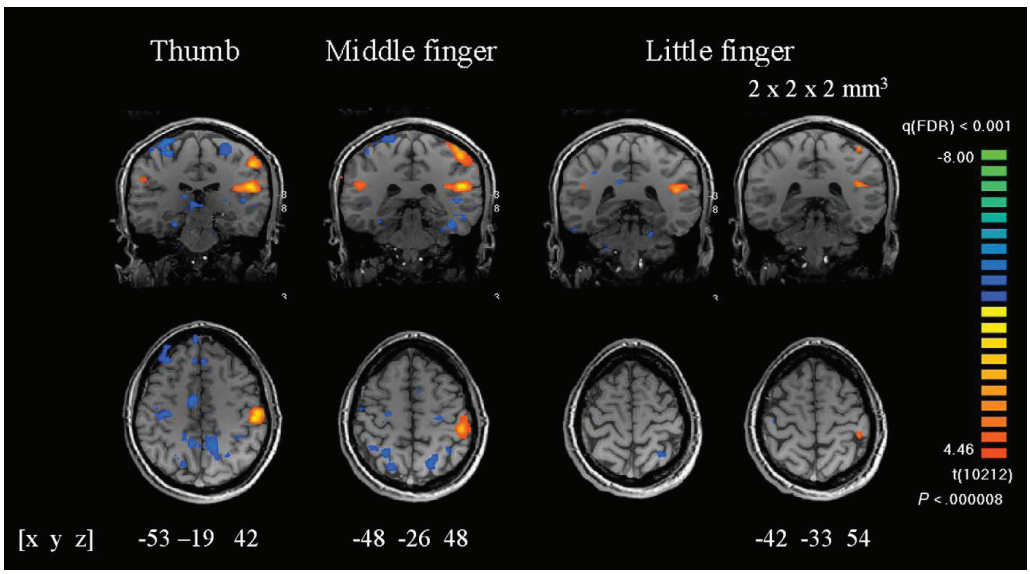

Fig. 4. Group activation for the thumb, middle finger and little finger at 3^3 mm^3. The little finger is also presented at 2^3 mm^3. The coordinates refer to the center of gravity of the cluster and indicate a somatotopic organization at group level. However, little finger activation in primary somatosensory cortex is absent at 3^3 mm^3.

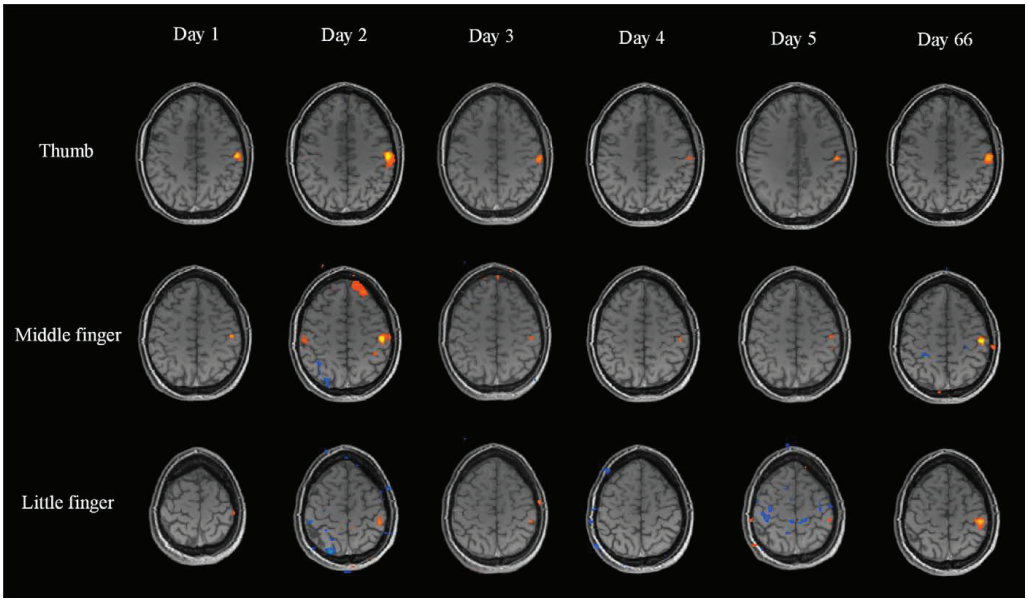

Fig. 5. Reproducibility study of Volunteer 22. Tactile stimulation of the thumb, middle finger and little finger was executed on five consecutive days (Day 1–Day 5) and on Day 66. A spatial resolution of 2^3 mm^3 and a 4-mm smoothing kernel width were used. Activation of the little finger was absent on Day 4, possibly due to the volunteer having problems being awake during parts of the session.

The reproducibility of finger activation during tactile stimuli was satisfying for mapping the somatotopy in SI (Fig. 5 and Table 3). The center-of-gravity coordinates for the different fingers were very stabile on both short and long terms. The cluster sizes varied more; however, this variation was expected as several parameters affect the cluster size in a complex way (e.g., variation in the degree of actual brain activation, scanner variations, physiological noise or statistical threshold based on FDR). In some sessions, additional activation was also seen in other regions of the brain, for example, prefrontal activation in Day 2. These activation clusters were assumed not directly connected to the tactile stimulation.

The overall function of the stimulation system was excellent in administrating a sensory stimulus to the different fingers in the MR environment. Although the sharp rectangular pulse stimulation is inevitably smoothed due to air compression in the tubes, it was not considered to hamper

Table 3
Investigation of reproducibility (Volunteer 22)

Day	Thumb				Middle finger				Little finger			
	Coordinates			Cluster size	Coordinates			Cluster size	Coordinates			Cluster size
	x	*y*	*z*		*x*	*y*	*z*		*x*	*y*	*z*	
1	−50	−18	41	924	−43	−19	47	70	−42	−25	60	34
2	−51	−17	39	3552	−44	−20	49	4790	−42	−26	52	225
3	−52	−21	41	512	−44	−24	46	38	−43	−31	54	63
4	−54	−19	40	396	−44	−22	47	40 **				
5	−48	−18	35	303	−43	−19	47	29	−42	−30	56	59 **
66	−52	−18	42	1820	−44	−20	51	395 *	−39	−27	55	1173
Mean	−51	−19	40		−44	−21	48		−42	−28	55	
S.D.	2.0	1.4	2.5		0.5	2.0	1.8		1.5	2.6	3.0	

q(FDR)<.05. Coordinates are given in Talairach space; 2^3 mm^3 spatial resolution and 4 mm smoothing kernel width are used. Cluster sizes in mm^3.
* q(FDR)<.01.
** q(FDR)<.1.

the study for the tube lengths used here. The actual stimulus was empirically evaluated prior to all subjects to ensure distinct, periodic and reproducible stimulation. However, for a setup using longer tubes, this might be an issue. The stimulation system proved able to map the distribution in SI on an individual level. The electronic control of the system ensures a highly reproducible tactile stimulus delivery. Another advantage is that the membranes can be attached to the fingertips without constraining the volunteer's hand and arm position, thus reducing the risk for problems of fatigue or discomfort during the experiment. The system ensures high patient comfort and is easy to work with in the MR environment.

An important limitation of using high spatial resolution in fMRI is the partial coverage of the brain. At 2^3 mm^3 or higher spatial resolution, it might not be feasible to cover the whole brain using typical GR-EPI sequences, due to insufficient gradient performance. Fast 3D fMRI methods based on steady-state techniques have been used for increasing the spatial resolution regionally beyond 2^3 mm^3 [24]. This could be an interesting option for mapping finger somatotopy at ultrahigh spatial resolution; however, these methods rely on a highly homogeneous magnetic field in the region of interest, which introduce new issues in whole-brain fMRI.

In a similar study, ipsilateral SI activation due to tactile stimulation was monitored [25], representing transcallosal fibres connecting the SI of both hemispheres. In our study, ipsilateral SI activation was rarely seen, and at group level, ipsilateral activation was only visible in the secondary somatosensory cortex, even at very low statistical thresholds. It has recently been suggested that area 3b in SI may have an ipsilateral and transient deactivation during tactile stimulation due to interhemispheric inhibition [26]. This weaker and negative activation contrast could potentially neutralise the positive activation contrast from nearby regions in SI. Another explanation could be that the ipsilateral response may be too weak to measure with the experimental setup presented in this study.

Although SI comprises four rather distinct regions (Brodmann areas 1, 2, 3a and 3b), each with a complete somatotopic representation of the body surface, with a variety of functional characteristics and complexity [9], the focus in this study is activation in either part of the SI. An investigation of activation in different Brodmann areas would be of great interest, but the scope of this study was to investigate the impact of spatial resolution and smoothing and to test the stimulation system for reproducible finger activation rather than a functional mapping of different Brodmann areas within SI.

In conclusion, high spatial resolution ($2\times2\times2$ mm^3) proved to be advantageous when mapping the SI and showed a reasonable sensitivity to tactile finger stimulation. Smoothing should be applied with caution as the sensitivity to individual finger activation decreased rapidly when increasing the kernel width. The presented system proved able to deliver a stimulus, resulting in distinct fingertip activation in SI, and was capable of mapping the somatotopy at an individual level. Finally, the stimuli system showed a remarkable reproducibility and seems promising for studies aiming to separate cortical finger areas such as studies of brain plasticity in hand and finger disorders and injuries.

Acknowledgment

The study was funded by the European Commission within the SMARTHAND project contract no. NMP4-CT-2006-0033423, the Swedish Council for Working Life and Social Research and the Swedish Medical Research Council.

References

[1] Lundborg G, Richard P. Bunge memorial lecture. Nerve injury and repair — a challenge to the plastic brain. J Peripher Nerv Syst 2003;8 (4):209–26.
[2] Lundborg G. Nerve injury and repair. Regeneration, reconstruction and cortical remodelling. 2nd ed. Philadelphia: Elsevier; 2004.
[3] Sakai K, et al. Functional mapping of the human somatosensory cortex with echo-planar MRI. Magn Reson Med 1995;33(5):736–43.
[4] Sanes JN, et al. Shared neural substrates controlling hand movements in human motor cortex. Science 1995;268(5218):1775–7.
[5] Geyer S, Schleicher A, Zilles K. Areas 3a, 3b, and 1 of human primary somatosensory cortex. Neuroimage 1999;10(1):63–83.
[6] Weibull A, et al. Investigation of spatial resolution, partial volume effects and smoothing in functional MRI using artificial 3D time series. Neuroimage 2008, doi:10.1016/j.neuroimage.2008.02.015.
[7] Geissler A, et al. Influence of fMRI smoothing procedures on replicability of fine scale motor localization. Neuroimage 2005;24 (2):323–31.
[8] Stippich C, et al. Somatotopic mapping of the human primary somatosensory cortex by fully automated tactile stimulation using functional magnetic resonance imaging. Neurosci Lett 1999;277(1): 25–8.
[9] Purves D, et al, editor. Neuroscience. Sunderland: Sinauer Associates, Inc.; 1997. p. 147–63.
[10] Overduin SA, Servos P. Distributed digit somatotopy in primary somatosensory cortex. Neuroimage 2004;23(2):462–72.
[11] van Westen D, et al. Fingersomatotopy in area 3b: an fMRI-study. BMC Neurosci 2004;5:28.
[12] Wienbruch C, et al. A portable and low-cost fMRI compatible pneumatic system for the investigation of the somatosensory system in clinical and research environments. Neurosci Lett 2006;398(3): 183–8.
[13] Kurth R, et al. fMRI assessment of somatotopy in human Brodmann area 3b by electrical finger stimulation. NeuroReport 1998;9(2): 207–12.
[14] Gelnar PA, et al. Fingertip representation in the human somatosensory cortex: an fMRI study. Neuroimage 1998;7(4 Pt 1):261–83.
[15] Edelstein WA, et al. The intrinsic signal-to-noise ratio in NMR imaging. Magn Reson Med 1986;3(4):604–18.
[16] Friston KJ, et al. To smooth or not to smooth? Bias and efficiency in fMRI time-series analysis. Neuroimage 2000;12(2):196–208.
[17] Benjamini Y, Hochberg Y. Controlling the false discovery rate: a practical and powerful approach to multiple testing. J R Stat Soc 1995; 57(1):289–300.
[18] Kurth R, et al. fMRI shows multiple somatotopic digit representations in human primary somatosensory cortex. NeuroReport 2000;11(7): 1487–91.

[19] Maldjian JA, et al. The sensory somatotopic map of the human hand demonstrated at 4 Tesla. Neuroimage 1999;10(1):55–62.
[20] Scouten A, Papademetris X, Constable RT. Spatial resolution, signal-to-noise ratio, and smoothing in multi-subject functional MRI studies. Neuroimage 2006;30(3):787–93.
[21] Triantafyllou C, Hoge RD, Wald LL. Effect of spatial smoothing on physiological noise in high-resolution fMRI. Neuroimage 2006;32(2):551–7.
[22] Worsley KJ, Friston KJ. Analysis of fMRI time-series revisited — again. Neuroimage 1995;2(3):173–81.
[23] Brett M, Johnsrude IS, Owen AM. The problem of functional localization in the human brain. Nat Rev Neurosci 2002;3(3):243–9.
[24] Miller KL, et al. High-resolution FMRI at 1.5T using balanced SSFP. Magn Reson Med 2006;55(1):161–70.
[25] Hansson T, Brismar T. Tactile stimulation of the hand causes bilateral cortical activation: a functional magnetic resonance study in humans. Neurosci Lett 1999;271(1):29–32.
[26] Hlushchuk Y, Hari R. Transient suppression of ipsilateral primary somatosensory cortex during tactile finger stimulation. J Neurosci 2006;26(21):5819–24.